PSEUDO-MOLECULAR ION FORMATION BY AROMATIC ACIDS IN NEGATIVE IONIZATION MODE ELECTROSPRAY IONIZATION MASS SPECTROMETRY

By

Kevin Albert Schug

Dissertation Submitted to the Faculty of the
Virginia Polytechnic Institute and State University
In partial fulfillment of the requirements for the degree of

DOCTOR OF PHILOSOPHY

IN

CHEMISTRY

_____
Harold M. McNair, Chair

_____ _____
Larry T. Taylor Jimmy W. Viers

_____ _____
Mark R. Anderson William A. Ducker

October, 2002

Blacksburg, Virginia

Keywords: adduct, electrospray, mass spectrometry, aromatic acids, pseudo-molecular ion, LC-MS.

PSEUDO-MOLECULAR ION FORMATION BY AROMATIC ACIDS IN NEGATIVE IONIZATION MODE ELECTROSPRAY IONIZATION MASS SPECTROMETRY

By

Kevin Albert Schug
Committee Chairman: Harold M. McNair
Department of Chemistry

ABSTRACT

Pseudo-molecular ion formation is an artifact common to most analyses performed by electrospray ionization mass spectrometry. These species are non-covalent complexes formed between an analyte of interest and any other components (such as mobile phase, additives, and impurities) present in the ionized sample band. Published literature addresses pseudo-molecular ion formation in routine analyses as well as in complicated molecular recognition processes. The majority of these works are directed towards the formation of complexes in the positive ionization mode. Consequently, investigation of pseudo-molecular ion formation in the negative ionization mode is a logical extension of work in this area.

Experiments presented here detail the work performed on elucidation of factors controlling ionization efficiency of aromatic acid pseudo-molecular ions by electrospray ionization in the negative ionization mode. Sets of tested acidic analytes, including ibuprofen derivatives and benzoic acid derivatives, were analyzed in the presence of various solution systems by flow injection analysis to determine the effect of pH, concentration, injection volume, and instrumental parameters on dominant ion forms observed in the mass spectra. These ion forms correspond to a deprotonated molecular ion ($[M-H]^-$), a hydrogen-bound dimer ion ($[2M-H]^-$), and a sodium-bridged dimer ion ($[2M-2H+Na]^-$). Report of the latter ion form is unique to this work.

Response of these ion forms were found to vary greatly with changing solution parameters, particularly in the presence of common LC-MS modifiers, such as triethylamine, acetic acid, formic acid, and ammonium formate. Results point to the formation of the sodium-bridged dimer ion during gas-phase processes following the release of ions from disintegrated droplets. *Ab initio* theoretical calculations and correlations with calculated solution phenomena (such as pK_a and log P) were used to elucidate structural arrangements and dominant factors controlling pseudo-molecular ion formation by aromatic acids in the negative ionization mode.

ACKNOWLEDGEMENTS

First and foremost, I would like to extend my thanks to my father, Dr. John C. Schug. Without his motivation and advice through the years, I would not have become the person who I am proud to be today. Even a semester of his dreaded graduate physical chemistry served as a reminder that to succeed, you have to practice and practice hard. Next I would like to thank my adviser and mentor, Professor Harold M. McNair. His exuberance and knowledge in the field of separation science has set the mark high, daring his students to jump higher. It is obvious his intentions are that we become a successful researcher and teacher to contribute, pass on, and build upon that which we have learned in our short time under his tutelage.

I would like to thank the members of Professor McNair's research group, past and present, for their knowledge, support and kindness in my years here at Virginia Tech. I would especially like to acknowledge Jennifer Smith, who has traveled the same path as I and has served as a teacher, a competitor, and most importantly, a friend to me.

I would also like to acknowledge the people at Shimadzu Scientific Instruments, specifically, Patrick Fromal, Robert Classon, and Chris Gilles for their time, their interest, and their instrumentation. Without their generosity, I would not have been able to perform the research presented in this dissertation. To Daniel Crawford at Virginia Tech, I extend my appreciation for use of his Gaussian98 program for performing *ab initio* calculations. To Michael McBrien of Advanced Chemistry Development, Inc., I extend my thanks for use of ACDlabs software to calculate solution-phase analyte properties.

Last, but not least, I extend my thanks to my professors and graduate research committee members, Larry Taylor, Jimmy Viers, Mark Anderson, and William Ducker for their fair assessment and critique of my work. Their high standards have motivated me to perform to the best of my ability and taught me to always look deeper into the problem at hand.

"I do not know what I may appear
to the world, but to myself I seem
to have only been like a boy playing
on the sea-shore, and diverting
myself in now and then finding a
smoother pebble or a prettier shell
than ordinary, whilst the great
ocean of truth lay all undiscovered
before me."

Sir Isaac Newton

TABLE OF CONTENTS

	Page
CHAPTER 1 INTRODUCTION AND BACKGROUND	1
1.1 Introduction	1
1.2 Theory and Mechanism of LC-MS	4
1.3 History of ESIMS	11
1.4 Noncovalent Interactions	15
1.5 Pseudo-Molecular Ion Formation and Alkali Metals	26
CHAPTER 2 EXPERIMENTAL	43
2.1 General Experimental	43
2.2 Experiment 1: Common Acidic Pharmaceuticals	49
2.3 Experiment 2: Simple Aromatic Acids	52
2.4 Experiment 3: Concentration and pH Effects in FIA-ESIMS	54
CHAPTER 3 COMMON ACIDIC PHARMACEUTICALS	57
3.1 Introduction	57
3.2 Results	58
3.3 Discussion	74
CHAPTER 4 BENZOIC ACID DERIVATIVES	83
4.1 Introduction	83
4.2 Results	85
4.3 Discussion	101
CHAPTER 5 pH and CONCENTRATION EFFECTS IN FIA-ESIMS	110
5.1 Introduction	110
5.2 Results	113
5.3 Discussion	127
CHAPTER 6 OTHER EXPERIMENTS	128
6.1 Addition of Alkali Acetate Salts to Ibuprofen Derivatives	128
6.2 Analysis of Parabens	135
6.3 Positive Mode Ionization of PABA with Extreme pH Adjustment	139
6.4 Analysis of Basis Set Selection in *ab initio* Simulations	141
CHAPTER 7 CONCLUSIONS	143

TABLE OF FIGURES

Figure	Detail	Page
1.2.1	Interface spray chamber for Shimadzu LCMS-2010 (Shimadzu Scientific Instruments, Columbia, MD, USA).	10
1.3.1	Publications involving the use of electrospray per year according to a popular search engine.	14
1.4.1	Generalized Scatchard plot used for the determination of dissociation constant for host – guest complexes.	20
2.1.1	General bench top set-up for the Shimadzu LCMS-2010.	44
2.1.2	LCMS-2010 interface probes for ESI and APCI operation modes.	45
2.1.3	Schematic diagram of the interface and ion lens configuration of a Shimadzu LCMS-2010 instrument.	45
2.1.4	Curved desolvation line (CDL) and CDL housing used for declustering gas-phase species and extraction of ions into the high vacuum region of the MS.	46
2.2.1	Structure, molecular weight, and pK_a for the six anti-inflammatory pharmaceuticals used in experiment 1.	51
2.3.1	Structures of *ortho*-, *meta*- and *para*-substituted benzoic acid analytes used in experiment 2.	53
3.2.1	Flow injection ESI mass spectrum of ibuprofen in 50/50 acetonitrile/water mobile phase with no modifiers in the negative ionization mode.	61
3.2.2	Geometry optimized structure of the deprotonated ibuprofen molecular ion at the 3-21G basis level using Hartree-Fock *ab initio* simulations.	61
3.2.3	Hartree-Fock ab initio geometry optimized structure for the sodium-bridged dimer ion of ibuprofen at the 3-21G basis level.	62
3.2.4	Effect of mobile phase modifiers on $[2M-2H+Na]^-$ of ibuprofen.	63
3.2.5	Geometry optimized structure of $[M-H]^-$ ion of carprofen.	64
3.2.6	Geometry optimized structure of $[2M-H]^-$ of carprofen.	64
3.2.7	Geometry optimized structure of $[2M-2H+Na]^-$ of carprofen.	65
3.2.8	Effect of additives on $[2M-2H+Na]^-$ of carprofen.	66
3.2.9	Effect of additives on $[2M-H]^-$ of carprofen.	66
3.2.10	Effect of additives on formation of $[M-H]^-$ by ketoprofen.	67
3.2.11	Geometry optimized structure for the sodium-bridged dimer pseudo-molecular ion of ketoprofen.	68
3.2.12	Geometry optimized structure of $[M-H]^-$ for naproxen.	69
3.2.13	Effect of additives on $[M-H]^-$ of naproxen.	70
3.2.14	Effect of additives on response for $[2M-2H+Na]^-$ of naproxen.	70
3.2.15	Geometry optimized structure of $[2M-2H+Na]^-$ for flurbiprofen.	71
3.2.16	Direct injection ESI mass spectrum of flurbiprofen in the presence of 5 mM formic acid.	72
3.2.17	Geometry optimized structure for the $[M-H]^-$ ion of fenoprofen.	73
3.2.18	Effect of additives on $[2M-2H+Na]^-$ of fenoprofen.	73
3.3.1	Effect of TEA on $[M-H]^-$ of six acidic anti-inflammatory pharmaceuticals.	76
3.3.2	Hartree-Fock *ab initio* simulation of hydrogen bonding in the	80

	homogeneous dimer ion of carprofen.	
4.2.1	Plot relating response of benzoic acid molecular ion ($[M-H]^-$) to percent organic as a function of concentration.	85
4.2.2	The effect of CDL voltage and temperature on the response of benzoic acid molecular ion ($[M-H]^-$).	87
4.2.3	Effect of CDL voltage and temperature on response for the sodium-bridged dimer ion of benzoic acid.	88
4.2.4	Deprotonated molecular ion of benzoic acid modeled with Hartree-Fock *ab initio* calculations at the 3-21G level of basis.	89
4.2.5	Most stable sodium-bridged dimer ion complex of benzoic acid modeled with Gaussian98 Hartree-Fock *ab initio* calculations at the 3-21G level of basis.	89
4.2.6	Three views of an alternate $[2M-2H+Na]^-$ ion form calculated by Hartree-Fock *ab initio* simulations at the 3-21G level of basis.	90
4.2.7	Response of $[M-H]^-$ for 0.01 mM halide-substituted benzoic acid model compounds in 50/50 acetonitrile/water.	92
4.2.8	Hartree-Fock *ab initio* simulations for the deprotonated molecular ion of halide-substituted benzoic acid molecules.	93
4.2.9	Steric interaction caused by halide-substituted benzoic acids in the *ortho*-position.	93
4.2.10	Response of [2M-2H+Na]- for 0.01 mM halide-substituted benzoic acid model compounds in 50/50 acetonitrile/water.	95
4.2.11	*Ab initio* Hartree-Fock structures modeled at the 3-21G level of basis for the *ortho*-halide substituted sodium-bridged dimer ion species.	96
4.2.12	Modeled structures for *meta*- and *para*-halide substituted benzoic acid complexes performed by Hartree-Fock *ab initio* calculations at the 3-21G level of basis.	97
4.2.13	Hartree-Fock *ab initio* geometry optimized simulation for t-butyl benzoic acid at the 6-31G(d) level of basis.	98
4.2.14	Hartree-Fock *ab initio* geometry optimized structures for *ortho*-, *meta*-, and *para*-amino benzoic acid $[M-H]^-$ pseudo-molecular ion forms at the 6-31G(d) level of basis.	99
4.2.15	Electrospray ion response of the deprotonated molecular ion and the sodium-bridged dimer ion pair for *ortho*-, *meta*-, and *para*-substituted amino benzoic acid analytes.	100
4.3.1	Effect of percent organic in solution on the intensity of the deprotonated molecular ion and the sodium-bridged dimer ion for benzoic acid.	102
4.3.2	Effect of: a) pKa; and b) log P on the ionization response for benzoic acid and halide-substituted benzoic acids.	103
4.3.3	Placement of charge density about the atoms in meta-fluoro benzoic acid according to *ab initio* calculations performed by Gaussian98 with the 6-31G(d) basis set.	109
5.2.1	Flow injection profiles for the total ion chromatogram of 0.5 mM para-amino benzoic acid at five injection volumes in the negative ionization mode.	114
5.2.2	Average intensity and percent RSD of $[M-H]^-$ and $[2M-2H+Na]^-$ pseudo-molecular ion response as a function of injection volume.	116
5.2.3	FIA-ESIMS profile for: a) negative; and b) positive ionization modes analysis of 0.5 mM PABA in the presence of 50/50 acetonitrile/water (pH ~ 6) with a 200 μL injection.	119

5.2.4	Pseudo-molecular ion response for PABA in 50/50 acetonitrile/water at five injection volumes and five concentrations.	121
5.2.5	Parts A – D represent the pseudo-molecular ion response for PABA at 0.1, 0.5, 1.0, and 2.0 mM, respectively.	122
5.2.6	Pseudo-molecular ion response of PABA in the presence of common LC-MS modifiers.	126
6.1.1	Aggregate pseudo-molecular ion formation by carprofen in the presence of 2.5 mM LiOAc.	129
6.1.2	Pseudo-molecular ion formation by flurbiprofen in the presence of 2.5 mM LiOAc.	130
6.1.3	Aggregation of alkali metal salts as a function of ionic radius of the cation.	131
6.1.4	Effect of added LiOAc on the response of $[M-H]^-$ for six ibuprofen derivatives.	132
6.1.5	Relative intensity of sodium and lithium adducts with carprofen and ketoprofen as a function of added LiOAc.	133
6.1.6	Hartree-Fock *ab initio* simulations of alkali metal-bridged dimer ions for benzoic acid a the 3-21G level of basis.	134
6.2.1	Structures of alkyl benzoate molecules.	135
6.2.2	Gradient elution of four alkyl (C1 – C4) parabens detected by: a) UV at 254nm; and b) negative ionization mode ESIMS.	137
6.2.3	Ionization response as a function of calculated log P values for the separation of four alkyl paraben analytes.	137
6.2.4	Hartree-Fock *ab initio* geometry optimized simulations of alkyl paraben deprotonated molecular ions at the 3-21G level of basis.	138
6.3.1	ESI mass spectrum of PABA in the positive ionization mode in the presence of 50/50 acetonitrile/water with 5 mM $HClO_4$ (pH ~ 2.0).	140
6.4.1	Hartree-Fock *ab initio* geometry optimization calculations for $[2M-2H+Na]^-$ of benzoic acid with three different basis sets: a) 3-21G; b) 6-31G(d); and c) 6-31+G(d).	142

TABLE OF TABLES

Table	Detail	Page
1.4.1	Interaction names and potentials for specific non-covalent interaction types.	16
1.5.1	Properties of Group 1 alkali metals.	26
1.5.2	Suitable and non-suitable solvents for use with ESIMS.	29
2.1.1	General operational settings for LCMS in the negative (and positive) ion mode.	47
2.4.1	Solution pH modifications made according to the Handbook of Chemistry and Physics.	56
2.4.2	pKa and measured pH values for modifiers and solutions commonly used in LC-MS and tested in experiment 3.	56
3.1.1	Common LC and LC-MS additives used in experiment 1.	58
3.2.1	Most intense base ion observed for the six anti-inflammatory pharmaceuticals.	59
3.2.2	Calculated pKa and log P values for the six ibuprofen derivative test analytes	60
3.3.1	Observation of specific pseudo-molecular ion species for ibuprofen derivatives during negative ionization mode FIA-ESIMS.	74
4.2.1	Solution phase data for benzoic acid and substituted benzoic acid model compounds.	91
4.3.1	Gas-phase basicities and proton affinities for selected analytes.	105
4.3.2	Deprotonated carboxylic acid charge density as a function of halide substitution calculated by the Hartree-Fock *ab initio* method at the 6-31G(d) level of basis.	108
5.2.1	Scan-by-scan reproducibility for FIA-ESIMS as a function of injection volume and number of scans averaged to obtain a mass spectrum.	117
5.2.2	Ionization response for PABA in the presence of bulky pH modifiers.	125
6.1.1	Ionic radii for alkali metal cations investigated in this experiment.	131
6.2.1	Calculated log P values for alkyl benzoate molecules.	136
6.4.1	Calculated values for distance and charge density according to results of Hartree-Fock *ab initio* calculations with three basis sets.	142

To My Mother:

Oh, how I wish you could see me now,

Though I know you really do!

CHAPTER 1

1.1 Introduction

Electrospray Ionization Mass Spectrometry (ESIMS) has been at the forefront of analytical science since the early 1990s. It has provided an efficient means of ionizing species in solution for mass analysis as well as a complementary detection technique for high performance liquid chromatography (LC). The ability of ESIMS to detect ions in diverse chemical settings, such as pharmaceutical, biological, environmental, and food science, to name a few, has allowed the technique to flourish rapidly. As evidence of its rapid expansion, ESIMS has been the subject of thousands of publications in recent years. Most publications report applications and methods for specific analytes and media. However, since the detailed mechanics behind the electrospray process are still widely debated, extensive investigation of the ionization process itself is a popular topic as well.[1]

Efficient ionization of polar and ionic, volatile and nonvolatile, and high and low molecular weight species in solution makes electrospray ionization (ESI) a suitable interface for combining liquid separation modes, such as liquid chromatography (LC) and capillary electrophoresis (CE), to mass spectrometer detectors.[2] Interfacing these systems allows for quantitative and qualitative analyses of simple and complex samples. Analysis of biological matrices by ESIMS is especially attractive due to its unique ability to detect high molecular weight molecules, such as proteins, peptides, and biopolymers, through the phenomenon of multiple charging.[2]

Another well-known aspect of ESI is that it is a ‘soft’ ionization technique.[3] This means that relatively small amounts of energy are imparted to molecules being

ionized and detected by ESIMS. During the process, the molecules are subject to a phase change from liquid to gas. As a result, solution-phase and gas-phase behavior and the chemical nature of an analyte influence the final ion form. Investigations of gas-phase molecular recognition (and chiral recognition) processes have been pursued as an avenue for exploiting associative behavior of molecules through the transition from solution phase to gas phase by ESI.[4] However, in many cases, detected ions that are composed of complexes formed by multiple species present during ESI, often called adduct or pseudo-molecular ions, can hamper quantitative and qualitative determinations. Often it is difficult to know which ions in a complex mixture originate from the analyte of interest. Many publications in the literature address pseudo-molecular ion formation in ESI, focusing mainly on association of species (particularly metal ion salts) to analytes in positive ionization mode. Several reviews detail the work performed on this subject.[3-8]

Efficiency of ion formation by ESI partly depends on a molecule's ability to associate and carry a charge. As a consequence, some analytes, such as amines and ethers, prefer positive ion formation while others, such as acids, phenols, and nitro-compounds, more easily ionize in the negative ionization mode.[9] Also, guidelines governing the formation of pseudo-molecular ions, especially in negative ionization mode, are not firmly established, since the pseudo-molecular ion makeup differs considerably depending on ionization mode and solution conditions.

The present work focuses on pseudo-molecular ion formation in negative ionization mode. The main groups of molecules studied are aromatic acids, which easily dissociate to form deprotonated molecular ions in most cases, but also form complexes with added salts and background ions that are detected as major pseudo-molecular

ions.[10] The goal of this thesis is centered on elucidating structure and interaction types of aromatic acid pseudo-molecular ions through the study of logical model compound sets with varying instrumental parameters. Flow injection analysis as a method for ESIMS sample introduction is investigated in detail with respect to injection volume and concentration of the analytes. The third facet of this thesis is the investigation of method transfer from LC to LC-MS, especially pertaining to pH, concentration and specific additive type and its effect on intensity and ionization of targeted and resultant pseudo-molecular ions. Theoretical *ab initio* calculations and geometry optimizations are used to determine the structures of pseudo-molecular ions of interest.

This work establishes guidelines governing formation of pseudo-molecular ions of acid molecules in negative ionization mode. The results can be directly applied to work in pharmaceutical and biological fields where molecules of acidic functionality, such as anti-inflammatory agents and amino acids, are encountered regularly. Secondly, a reliable method for performing such analyses, flow injection analysis (FIA) with large volume injections, is proposed as a better way to study complex formation in ESIMS compared to traditional LC methodologies. Solution composition and functional complexity of substitutions on aromatic acids are shown to be major factors contributing to the efficient ionization and formation of specific pseudo-molecular ions. As an underlying goal, the results are interpreted, compared and assimilated to provide new insight into the mechanics governing the ESIMS process.

1.2 Theory and Mechanism of LC-ESIMS

Electrospray ionization is a process by which polar and ionic species in solution can be converted efficiently into gas-phase ions. A large host of factors, instrumental and system-related, control the process. Despite debate over the specifics of theoretically describing the ESIMS theory, experimentally determined dependencies are not focused on one single dominating factor, but on a whole host of variables. The variables encompass the solution and gas phase and the transition between them. ESI is strongly dependant on solution chemistry (pK, diffusivity, and surface activity), electrophoretic migration, ion affinity, and molecular structure of the analyte, as well as the instrumental conditions used, such as solution composition (pH, type of additives, and organic/aqueous percentages), interface parameters (voltage, bath gas, and dimensions), and mass spectral sampling parameters (temperature, voltage, and type of orifice).[11]

Adding to the complexity of elucidating effects of individual parameters, the mechanism controlling the process is widely debated.[1] Two main mechanistic theories have been proposed and subsequently critiqued and modified since their conception. They are the Ion Evaporation Model (IEM), proposed by Iribarne and Thomson in the late 1970s[12,13] and the Charge Residue Model (CRM), coined by Dole in the 1960s.[14] The main difference between these models is the point where desorption of ions occurs from highly charged droplets. The debate over the mechanism of ionization has been the subject of many research and review articles to date.[1,2,15-30]

The IEM is based on the assumption of a late transition state for evaporation of ions from charged droplets. A late transition state means that during the formation of gas-phase ions, a transition state exists where the form of the species undergoing

transformation to the gas-phase more closely resembles the final state of the ions, or product ions, formed rather than reactant molecules present in solution. Evaporation of ions is possible because the analytes associate into a cluster (containing neighboring solvent and ionic species). In the presence of a high electric field and a droplet with decreasing volume, cluster formation and local droplet surface deformations lower the free energy of evaporation for species from solution to the gas phase.[12] The interaction energy between the analyte of interest and a nearby charge depends on the strength of the partial charges, the distance between partial charges, and the dielectric of the surrounding medium. This approach labels solvation free energy of a molecule as the dominant factor controlling ionization. In other words, as the solvation energy of a molecule decreases, the observed ion intensity increases. Plots of the natural logarithm of intensities versus standard hydration free energies of analytes show a negative linear relationship and thus a strong correlation between the solvation free energy of a molecule and ionization efficiency.[31] Equation 1, derived from absolute reaction rate theory, describes the dependence of the ion evaporation rate constant on transition state free energy ($\Delta G^{\ddagger}$) by:

$$k_I = (kT/h)e^{-\Delta G^{\ddagger}/RT}; \qquad \text{(eq. 1)}$$

where k_I is a reaction rate constant for a given species, k is Boltzmann's constant, T is temperature, h is Planck's constant, and R is the universal gas constant.

The CRM says that, rather than evaporating from charged droplets, the ions formed are a result of electrohydrodynamic disintegration of the droplets due to Rayleigh instability. Rayleigh instability occurs when the coulombic repulsion at the surface of a droplet overcomes the cohesive energy holding the droplet together. Mathematically, the Rayleigh stability condition is:[32]

$$E_R = 6.6 \times 10^{-4} (\gamma / R)^{1/2}, \qquad \text{(eq. 2)}$$

where γ is the surface tension of the liquid phase (N m^{-1}), R is the droplet radius, and E_R is coulombic repulsion energy . When this condition is reached, the result is uneven fission of the droplet into smaller droplets. Successive disintegrations ultimately result in a charged residue where the analyte of interest is present in the gas-phase as an ion that can be sampled into the mass spectrometer for mass to charge (m/z) analysis.

Other possible mechanistic schemes have also been proposed.[29,32,33] Generally, proposed changes to the established models have been minor and based on combination of aspects of both the IEM and CRM models. The changes are made based on inconsistencies uncovered by experiments specifically designed to probe different aspects of the spray process. As a consequence, changes to the theory are not all-encompassing, and serve only to slightly modify the proposed theories. In general, many researchers have agreed that the IEM is more applicable to ionization of small molecules, whereas large molecules are believed to ionize closer to the mechanics explained by the CRM.[14]

For obvious reasons, the analyte of interest is the main concern in method development for a particular ESIMS procedure. Neither of the two popular ESI mechanisms predicts how the desolvation dynamics will affect the measurement of equilibrium distributions of complexes in solution.[34] This has been a constant concern for researchers interested in correlating gas-phase ions to solution phase behavior, particularly if a quantitative comparison between equilibrium solution compositions and host-guest complex ion intensities is desired.[34] In these studies, correlations are very

analyte dependant. General effects can be summarized by addressing the analyte's behavior in solution phase, gas phase, and the transition between the two phases.

The solution phase composition has been deemed the most dominant factor controlling ionization in ESIMS. Basic interactions caused by inductive effects, steric interactions, acid-base chemistry, and dielectric of the medium strongly influence the state of an analyte in solution, and in the case of ESI, its ability to associate a charge and release into the gas phase. In addition, the mobile phase used affects spray performance and hence, gas-phase ion production.[35] For a typical solution phase made up of aqueous and organic parts, the aqueous solution serves to provide conductance when a high voltage is imparted, whereas the organic component serves to lower the surface tension of the solution and increase its vapor pressure. A lower surface tension allows for the formation of smaller droplets at the spray tip and consequently higher ionization efficiency. Solution compositions with higher vapor pressure allow the solvent to evaporate quickly, leaving behind the desired ion product.

The formation of highly charged droplets from charge repulsion caused by an electric field is the heart of the ESI process. At the onset of electrospray, a cone of droplets (often referred to as a Taylor cone[36]) is emitted from the spray capillary. In the few microseconds it takes for an analyte to undergo phase transition from solution to the gas-phase, a number of important parameters come into play. Interface parameters, such as solution flow rate, probe voltage, capillary diameter, and bath gas flow rate; analyte characteristics such as surface activity, concentration, free energy barrier to evaporation, and vapor pressure; and solution phase parameters such as pH, organic/aqueous composition, dielectric, vapor pressure and additive type and amount all

influence the conversion of an analyte from the solution phase into a gas-phase ion. As a droplet evaporates the local environment of the solution inside the droplet changes drastically. All species present are effectively concentrated in the droplet and approach close proximity with each other.

Once in the gas phase, parameters such as gas-phase basicity and proton affinity of the mobile phase components can also have a marked effect on ion formation. Proton affinity (PA) and gas-phase basicity (GB) are defined by standard thermodynamics of the simple protonation reaction:

$$M + H^+ \rightarrow MH^+, \qquad \text{(eq. 3)}$$

where M denotes the analyte of interest. The enthalpy of this reaction (ΔH_{rxn}) is equal to –PA and the Gibbs free energy of reaction (ΔG_{rxn}) is equal to –GB.[37] Thus, a solvent or additive with a higher proton affinity in the gas-phase than an analyte can limit the formation of a positive molecular ion by stripping away potential protonating hydrogens from the analyte. Conversely, mobile phase species present with a high PA can aid in formation of a negative molecular ion when a hydrogen ion is available for abstraction.

Figure 1.2.1 depicts an interface spray chamber for ESIMS. Flow and sample introduction are provided by the HPLC system, either as separated sample bands or simply as a flow injection solution system band. The capillary, made from fused silica is jacketed by a stainless steel capillary, onto which is imparted a high voltage. The consequence is the formation of an electric field. Equation 4 allows calculation of the electric field present at the tip of a capillary electrode assuming a planar counter electrode:[38]

$$E_c = \frac{V_c}{r_c \ln(4d / r_c)}. \qquad \text{(eq. 4)}$$

Here, V_c is the voltage difference between the capillary and the counter-electrode, r_c is the radius of the spray capillary, and d is the distance between the spray capillary and the counter electrode. Equation 5 describes the conditions necessary for the onset of electrospray:[29]

$$E_0 = \left(\frac{2\gamma \cos 49^\circ}{\varepsilon_0 r_c} \right)^{1/2}, \qquad \text{(eq. 5)}$$

where 49° is the half-angle of the Taylor cone and ε_0 is the permittivity of vacuum.
In both cases, the values are shown to be highly dependent on the capillary radius. The size of the capillary affects the size of the droplet formed (smaller capillaries induce the formation of smaller droplets). A bath gas is present, in most cases high-purity nitrogen, which flows concentrically on-axis with the solution from the capillary. The bath gas pneumatically assists the evaporation of solvent from electrosprayed droplets. The major solution phase parameter contributing to the onset of electrospray is viscosity of the liquid phase.

The spray is emitted into the atmospheric pressure region (generally equilibrated at slightly less than atmospheric pressure due to the presence of the vacuum provided by the MS inlet). Sampling of the emitted gas-phase ions in this instrumental configuration is through a curved desolvation line (CDL). The CDL is a curved stainless steel tube (150 μm diameter) which is heated and thermostatted by a heated block. The CDL serves as the planar electrode. A small voltage of approximately tens of volts is applied to pull ions in the spray chamber region toward the orifice. The CDL is designed in such a shape as to provide maximum declustering of ions as they are sampled by the MS.[39]

Further details of this experimental set-up, including standard operating conditions, are given in Chapter 2.

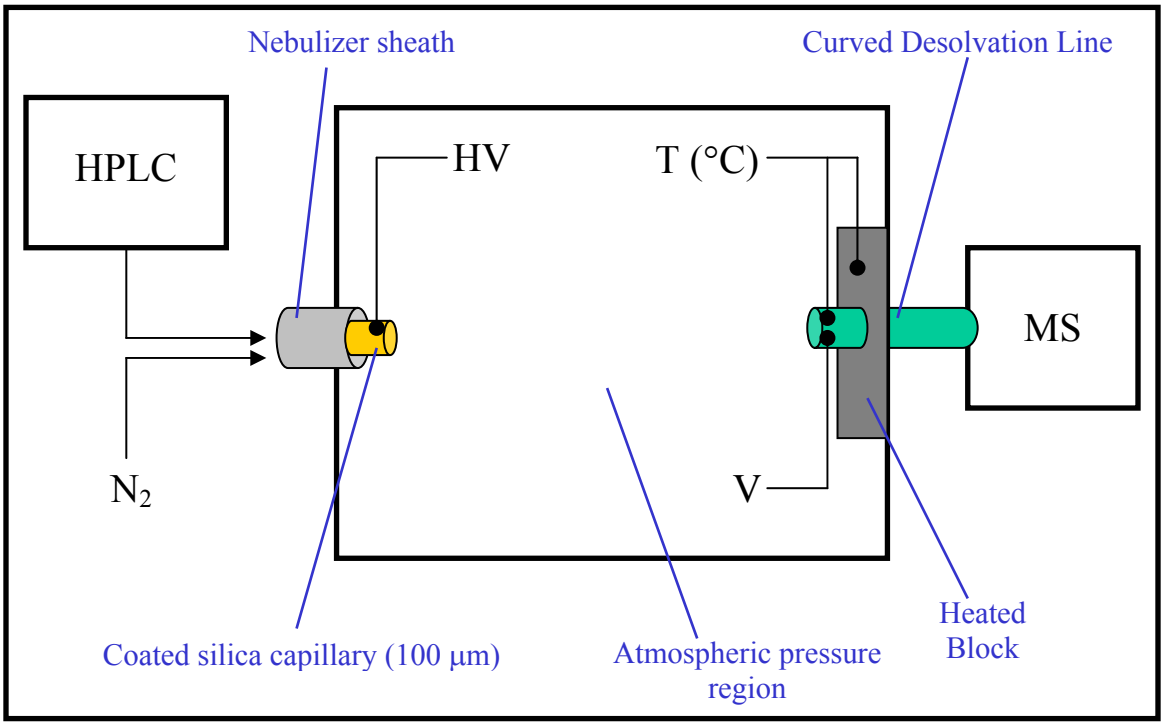

Figure 1.2.1 Interface setup for ESIMS, based on the Shimadzu LCMS-2010 (Shimadzu Scientific Instruments, Columbia, MD, USA).

1.3 History of LC-ESIMS

Prior to the use of ESIMS as a detector for liquid separations, electrospray had been used extensively in the fields of pollution research, crop spraying, electrostatic printing, spray painting, propulsion of space vehicles, and emulsification.[34] The process of spraying electrified droplets has a long history dating back to the middle of the 18th century with the work of Bose.[40] Later, in 1882, Lord Rayleigh published his theoretical calculations that established the condition known today as Rayleigh instability.[41,42] The investigation of the electrospray process was not published in the scientific literature again until Zelany studied the formation of a mist of fine droplets in 1917.[43] This work is credited as the first systematic study of the generation of a charged aerosol beam at atmospheric pressure where the shape of the emitted droplet spray was studied as a function of voltage. Work on the investigation of mobility of ions created from spraying and bubbling of aqueous solutions was investigated by Chapman in 1937 and 1938 through the use of an Erikson mobility tube.[44-46] Solutions of different compositions, containing species such as sugars, salts, acids, and bases, were investigated for the release of ions by the application of a applied current. Through this work, Chapman assessed the effect of capillary size on the size and charge of the droplets formed from the nebulization processes.

In the mid-1950s, a renewed interest in the electrospray process was shown as Vonnegut and Neubauer studied the production of monodisperse liquid droplets by electrical atomization by placing a high voltage on a reservoir of water attached to a capillary.[47,48] In a follow-up article, they studied the behavior of the spray with varying solution conductance and applied voltage. Shortly after this work, Drozin

showed the importance of the dielectric of the medium and the radius of curvature of a liquid in a capillary to the dispersion process.[49] He showed that nonpolar liquids, having small dielectric constants could not be dispersed by the application of a high voltage.

In the late 1960s and early 1970s, Dole and co-workers published the first studies using electrospray for the generation of gas-phase ions.[14,50-53] These works involved the investigation of ion mobility of large polymer molecules. Herein were established the guidelines outlining the charged residue mechanism where droplets were hypothesized to dry to the form of a charged residue containing one analyte of interest and an associated charge. Dole's work prompted the investigations of the ionization process by Iribarne and Thomson in the late 1970s.[12,13,54] Contrary to the CRM proposed by Dole, Iribarne and Thomson laid the groundwork for their own theory of ion evaporation, where an ion is ejected into the gas-phase once the free energy barrier for evaporation is surmounted in the presence of a high electric field. All of the mechanistic studies published since these banner works have addressed one or both of these models. Individually, neither the CRM nor the IEM are considered all-encompassing for the analysis of the wide array of molecule types studied today by ESIMS.

In 1980, Vestal and co-workers were the first to use charged droplets as an ion source.[55-57] However, these studies were performed by a technique now termed thermospray, which is overall significantly different than the traditional electrospray process. In 1984, Yamashita and Fenn at Yale University and Aleksandrov and co-workers in the former Soviet Union combined electrospray ionization with conventional mass analyzers.[58-60] In these works by the Aleksandrov and Fenn groups, ESI was

realized as an efficient on-line interface for combining liquid separations, such as capillary electrophoresis and liquid chromatography, to mass spectrometry detectors.

Pneumatic assisted electrospray, where a nitrogen sheath gas is added to the spray process to aid evaporation, was introduced in 1987.[15] The addition of a bath gas flowing concentrically on-axis with the spray allows for the use of higher liquid flow rates, since a greater amount of solvent can be removed from the droplets in a shorter period of time. Following this development in the late 1980s and in the early 1990s, commercial instrumentation for on-line LC-ESIMS was introduced.[61,62] At this same time, the benefit of using ESIMS for the analysis of large biopolymers was presented by Fenn and co-workers.[63] Molecules with molecular weights up to 40,000 Da were shown to associate up to 45 positive charges, allowing conventional mass analyzers, such as quadrupole instruments, to be used for high molecular weight determinations.

The middle to late 1990s saw improvements in ESIMS instrumentation with modifications such as the orthogonal spray interface.[64,65] In this configuration, the spray capillary is placed perpendicular to the mass spectrometer inlet, further increasing the range of operational flow rates and allowing for more sensitive detection due to decreased noise. A high sensitivity technique, coined nanospray, was also introduced.[66] Nanospray utilizes small bore capillaries and is advantageous for ultra-trace analysis without the need for pneumatic assistance or large sample sizes. Extremely low flow rates are achieved without the use of pumping systems due to flow from capillary action once a high voltage is applied to the capillary tip.

Today, publications involving the use of electrospray ionization cover a wide array of fields of research and are too numerous to completely recount. In five years, the

number of research articles associated with electrospray has doubled from 250 per year in 1995 to over 500 per year in 2001. Figure 1.3.1 shows the number of publications associated with electrospray in the past seven years according to a popular internet search engine.[67] The search for an all-encompassing ionization technique for the analysis of a wider array of molecule types will encourage further development of the electrospray process.

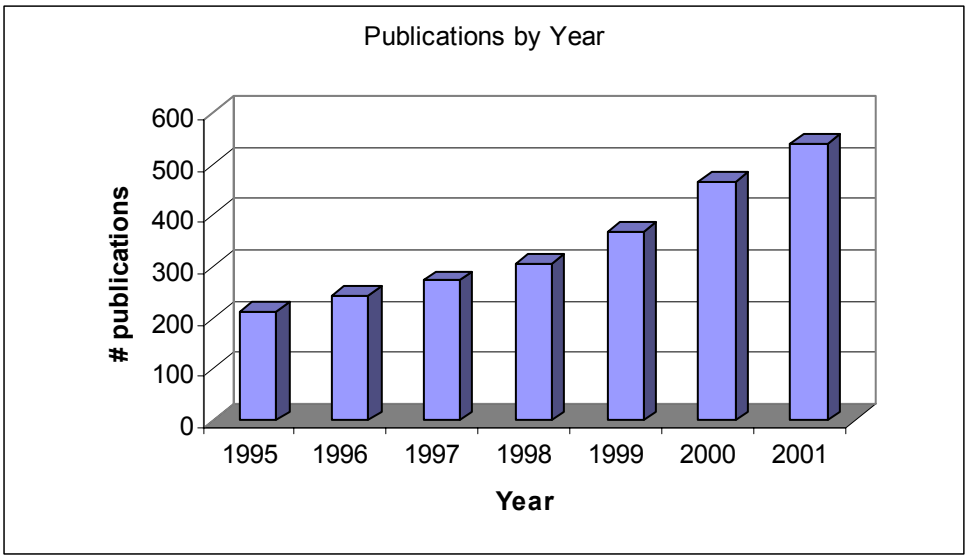

Figure 1.3.1 Publications involving the use of electrospray per year according to a popular search engine (www.ingenta.com).

1.4 Noncovalent Interactions

Since the introduction of the electrospray process, results have been encountered where the traditional molecular ion of interest is not always the observed ion form. Instead, pseudo-molecular ions, or noncovalent complex ions, are commonly encountered. These are formed by either association between species present in the solution system that are preserved due to the soft ionization of the electrospray process or to the presence of gas-phase collisions in the spray chamber prior to sampling by the mass spectrometer. More often than not, the formation of adduct ions hamper qualitative and quantitative results, especially when unexpected. However, these associative processes have also created interest in the study of formation of solution and gas-phase complexes which benefit from the ability of ESIMS to provide accurate mass analysis and stoichiometric measurements for complex formation in a variety of molecular systems.

Non-covalent interactions are interactions between two species that do not involve covalent bonds. Associations of this nature cover a variable range of energies and depend explicitly on the structure and functionality of the species involved in the formed complex as well as the local environment of the complex. Table 1.4.1 lists the interaction potentials for the major contributions to non-covalent interactions.[3] The equations listed for interaction types represent the free energy associated between two species. All of the interactions are attractive in nature, except for coulomb-coulomb and dipole-dipole which may be attractive or repulsive, depending on the signs of the charges or the relative angular orientation of the dipoles, respectively. Permanent and induced dipoles accommodate the forces acting upon them and do so to cause an attractive interaction.

Table 1.4.1 Interaction names and potentials for specific non-covalent interactions.

Interaction Type	**Formula**
Charge-charge (Coulomb energy)	$\frac{Q_1 Q_2}{4\pi\varepsilon\varepsilon_0 r}$
Charge-dipole (fixed dipole)	$-\frac{Qu\cos\theta}{4\pi\varepsilon\varepsilon_0 r^2}$
Charge-dipole (freely rotating dipole)	$-\frac{Q^2u^2}{6(4\pi\varepsilon\varepsilon_0)^2 kTr^4}$
Dipole-dipole (fixed dipole)	$-\frac{u_1 u_2}{4\pi\varepsilon\varepsilon_0 r^3}(2\cos\theta_1\cos\theta_2 - \sin\theta_1\cos\phi\sin\theta_2)$
Dipole-dipole (freely rotating dipole) (Keesom energy)	$-\frac{u_1^2 u_2^2}{3(4\pi\varepsilon\varepsilon_0)kTr^6}$
Charge-nonpolar	$-\frac{Q^2\alpha}{2(4\pi\varepsilon\varepsilon_0)^2 r^4}$
Dipole-nonpolar (fixed dipole)	$-\frac{u^2\alpha(1+3\cos^2\theta)}{2(4\pi\varepsilon\varepsilon_0)^2 r^6}$
Dipole-nonpolar (freely rotating dipole) (Debye energy)	$-\frac{u^2\alpha}{(4\pi\varepsilon\varepsilon_0)^2 r^6}$
Nonpolar-nonpolar (London Dispersion energy)	$-\frac{3}{2}\frac{\alpha_{01}\alpha_{02}}{(4\pi\varepsilon\varepsilon_0)^2 r^6}\frac{I_1 I_2}{I_1+I_2}$
Hydrogen bond	Special, directed interaction
Hydrophilic	Special
Hydrophobic	Special

Q = charge, r = distance, α = polarizability, ε = dielectric constant, I = first ionization potential, θ = angle between dipole and vector connecting the interacting particles, φ = polar angle of second dipole relative to the first.

Particles with no charge or dipole associated with them can attract each other due to London dispersion forces invoked by the polarizability of the particle. All of the forces are distant dependent as noted by the presence of the $1/r^n$ term. Also notable is the presence of the dielectric constant of the medium in the denominator of each equation. The presence of the $1/\varepsilon$ term implies that a solvent with a high dielectric constant, such as water, will reduce interaction energies. This term also represents the major difference between forces present in solution- versus gas-phase, where the dielectric of the solvent is not present. Energies of interactions based on charges, dipoles, or polarizability are expected to increase as the effect of solution is removed. An exception to this is hydrophobic interactions between two nonpolar particles, where the absence of water decreases the attraction between the particles.

Hydrophobic, hydrophilic, and hydrogen bonding interactions are not easily described. Hydrogen bonding interactions are primarily electrostatic and directional in nature, meaning the alignment of potential hydrogen bonding groups greatly affect the degree of interaction. Hydrophobic and hydrogen bonding forces are extremely important in the structural arrangement of many molecules, and are particularly relevant to large biomolecules and the formation of many non-covalent complexes.

Several methods are used routinely in the literature to determine degree of binding between species. These methods are composed of techniques used to study solution phase interactions as well as gas-phase processes. Common methods used to probe solution reactions are melting curve analysis, titration, and competition techniques. Gas-phase techniques include in-source collision induced dissociation (CID), CID with tandem MS, heated capillary dissociation (at the MS inlet), guided ion beam MS, high

pressure MS (HPMS), equilibrium measurements, photodissociation, and kinetic methods.[3]

For the measurement of solution phase parameters by MS, it is necessary to ensure that solution phase parameters and not gas-phase properties are being measured and are reflected in the mass spectra. For this to be the case, the ionization process should not cause a shift in the solution equilibrium that is being measured. For many analyte types, this is not the case with ESI analysis, and should be investigated on an individual basis for each experiment. A notable study performed by Wang and Agnes showed that solution phase equilibria deviated very little during ESIMS of a strontium/EDTA complex.[68] The reaction

$$Sr^{2+} + EDTA^{4-} \xleftrightarrow{k_1, k_{-1}} [Sr \cdots EDTA]^{2-} \qquad \text{(eq. 6)}$$

is interesting due to the very slow rate constant associated with the reverse reaction (k_{-1} = 1 s^{-1}). Relative to the approximate time period of the ESI process (~ 10^{-2} s), the reverse reaction is very slow. It may be expected that the dynamics of the reaction during the change in solution environment may proceed to formation of more products during the ESI process, however very little deviation from equilibrium was observed in the ESI process, indicating that ESI is a viable technique for measuring solution phase equilibrium in this system.

A technique used commonly in oligonucleotide analyses is the construction of a melting curve. Here, the fraction of intact complex, α, is measured as a function of solution temperature. The slope of the α-T plot gives the transition enthalpy for complex dissociation or conformational change of interest by[69]

$$\Delta H = (2+2n)RT_m^2\left(\frac{\partial \alpha}{\partial T}\right)_{T=T_m}, \qquad \text{(eq. 7)}$$

where n is the molecularity of the association reaction (e.g. n = 2 for a dimer), and T_m is the melting temperature for α = 50%. Such measurements can be done optically by ultra-violet, fluorescence, or circular dichroism spectroscopy, or by MS methods, by heating the solution or spray capillary prior to ionization. Smith and coworkers published a paper comparing the dissociation of a dimer complex between synthetically prepared DNA analogs and naturally occurring DNA.[70]

Specific associative experiments designed to probe selectivity and molecular recognition are commonly set-up with host(s) and guest(s) present in a MS titration study. To titrate, analyses can be performed where the host is held at a constant concentration and the concentration of the guest is varied over a wide concentration range. Analogous to this, the set-up can also be reversed, varying the host concentration and holding the guest constant. A critical assumption is made that the ionization process does not affect the equilibrium between solution associations. Data are analyzed by comparing the intensity of the complex species (HG, for a host – guest complex) to that of the free host or guest (H or G, respectively) in the form of a Scatchard plot, which has the form:

$$\frac{[HG]}{[G_F][H]_0} = \frac{-1}{K_D}\frac{[HG]}{[H]_0} + \frac{n}{K_D}. \qquad \text{(eq. 8)}$$

Here, $[H]_0$ is the total host concentration, n is the number of guests per host molecule, K_D is the dissociation constant, and [HG] and $[G_F]$ are the intensities of the complex ion and the free guest, respectively. Figure 1.4.1 shows the general layout of a Scatchard plot, where the slope is used to obtain the dissociation constant.

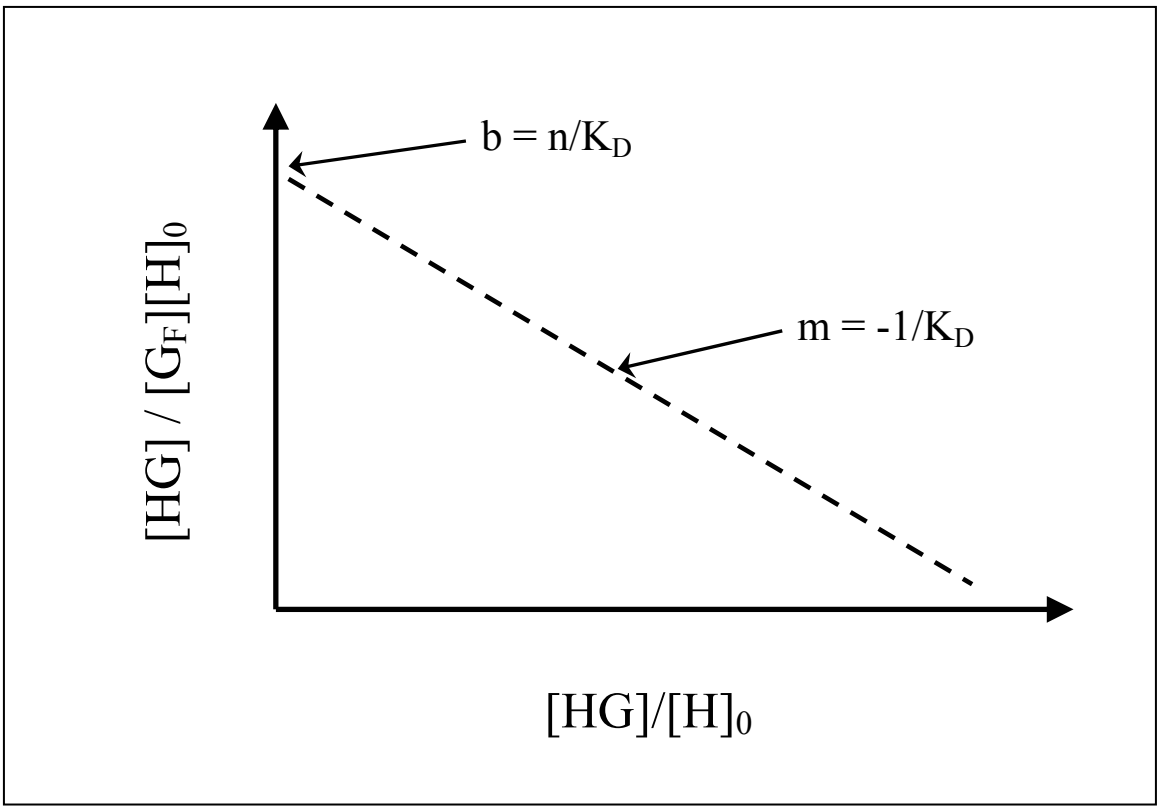

Figure 1.4.1 Generalized Scatchard plot used for the determination of dissociation constant for host – guest complexes.

Sannes-Lowery and coworkers reported use of the titration method for determination of binding between RNA and aminoglycosides.[71] Two types of experiments were carried out. One experiment held the concentration of RNA (host) constant and varied that of the aminoglycoside (guest). The second held the concentration of the guest constant and varied that of the host. Surprisingly, different results were obtained for K_D. Results determined from the first experiment where the host is held constant are believed to be more accurate, however this case indicates that caution must be practiced when performing experiments in this manner.

An important implication of studying solution-phase complex formation has been stated and should be addressed. That implication is that the ionization process and mass

analysis system do not affect the relationship between species in solution and the observed mass spectra. In most systems, this is not the case. However, the relationship depends explicitly on the relative vaporization and ionization efficiencies of all species present. The definition and determination of transfer coefficients is an important consideration when addressing the effect of the ionization processes on the pseudo-molecular ion observed. For molecule X, we define a transfer coefficient t_X, which accounts for all instrumental and chemical effects X undergoes during the ionization and mass analysis process. In other words, t_X accounts for transfer of X from solution phase to formation of a gas-phase ion, as well as sampling and measurement of response of X by the specific instrument configuration employed.

The dependence of the ionization efficiency on species type is largely a result of solvation energy. A study by Leize and coworkers showed that for equimolar mixtures of LiCl, NaCl, KCl, RbCl, and CsCl, Cs^+ shows the greatest ionization efficiency relative to the other cations in positive ionization mode ESIMS.[72] In fact, the response factor for Cs+ ($k_{M,Cs+}$, defined below in equation 9) was found to be fifty times greater than that for Li^+. The response factor varied experimentally with the solvation energy, E_M and a constant C which contains variations due to ion charge, ion concentration, and instrumental parameters by:

$$k_M = C\exp(-0.015E_M). \qquad \text{(eq. 9)}$$

This work demonstrated the necessity for considering those factors controlling relative ionization efficiency between different species. Most of the time, however, only instrumental transfer parameters are considered and a general transfer coefficient is used and assumed to be equal for all species present in the system.[3]

A different approach used to study selectivity between species is the competition method. With this technique, multiple host-guest complexes are monitored simultaneously to determine relative or absolute binding affinities or selectivity for different guests. These experiments are easily performed with multiple hosts present or multiple guests present. A good example of the use of this method for the determination of absolute binding constants for guest molecules with vancomycin and risocetin was performed by Jørgensen and coworkers.[73] The method is based on measurement of relative peak intensities of the free host and three complexes with three guests, all present in equimolar concentrations. A determination of the selectivity can be represented by:

$$[H_i] = \frac{H_i[H_i]_0}{H + HG_1 + HG_2 + HG_3}, \qquad \text{(eq. 10)}$$

where H_i represents any form of the host molecule, $[H_i]_0$ is the initial host concentration, and H, HG_1, HG_2, and HG_3 represent the peak intensities for the free host and the complexes formed with the three guests, respectively. Remembering that equimolar mixtures must be employed in this experiment, a binding constant can be determined for any of the observed complexes as:

$$K_{HG_1} = \frac{[HG_1]}{[H][G_1]} = \frac{[HG_1]}{[H]([H]+[HG_2]+[HG_3]}, \qquad \text{(eq. 11)}$$

where brackets denote molar concentration values. This system also assumes identical ionization efficiencies for all species.

Determination of binding by gas-phase methods has been performed in a variety of different ways. However, with a few exceptions, binding constants determined by solution-phase methods and gas-phase methods rarely agree. This is due to the nature of the forces involved in the formation of noncovalent complexes and the difference

between the strength of the forces in the presence and absence of solvent. Electrostatic and dipolar noncovalent interactions are strengthened in the absence of a dipolar solvent, whereas the very nature of solvophobic forces (attraction between two species due to repulsion from solvent), such as hydrophobic interactions, require the presence of solvent to exert a significant attraction. Gas-phase methods for the determination of binding constants are centered around dissociative experiments where collisions are induced by either an inert reactant gas or an applied electric field. These methods include in-source CID, CID with tandem MS instrumentation, heated capillary dissociation (at the MS inlet), HPMS,[74-79] guided ion-beam MS,[80-82] equilibrium dissociation methods,[83,84] photodissociation,[85-89] and the kinetic method of Cooks and coworkers.[90-92] Though many aspects of these techniques are beyond the scope of this work, their applicability in studying noncovalent interactions cannot be overlooked. References are provided above for further information on several of these topics.

In-source CID, the technique whereby a higher than normal voltage is placed on the MS inlet region to influence the kinetic energy of gas-phase ions in the spray chamber, has previously been called "poor man's MS/MS." An increase in voltage increases the kinetic energy acquired by ionic species, and thus, the probability for excitation when a collision occurs with other gaseous molecules. The draw-back to this technique relative to more elaborate tandem MS methods is that there is no mass filtering prior to the collision cell. All ionic species in the spray chamber are susceptible to increased collisions. This leads to fragmentation patterns that are difficult to deconvolute. A stability parameter VC_{50} can be assigned based on the cone voltage necessary to dissociate 50% of a gas-phase complex.

Tandem MS techniques are most often employed experimentally when collisional fragmentation of complex ions is desired. In the simplest configuration, a triple quadrupole MS, with three quadrupole mass filters (Q1, Q2, and Q3) arranged in a linear configuration, can be used to fragment gas-phase ions. Q1 is used to select a particular mass/charge ratio of an ion of interest (parent ion). Q2 acts as the collision cell where an inert gas is leaked in to provide for collisional dissociation of molecular or complex ions. A m/z scan in Q3 gives the daughter ion spectra for the fragmentation of the parent ion. The internal energy E_{int} acquired by ions passing through a collision cell is:[3]

$$E_{\text{int}} = \frac{m_t}{M}\phi\frac{m_p E_0}{m_t C_D}\left\{1-\exp\left(\frac{-C_D n m_t \sigma l}{m_p}\right)\right\}, \qquad \text{(eq. 12)}$$

where m_p is the mass of the analyte ion, m_t is the mass of the target, $M = m_p + m_t$, φ is the average fraction of center of mass energy transferred to internal energy of the ion in a collision, C_D is the drag coefficient, E_0 is the laboratory frame kinetic energy, n is the number gas density, σ is the collision cross-section, and l is the length of the collision cell. The laboratory frame kinetic energy is related the center of mass kinetic energy E_{COM} by:

$$E_{COM} = E_0[m_t/(m_t + m_p)]. \qquad \text{(eq. 13)}$$

Also used for studying dissociative processes is heated capillary dissociation. In solution phase measurements, the heated capillary technique referred to is the spray capillary, whereas here, the capillary that is heated is the transfer line between the spray chamber and the high vacuum MS. The transfer line can be heated to dissociate complexes. A plot of normalized intensity versus capillary line temperature yields binding energies that correlate well with tandem MS CID.

Of the other techniques used in gas-phase analysis of noncovalent species, Cook's Kinetic Method and work with specially designed reactors such as guided ion-beam MS and HPMS are of interest. The use of the Kinetic method to perform chiral selectivity experiments in the gas-phase with MS detection is very valuable, especially in the biochemical and pharmaceutical realms. Here, the methodology employed and the linear relationship between the logarithm of the fragment ion abundance ratio and the optical purity allows for determination of enantiomeric excess. Studies performed using specially designed reaction chambers are of interest because of the experiments performed on alkali metal complexation. These techniques will be addressed with respect to work done with alkali binding in the next section.

1.5 Pseudo-Molecular Ion Formation and Alkali Metals

The elements in Group 1 of the periodic table are the alkali metals. These metals are characterized with the lowest ionization potential of all the elements and easily form singly-charged cations to achieve noble gas configuration. Alkali metals are highly reactive and are excellent reducing agents. Due to their highly acidic character, the cations readily form complexes with a variety of Lewis bases (hence, "alkali"). Table 1.5.1 lists some properties of the group 1 elements.[93]

In ESIMS, formation of complexes of analytes with alkali metal ions is generally observed due to background Na^+ or K^+, present in almost all research grade solvents and analytical glassware. It is nearly impossible to remove all salt impurities from the system prior to analyses and as a consequence, adduction by analytes to these species can occur. Estimations suggest that the average concentration of background electrolytes in a normal solution system is approximately 10^{-5} M.[94]

Table 1.5.1 Some properties of Group 1 alkali metals.

Elements	Ionization Energy (kJ mol-1)	Electron Affinity (kJ mol-1)	Electronegativity (Pauling)
Li	520	60	0.98
Na	496	53	0.93
K	419	48	0.82
Rb	403	47	0.82
Cs	376	46	0.79

Many references in the literature address the binding of alkali metals to analytes by ESIMS. These studies provide a good basis for the mechanism of these cations binding to a wide variety of analyte structures. Also important to the understanding of

complex formation with alkali metal cations are studies performed in the gas-phase with techniques such as high pressure MS (HPMS) and guided ion-beam MS (GIBMS). The following is a review of some of these experiments and serves to elaborate on the behavior of alkali metal cation binding to analytes during ESIMS, resulting in the formation of pseudo-molecular ions.

Some of the earliest work in the field of ESIMS was performed in the analysis of salt species. In 1984, Yamashita and Fenn published an important paper that showed the effect of probe voltage on systems containing methanol, water, and acetonitrile with additives such as LiCl, NaCl, $(CH_3)_4NI$, and HCl.[58] The pseudo-molecular ion form was monitored for a variety of system compositions and was determined to depend on composition and flow rate of solution, temperature and composition of bath gas, as well as the applied spray capillary voltage. Studies performed with high concentrations of LiCl appeared to be more amenable to the ion evaporation model (IEM) of Iribarne and Thomson,[12,13] rather than the charge residue model (CRM) of Dole and coworkers.[14] This is inferred from the fact that more singly lithiated clusters are detected. A charged residue at high concentration of salt would be expected to contain a greater number of lithium adducts do to their sheer number and proximity in a disintegrated droplet. Fenn and coworkers also pointed out that Iribarne and Thomson brought about charging by spraying, whereas in true ESI, spraying is achieved through charging.

Early in ESI development, Kebarle and coworkers began basic studies on pseudo-molecular ion formation for thirty organic nitrogen bases (B) with NH_4^+, Na^+, K^+, Cs^+, and Ca^{2+} cations.[95] Each of the metal ions was found to cluster when MeOH and H_2O

was in the system. Little adduction with nitrogen bases was observed until high concentrations of salt and analyte were employed. When the salt concentration was kept low, below 10^{-4} M, the limit of detection for the protonated molecular ion of the analyte was found to be in the sub-femtomole to attomole range. Increasing salt concentration led to an increase in population and the numbers of gas-phase collisions, which resulted in adduct formation through ion/molecule reactions. The effect of additives with a high gas-phase base showed a pronounced impact on protonated analyte ion response due to the ability of the additive to induce charge transfer reactions in the gas-phase, thus suppressing analyte ion formation and decreasing response. Such a scheme is plausible, since the residence time of a gas-phase ion in the spray chamber was estimated to be approximately two milliseconds. Also notable was the decrease of protonated analyte ion response with an increase in electrolyte concentration due to effective competition of the salt species for sites on the droplet surface. This effect was investigated in detail by Kebarle and coworkers.[16,19] The implication of decreased sensitivity with increased modifier concentration does not bode well for efficient combination of ESIMS with LC systems, where modifier concentrations are generally employed in large amounts to effect chromatographic separation.

The subject of suitable solvent use for ESIMS was addressed by Hiraoka and coworkers in 1990.[96] The effect of different solvent, needle voltage, surrounding gas and gas temperature on positive and negative ionization mode ESIMS were investigated. Table 1.5.2 shows those solvents found to be suitable for ESIMS as well as those that are not.

Table 1.5.2 Suitable and non-suitable solvents for use with ESIMS.[96]

Suitable Solvents	Non-suitable Solvents
Water	Benzene
Methanol	Toluene
Ethanol	Ligroin
n-Propyl alcohol	Carbon tetrachloride
Isopropyl alcohol	Carbon disulfide
t-Butyl alcohol	Styrene
Acetonitrile	Formamide
Acetone	Hexane
Pyridine	Cyclohexane
Tetrahydrofuran	
Aniline	
Nitromethane	
Acetic acid	
Chloroform	
Hexamethylphosphorotriamide	
N-Methylformamide	
Dimethylformamide	
Dimethyl sulfoxide	
Dichloromethane	
1,2-Dichloroethane	
Tetrachloroethane	

Clusters of solvent molecules such as H_2O and MeOH with background species were abundant in the mass spectra in the positive ionization mode. The extraction of negative ions from solution was found to be more difficult due to the lower breakdown voltage in the negative ionization mode. Often, gaseous discharges result in drastically reduced sensitivity. Addition of a gaseous scavenger, such as SF_6, or a liquid reagent, such as CCl_4, greatly reduced the appearance of discharges in negative ionization mode leading to a more stable spray at higher voltages.

The adduction of alkali metal cations with high molecular weight species in ion/ion reactions was first investigated by R.D. Smith and coworkers by use of an Y-shaped dual ESI flow reactor source.[97,98] Reactions between protein and peptide molecules such as melittin, bradykinin, cytochrome c, and myoglobin were investigated in multiple mode combinations (+/+, +/-, -/-, for each of the dual ESI probes) for

reactions between gas-phase species produced by each probe, multiple bath gas types, and, for some cases, in the presence of a gaseous discharge. Multiply charged ions were produced, and in many cases, multiple Na^+ adducts such as $[2M-7H+4Na]^{3-}$ and $[M-3H+2Na]^-$, were observed.

Other novel source designs were investigated by Hiraoka and coworkers in 1995.[64] They showed a parallel ion spray set-up to have higher sensitivity, to be more robust, to virtually eliminate contamination, and to allow higher flow rates relative to traditional source designs for the analysis of peptide chains. Studies were performed on Lys-Lys-Lys-Lys-Lys in an acetic acid modified $MeOH/H_2O$ system with variation of capillary voltage, capillary distance and flow rate. Positive ionization mode results showed adduction of the peptide molecule with multiple sodium cations (e.g. $[M+2Na]^{2+}$).

The study of binding of Na^+ and NH_4^+ background species to a host of secondary metabolites of plant and microbial origin was investigated by Zhou and Hamburger with ESIMS and a variety of solution-phase modifiers.[9] The MS characteristics of different compound classes (macrolides, peptides, aminoglycoside, polyethers, polyenes, alkaloids, terpenoids, purines, amides, phenolics and glycosides) were determined based on dominant pseudo-molecular ion observed. Acetic acid, formic acid, trifluoroacetic acid, ammonium acetate, and triethylamine were used as additives to investigate their effect on ion form and sensitivity. Sodium cation adducts were observed for all oxygen-containing metabolites. Those oxygen-containing metabolites lacking amino functional groups also showed significant adduction to NH_4^+, forming an $[M+NH_4]^+$ pseudo-molecular ion.

The use of stability constants ($\log K_s$) for determining binding of metal-ion complexes was performed by Liu and coworkers.[99] As test probes, these researchers

used the well-characterized crown ether compound class. For metal binding, Li^+, Na^+, and K^+ were introduced into the system. The method for determination of K_s was akin to a competition method. Transfer coefficients were taken into account to correlate response to solution-phase behavior by:

$$C_{complex} = t \times I \,, \qquad \text{(eq. 14)}$$

where $C_{complex}$ is the concentration of the complex in solution, *t* represents the transfer coefficient, and *I* is the observed peak intensity for the complex ion. Once *t* and *I* are known, $C_{complex}$ and K_s can be estimated. By using an internal standard in the system, and measuring the respective peak heights of the internal standard and the analyte ion, the ratio of the two *t* values can be determined easily and accurately. The ratio of the *t* values is defined as the cationization efficiency (S).

For the two reactions:

$$C + M_a^+ \rightarrow CM_a^+ \qquad \text{(eq. 15a)}$$

$$C + M_b^+ \rightarrow CM_b^+ \,, \qquad \text{(eq. 15b)}$$

stability constants can be defined as:

$$K_{sa} = fcm_a[CM_a^+] / \, fc[C] fm_a[M_a^+] \qquad \text{(eq. 16a)}$$

$$K_{sb} = fcm_b[CM_b^+] / \, fc[C] fm_b[M_b^+] \,, \qquad \text{(eq. 16b)}$$

where $[CM_a^+]$ and $[CM_b^+]$ are the concentrations of the complexed cation with metals "a" and "b"; [C] is the concentration of the crown ether; $[M_a^+]$ and $[M_b^+]$ are the concentrations of the metal ions; and fcm_a, fcm_b, fc, fm_a, and fm_b are activity coefficients for the respective species. In dilute solutions, all of the activity coefficients approach unity and a ratio between K_{sa} and K_{sb} can be used to determine cationization efficiency by:

$$\frac{K_{sa}}{K_{sb}} = \frac{[CM_a^+]}{[CM_b^+]} \cong \frac{t_a I_{CM_a^+}}{t_b I_{CM_b^+}} \cong S \frac{I_{CM_a^+}}{I_{CM_b^+}}. \qquad \text{(eq. 16)}$$

Once a K_s value is defined for a species, it can be used iteratively to determine other K_s values. Results of this experiment were found to correlate well with literature values of crown ether-metal binding.[100]

Brodbelt and coworkers also performed extensive research in the field of cation binding with crown ethers in ESIMS. One such study compared the binding of Li^+, Na^+, and K^+ to several bibenzo-16-crown-5 lariat ethers.[101] The lariat ethers differed by placement of a pendant functional groups such as methoxy, carboxylic acid, ester, or amine. Complexes observed were compared to *ab initio* structure determinations. Results showed that there are three major factors determining the selectivity of lariat ethers for alkali metal cations. They are cavity size of the lariat ether, solvent effects that control the placement of the metal cation in the complex (perching versus nesting), and the basicities of the pendant groups, which effect the extraction of the metal ion from solution. Logically, lariat ethers with a larger cavity favor larger cations and those with smaller cavities favor smaller cations. The addition of pendant groups also affects the shape and size, and therefore, selectivity, of the cavity.

Similar selectivity experiments were also performed on a family of calixarene model compounds.[102] The basic structure of a calixarene is an oligomeric benzyl ether. Multiple substitutions were investigated to determine the sites for binding as well as to study their affect on sensitivity. CID results indicate the phenyl oxygens are the primary binding site. Also, addition of groups such as a t-butyl on the upper rim of the molecule can be used to switch the selectivity of the complex from Na^+ selective to K^+ selective.

In a separate experiment it was also possible to modify the calixarene structure to be selective for Cs^+.[103] Preferential binding of Cs^+ was determined to be due to the large cavity size and π-metal interactions that help stabilize the complex.

Silicon-containing analogs of the calixarene family were studied to elucidate their binding characteristics with alkali metal cations by Yoshida and coworkers in Japan.[104] Oligo[(dimethylsilylene)phenylene]s form cyclic structures that are selective for Rb^+ and Cs^+. Results were compared with *ab initio* calculations to determine the effect of silyl groups on the position of alkali metal binding. It appears that competition between cation-π complexation and solvation by species in the solvent matrix is essential for understanding the hole-size selectivity of the π-basic macromolecular host molecules.

Gates and coworkers in Brazil and the UK studied the effect of pH, solvent system, cone potential, and addition of crown ethers on the formation of $[M+H]^+$ of monensin.[105] It was found that the addition of 15-crown-5 and 18-crown-6 as coanalytes caused an increase in the protonated molecular ion of monensin due to effective competition of the crown ethers for background alkali metal ions that might otherwise complex with monensin. Of the two crown ethers used, 15-crown-5 was the most effective in increasing sensitivity.

Recently, Matsuda and coworkers in Japan have studied the solvation of lithium ions in organic electrolyte solutions by ESIMS.[106] Ethylene carbonate, propylene carbonate, and gamma-butyrolactone were used to simulate the environment inside of advanced batteries. Single lithium adducts to one or more analyte molecules were observed in the form $[Li\text{-}(Analyte)_x]^+$ where x = 1 to 3.

A large variety of other studies have been employed to study adduct or complex formation by alkali metal cations. The methodology involved in most of these works was the incorporation of a series of test probes for elucidation of trends in the data due to specifically functionalized molecules or molecular units. Thirty-five pharmaceutical test compounds, including amoxicillin, caffeine, reserpine, tryptophan, etc. were analyzed to determine the effect of different additives and solvents on the formation of pseudo-molecular ions.[107] It was found that methanol, rather than acetonitrile, and formic acid, rather than trifluoroacetic acid (TFA) and ammonium formate, were preferable due to slight enhancement in sensitivity and lower variation of response with changing additive concentration. A similar study was performed by Matsuura and coworkers on the positive and negative ionization mode pseudo-molecular ion formation of tiopronin – thiol acid derivatives.[11] Seven structurally diverse acrylic acid analogues were added to tiopronin via Michael addition. The response characteristics of pseudo-molecular ions were monitored in the presence of acetic acid, TFA, ammonium acetate, and ammonium hydroxide. Acetic acid and ammonium hydroxide were found to be preferable to TFA and ammonium acetate for promoting ionization in both ionization modes. The differences based on modifier used were also found to rely heavily on the spray current of the ESI capillary.

Computer simulation experiments have been widely used to study complex formation between different test species and alkali metal ions. Techniques vary, however, *ab initio* or molecular dynamics programs are most often used to achieve this goal. Simulation techniques can provide insight into types and sites of interactions and geometry of formed complex. Changes in these interactions and geometries can also be

monitored for a variety of functional substitutions in the system. A good example of such work is the *ab initio* molecular orbital simulation of cation-π interactions for Li^+, Na^+, and K^+ with several π-rich systems such as benzene, toluene, ethylbenzene, and t-butylbenzene.[108] Calculations showed an increase in cation-π interaction energy with the substitution of alkyl groups on the aromatic ring. T-butylbenzene reportedly increased interaction energy for Li^+ and Na^+ by 4.3 and 3.1 kcal/mol, respectively, relative to benzene.

Cubero and coworkers and Dougherty and coworkers have also studied cation binding to benzene and benzene derivatives. Cubero's group used theoretical calculations[109] whereas Dougherty's group employed ESI with CID to study interaction potentials.[110] Theoretical simulations focused on the correlation of electrostatic and induction interactions to complex formation using generalized molecular interaction potentials with polarization (GMIPp) for a variety of benzene derivatives including multiple ring structures, halide and amine substitution, and the incorporation of heteroatoms in the ring structure. Results showed that the introduction of electron-withdrawing groups leads to a large decrease in electrostatic interaction energy, whereas polarization interactions show little variation. In fact, polarization energy appeared to be the major contribution to cation binding when benzenes with several electron-withdrawing groups were simulated. Dougherty and coworkers assess the contribution of electrostatic interactions to binding to be major, however, inductive polarization effects generally account for ~12 kcal/mol of binding energy for substituted benzene – cation interactions. This experimental investigation was in agreement with the theoretical arguments of Cubero and coworkers.

Stone and coworkers used pyocyanin as a model to study cation binding to riboflavin using CID.[111] Results of this work showed Li^+ and Na^+ to form a bidentate chelation between the nitrogen heteroatom in the ring and the carbonyl oxygen in a specific resonance form.

Kebarle and coworkers used a set of amide and amino acid molecules to study cation binding for the purpose of mimicking movement or transfer through transmembrane channels.[112] Sodium and potassium cation binding to acetamide, N-methylacetamide, N,N-methylacetamide, glycine, and glycylglycine were studied with ESIMS and CID. The ion-dipole and induced dipole interactions which dominate the bonding in alkali metal complexes involve weaker, but long-range, forces. The major contribution to binding in these complexes is electrostatic in nature and attributed to the presence of amide functionality, because of the expected dominance of electrostatic interactions and the large bond dipole and polarizability of the carbonyl group. Other groups, such as $-NH_2$, $-NHCH_3$, $-N(CH_3)_2$, and -OH also make significant contributions to binding as shown by a change in ΔH^0 of the CID dissociation reaction when these substitutions are employed. The largest interaction potential for Na^+ and K^+ with this series of test compounds is with glycine, succinamide, and glycylglycine. With these molecules, the largest contribution to binding is attributed to the presence of an amino group.

Series of alcohols have been studied for their ability to associate a cation. Rodgers and Armentrout studied the effect of binding Li^+ with MeOH, ethanol (EtOH), n-propanol, (n-PrOH), isopropanol (i-PrOH), n-butanol (n-BuOH), isobutanol (i-BuOH), sec-butanol (s-BuOH), and t-butanol (t-BuOH).[113] This sequence is interesting due to

the variation in size of the alkyl group and its effect on binding interaction. This study was performed by CID with guided ion-beam MS (GIBMS). $[Li\text{-}ROH]^+$ is dissociated in the presence of Xenon gas to a loss of neutral alcohol as the primary product. In this specially designed reaction chamber, tandem MS is employed. Q2 in this setup is a specially designed octapole ion guide which traps ions in the radial direction, allowing collisions with the target gas molecules at low pressures (0.03 – 0.20 mTorr). Geometry optimizing simulations (semi-empirical PM3) were used to correlate the stability of the lithiated alcohols with experimental results. In all cases, the lithium cation prefers to bind to the oxygen. The alkyl group closes around the metal ion to encapsulate the lithium cation next to the oxygen atom. Enthalpies and free energy of binding were shown to increase with the size of the alkyl chain.

Pseudo-molecular ion formation by ESIMS for actinomycin D (a cyclopeptide antibiotic), digitoxin, reserpine, and quercetin (plant derived natural products) in the presence of formic acid, ammonium formate, and sodium acetate was investigated by Zhou and Hamburger.[35] Each test probe was shown to behave slightly different based on their respective gas-phase and solution-phase character. Actinomycin D showed a relatively high affinity for both H^+ and Na^+. Reserpine, an alkaloid with a high proton affinity, predominantly formed $[M+H]^+$. Neither actinomycin D nor reserpine showed adduction to NH_4^+. Digitoxin, a glycoside, readily adducts sodium and ammonium ions to form stable pseudo-molecular ions. The polyphenol, quercetin, with multiple weakly acidic phenolic groups, adducts Na^+ and H^+ in positive ionization mode, but has a much higher response when ionized to form a negative deprotonated ion in the negative ionization mode.

These works and the works of others show that the degree of binding of an alkali metal to a molecule of interest is dependent on a host of factors. These factors include solution-phase behavior of the molecules including acid-base chemistry (pH dependences), solvation energies of analytes in multiple solvent/modifier systems, inductive effects between the metal and analyte, surface activity, and competition between free and complex species in a droplet. All of these factors vary with analyte structure and functionality and with metal type and size. Gas-phase reactions in ESIMS are generally considered as a secondary process in the formation of gas-phase ions; however, techniques such as in-source CID, tandem MS CID, and other gas-phase reactor configurations (e.g. GIBMS) make gas-phase behavior of electrosprayed ions particularly relevant. In the gas-phase, analyte and complex activity are governed by factors such as instrumental settings (control of internal and kinetic energy, residence times), size of the species and target ions (collision dissociation), transfer effects (e.g. solution to gas-phase transfer and MS discrimination), and effects relating to amounts and activity of particular analyte species (concentration dependence, number of collisions, proton affinity, and gas-phase basicity).

Also complicating spectral interpretation are pseudo-molecular ions formed between all of the other species present in solution, such as dimers ($[2M \pm H]^{\pm}$) and gas-phase reaction products (e.g. $[M+H_2O]^{\pm}$, $[M+Organic]^{\pm}$, and fragment ions). The majority of work investigating adduction of alkali metals to analytes is performed in the positive ionization mode, where the cation provides a charge, forming a complex with a neutral molecule. Complex formation with alkali metal cations in the negative ionization mode has scarcely been reported due presumably for the need for two negative charges to

counter the positive cation to create a negatively charged complex species. It is more likely one observes complexes with the alkali metal counterion in the negative ionization mode.

The observation of non-covalently bound dimers has also been reported. These complexes are due to strong associations between two analyte ions. In some cases, this association is mediated by a metal ion. To make a clear distinction between those associations that are a result of intermolecular attraction where no metal ion is included and those where the dimer complex is bridged by a coordinated or complexed metal, the former will be referred to strictly as a dimer ion, whereas the latter will be referred to as a metal-bridged dimer ion.

Dimer formation is of course not restricted to these two cases. Reports in the literature show a wide array of dimer types. Formation of dimers in solution can be used to probe the relative activity and selectivity of molecule functional units in a variety of solution environments. Research strongly supporting this path is that involving gas-phase chiral and molecular recognition experiments with MS detection. Regardless of the direction of the experiment, dimer ions, whether mediated by another species or not, are commonly encountered for a wide array of molecule types during ESIMS.

The report of an anion bridged dimer ion was observed by Keely and coworkers for a series of quaternary ammonium pesticides.[114] These positively charged species in solution were shown to form positively-charged complexes with acetate and chloride (A^-) in the form $[2M^+ + A^-]^+$. However, as previously addressed, a thorough survey of the literature shows no observation of a *metal*-bridged dimer ion in negative ionization mode. Work by Schug and McNair on the pseudo-molecular ion formation of aromatic

carboxylic acids has shown the formation of a negatively charged sodium-bridged dimer ion for the first time.[10] Current work at Virginia Tech has been directed towards a more complete study of this negative ion form, particularly in the realm of small aromatic acid molecules with a variety of substituents.

The example cited above refers to the presence of two analyte molecules of the same type associated in a complex. This can be referred to as a homogeneous dimer ion. In the realms of macromolecule chemistry and molecular recognition, selectivity experiments exploiting the formation of dimer ions are better served when species of different types are allowed to associate. In such experiments, a heterogeneous dimer ion is observed. These species can also be bridged with or without a metal ion.

In a study by Rebek, Jr. and coworkers, molecular recognition processes between calixarene based macromolecules and various alkyl and aromatic quaternary ammonium ions were investigated for selectivity of dimer ion formation.[115] Modeling shows the calixarene molecules to be held together by a seam of hydrogen bonds which forms a cavity for small molecules. These complexes are very stable with energies of dissociation approaching that of covalent bonds. The heterogeneous dimer ion formed between a single calixarene and a single guest ammonium ion is dissociated at a much lower energy and is less stable due presumably to the lack of multiple hydrogen bonds. Data for complexation of a second ligand are often available from ion equilibria measurements. For example, the enthalpy to fully dissociate two acetone molecules bound by Na^+ is approximately 1.75 times greater than the enthalpy for dissociation of one acetone molecule bound to sodium.[112]

Multiple dimer ions were also observed by Stone and coworkers in their work with pyocyanin.[116] Mixtures of piocyanin with bipyridine and a wide array of metal cation types showed the formation of a variety of dimer pseudo-molecular ion types. This system demonstrated that the complex of two pyocyanin or one pyocyanin and one bipyridine molecules and a metal ion is more hydrophobic than the free molecule ion and thus shows a greater sensitivity during ESIMS. In general, dimer complexes are expected to have greater surface activities, lower solvation energies, and thus produce higher ESIMS signals. The formation of dimer complexes complicates the interpretation of data, and likely reflects the enhanced desolvation efficiencies of complexes in which the ionic charge is strongly solvated by ligands rather than directly by solvent molecules.[34]

Probably the most interesting aspect of complex formation by ESIMS, is its use in performing chiral recognition experiments in the gas-phase. Cooks and coworkers have performed Cu(II) assisted chiral recognition studies[117] using the kinetic method[90] for determination of enantiomeric excess. The method uses chiral reference ligands (ref*), chosen from the natural α-amino acids, to separate enantiomers of other amino acids (A). Singly charged Cu(II)-amino acid cluster ions $[Cu^{II}(A)(ref^*)_2\text{-}H]^+$ dissociate by CID to form dimeric complexes $[Cu^{II}(A)(ref^*)\text{-}H]^+$ and $[Cu^{II}(ref^*)_2\text{-}H]^+$. The abundance of these fragment ions depends strongly on the stereochemistry of the ligands in the precursor complex ion and specifically on the chirality of the amino acid of interest. An energy quantity for the bond dissociation energy is predicted from the kinetics of the dissociation reaction and shown to serve as a thermochemical indicator of chiral recognition. The use of ESIMS for chiral recognition processes is very attractive and shows promise for future applications. A detailed review of this field is beyond the scope of this thesis; however,

all research directed towards elucidating the nature of non-covalent interactions by ESIMS are considered to be stepping stones for more complex analyses such as those involved in chiral recognition processes.

The ability of ESIMS to produce and detect non-covalently bound pseudo-molecular ions of varying form can be a help or a hindrance. The presence of background electrolytes in nearly all solution systems ensure that adducts will be formed whether they are desired or not. Those researchers who are focused on developing specific analytical applications must be aware of these processes, especially relating to specific molecular functionality of the analyte of interest. If an adduct ion form is not anticipated, such as in high-throughput screening, analytes of interest may be missed or improperly quantified. In more complex processes, where non-covalent interactions are desired to investigate selectivity and recognition processes, ESIMS is a powerful tool for making equilibrium measurements in solution. When gas-phase processes such as CID are incorporated, the technique allows for quantitative binding determinations for a variety of complex ion types and configurations.

CHAPTER 2

2.1 General Experimental

Results for the formation of pseudo-molecular ions by aromatic acids in negative ionization mode ESIMS are products of three primary and three secondary experiments performed under a variety of instrumental conditions. The specific details for each experiment are addressed individually below. All ESIMS experiments were performed on a Shimadzu LCMS-2010 (Shimadzu Scientific Instruments, Inc., Columbia, MD, USA). Figure 2.1.1 shows a picture of a general bench top set-up for an LCMS-2010 system. The LCMS-2010 allows use of two interchangeable atmospheric pressure interfaces for ionization of analytes by ESI or by atmospheric pressure chemical ionization (APCI). Figure 2.1.2 shows the two interface sources available with this instrument. The ESIMS interface was used for all analyses of aromatic acid analytes in the experiments described below. Both positive and negative ionization modes were employed for all test probes used. Ionization efficiencies were best when the negative ionization mode was used and generally poor when the positive ionization mode was used. Figure 2.1.3 shows a schematic diagram of the interface, ion lenses, and quadrupole mass filter arrangement for an LCMS-2010.

Standard Shimadzu LC-10AD VP dual-piston pumps with high pressure mixing provided flow for the interface and detector. The pumps were operated isocratically at 0.1 mL/min with a mobile phase of 50/50 acetonitrile (Burdick & Jackson, Muskegon, MI)/deionized water (obtained and filtered in-house). Samples were injected by the SIL-10AD VP auto-sampler outfitted with a 500 μL injection loop. Ultra-high purity nitrogen gas (Holox, Norcross, GA) at a flow rate of 4.5 L/min was used as the bath gas for

pneumatic assistance in droplet desolvation. All analyses were performed in flow injection mode with no chromatographic column present. In this configuration, analytes in the presence of various solution compositions and modifiers are directly infused into the interface for ionization.

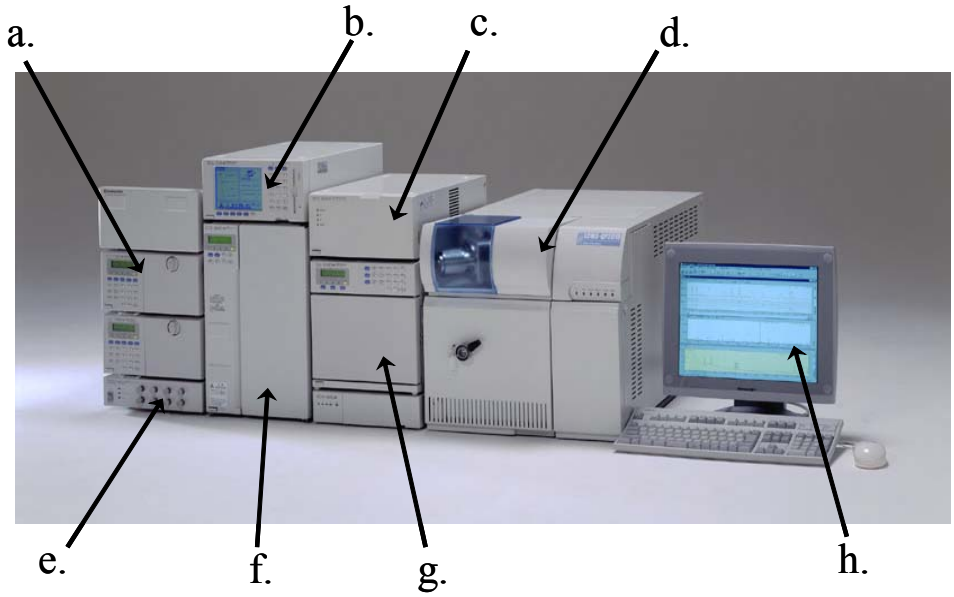

Figure 2.1.1 General bench top set-up for the Shimadzu LCMS-2010. The components of the system correspond to: a.) two LC-10AD VP dual piston pumps; b.) SCL-10AD VP system controller unit; c.) SPD-10AV VP variable wavelength UV-Vis detector; d.) LCMS-2010 API MS; e.) DGU-14A solvent degasser; f.) CTO-10AC VP column oven; g.) SIL-10AD VP auto-sampler unit; and h.) computer data system with LCMS LabSolutions software package.

a. ESI Interface Probe

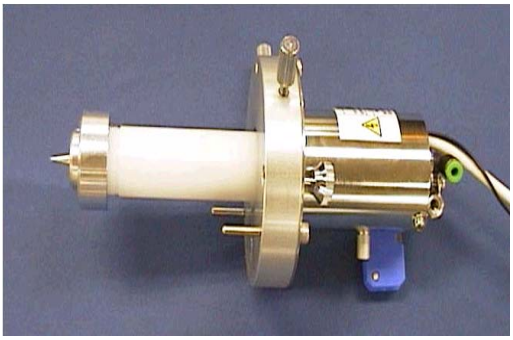

b. APCI Interface Probe

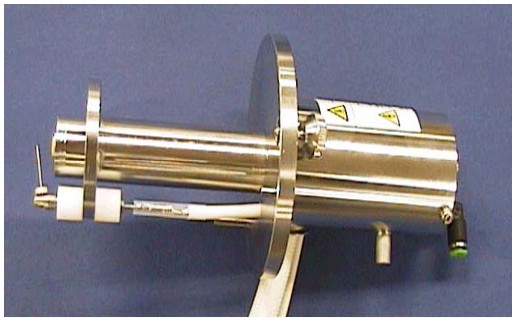

Figure 2.1.2 LCMS-2010 interface probes for (a.) electrospray ionization and (b.) atmospheric pressure chemical ionization operation modes.

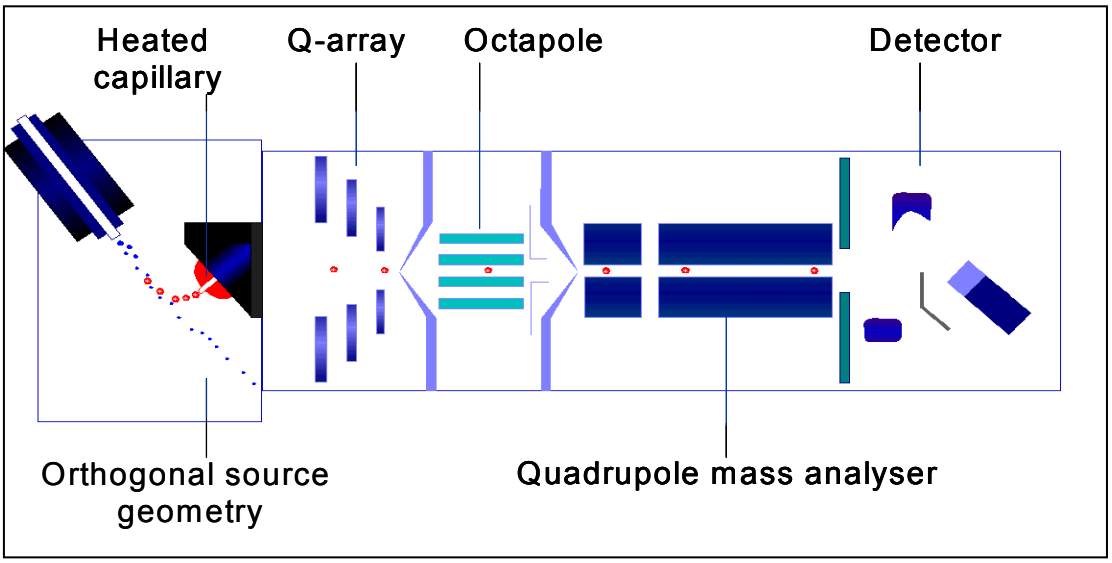

Figure 2.1.3 Schematic diagram of the interface and ion lens configuration of a Shimadzu LCMS-2010 instrument.

The mass spectrometer on the LCMS-2010 is a single quadrupole mass filter and is capable of detecting singly and multiply charged ions in the 10 – 2000 m/z range. This instrument makes use of an in-line Q-array (patent pending) and octapole ion lens system for focusing the ion beam. Ions are extracted into the high vacuum region of the instrument by a heated capillary transfer line set orthogonal to the spray capillary, called a curved desolvation line (CDL). The CDL is configured to provide optimal declustering of gas-phase species prior to mass filtering and has an internal diameter of 150 μm.[39] The orthogonal configuration serves to minimize sampling of background species, such as non-volatile solutes and high concentrations of solvent vapor. Figure 2.1.4 is a picture of a CDL used in Shimadzu LCMS instrumentation. The MS was run in both scan and selected ion monitoring (SIM) modes where applicable for detection of desired pseudo-molecular ion products. Table 2.1.1 lists the MS voltages and temperatures used. These settings were not changed unless otherwise noted in specific experiments.

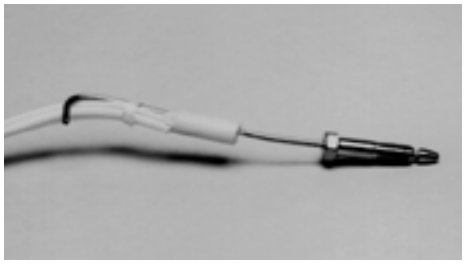

Curved Desolvation Line

CDL Housing

Figure 2.1.4 Curved desolvation line (CDL) and CDL housing used for declustering gas-phase species and extraction of ions into the high vacuum region of the MS.

Table 2.1.1 General operational settings for the LCMS-2010.

Instrument	**Shimadzu LCMS-2010**
Ionization Mode	ESI negative (positive)
Probe Voltage	-3.5 kV (+4.5 kV)
Nebulizer Flow (N_2)	4.5 L/min
CDL Temperature	250 °C
Block Temperature	250 °C
CDL Voltage	-25 V (10 V)
Q-Array Voltage	Scan
Q-Array RF	150.0
Mass Range	50-350 amu
Interval	0.3 sec
Scan Speed	1000

Three experiments for the elucidation of pseudo-molecular ion formation by aromatic acids in negative ionization mode are outlined below. They are:

- Experiment 1: Adduct Formation by Common Acidic Pharmaceuticals;
- Experiment 2: Adduct Formation by Simple Aromatic Acids;
- Experiment 3: Concentration and pH Effects in FIA-ESIMS;

Other experiments performed included work presented at various conferences and as supplemental data to clarify the results reported in experiments 1 – 3. These are addressed in Chapter 6.

Where applicable, results were correlated with calculations from two computer software programs. Calculations of solution phase parameters, such as pK_a and log P, for individual analytes were made using ACDlabs SpecManager program (Advanced Chemistry Development, Inc., Toronto, Ontario, Canada). pK_a is a measure of the ability of an acidic analyte to give up one proton. pK_a values are approximately equivalent to the pH necessary to obtain 50% of the analyte in the neutral form and 50% in the ionic form. Multiple dissociation values (pK) were obtained where an analyte contained more than one ionizable group. Values for log P correspond to the logarithm of the octanol/water partition coefficient of a given analyte in an aqueous system. Though analyses were performed here in 50/50 acetonitrile/water, log P was used as a relative measure of the ability of different analyte species to move from a hydrophilic solution phase to a hydrophobic gas phase during ESIMS droplet formation and ion evaporation.

Due to our unique finding of a sodium-bridged dimer ion in these experiments, it was interesting to determine the most favorable orientation of this complex ion through molecular modeling techniques. Gaussian98[118] was used to perform *ab initio* geometry optimization calculations with Hartree-Fock self-consistent field theory. Due to the complex nature of these species, simulations were performed with relatively simple basis sets, such as 3-21G and 6-31G(d). These basis sets are defined as Gaussian-type or Pople-type split valence basis sets. Due to the nature of the weak interactions encountered in non-covalent complex ions, some work was performed with a more diffuse basis set, 6-31+G(d), to account for longer-ranged interactions. A comparison of these results is offered in Chapter 6.

2.2 Experiment 1: Adduct Formation by Common Acidic Pharmaceuticals

The purpose of this work was to optimize the generation of specific pseudo-molecular ions by studying the effect of common LC mobile phase additives on the intensity of ions formed by six common anti-inflammatory pharmaceuticals. The analytes used in this study were ibuprofen, carprofen, ketoprofen, naproxen, flurbiprofen, and fenoprofen. All analyte standards were obtained from Sigma-Aldrich (St. Louis, MO). Figure 2.2.1 shows the structure, molecular weight, and pK_a for these compounds used in this experiment. These standards were chosen due to the presence of a common phenylacetic acid moiety. Differences in ionization efficiency and type of pseudo-molecular ion formed by each molecule were therefore due to the functionality pendant to the aromatic acid group. Three acidic and three basic mobile phase modifiers were chosen based on their routine use in LC-MS analyses. These were: formic acid (FA); acetic acid (HOAc); trifluoroacetic acid (TFA); ammonium acetate (NH_4OAc); ammonium carbonate ($(NH_4)_2\ CO_3$); and triethylamine (TEA). Each additive was mixed 1:1 at three different concentrations (20, 10, 5 mM) with each analyte in an auto-sampler vial. All analytes were present at 100 ppm (w/w) concentration. Four microliters of the mixture was flow injected at 0.2 mL/min. A 100 μL dead volume loop was placed in the flow path to band broaden the peak for optimal scanning by the quadrupole mass analyzer.

The LCMS-2010 was operated in negative scan ESI mode. Ionization in the negative mode was facilitated by the presence of the acidic functional unit. Scans were made from 200 – 600 amu at 0.5 second intervals. The temperature and voltage of the curved desolvation line (the inlet for the high vacuum region) were set to 250 °C and -25 V, respectively. These operating conditions were mild enough to preserve association

between solution phase species, so pseudo-molecular ions could be observed in ESI spectra. The ions of interest which were monitored and chosen due to their relatively high abundance in the mass spectra were the deprotonated molecular ion ($[M-H]^-$), a homogeneous dimer ion ($[2M-H]^-$), and a sodium-bridged dimer ion ($[2M-2H+Na]^-$).

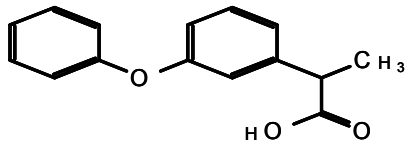

Fenoprofen (242.27) (pKa = 4.20)

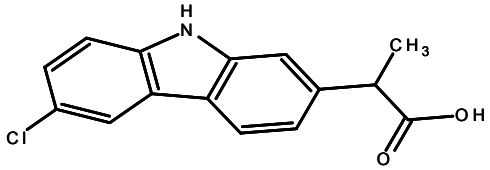

Carprofen (273.71) (pKa = 4.39)

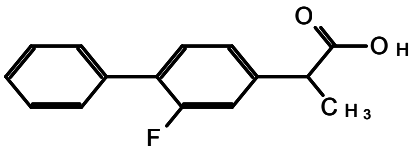

Flurbiprofen (244.26) (pKa = 4.14)

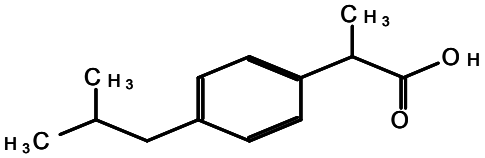

Ibuprofen (206.28) (pKa = 4.41)

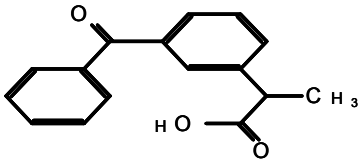

Ketoprofen (254.28) (pKa = 4.23)

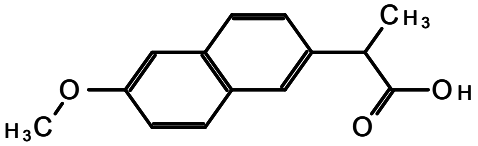

Naproxen (230.26) (pKa = 4.40)

Figure 2.2.1 Structure, molecular weight, and pKa for the six anti-inflammatory pharmaceuticals used in experiment 1.

2.3 Experiment 2: Adduct Formation by Simple Aromatic Acids

Results of experiments where pseudo-molecular ions were formed by common acidic pharmaceuticals, showed the structural diversity of the test probes to be too complex to derive concrete conclusions relating molecular functionality and ion type formed. These results are addressed in Chapter 3. It was therefore necessary to choose a less complex set of analytes to elucidate effects controlling pseudo-molecular ion formation. A series of standards including benzoic acid (BA), halide substituted benzoic acids, amino benzoic acids, and t-butyl BA where the point of substitution is varied between the *ortho*-, *meta*-, and *para*- positions on the ring were chosen. *Meta*-bromo-benzoic acid (3-Br BA), *meta*-chloro-benzoic acid (3-Cl BA), *para*-chloro-benzoic acid (4-Cl BA), *meta*-amino-benzoic acid (3-amino BA), and *para*-amino-benzoic acid (4-amino BA) were obtained from Sigma – Aldrich (St. Louis, MO). *ortho*-bromo-benzoic acid (2-Br BA), *para*-bromo-benzoic acid (4-Br BA), *ortho*-chloro-benzoic acid (2-Cl BA), *ortho*-fluoro-benzoic acid (2-F BA), *meta*-fluoro-benzoic acid (3-F BA), *para*-fluoro-benzoic acid (4-F BA), and *para*-t-butyl-benzoic acid (4-t-butyl BA) were obtained from Lancaster (Pelham, NH). *Ortho*-amino-benzoic acid (2-amino BA) was obtained from Acros Organics (Fisher Scientific, Geel, Belgium). Figure 2.3.1 shows the structures of these analytes.

The LCMS-2010 was operated in negative ionization ESI scan and selected-ion monitoring (SIM) mode. Scans were made from 50 - 500 amu at 0.5 second intervals (scan speed = 1000 amu/sec). Selected ion monitoring (SIM) was used for unsubstituted BA experiments at m/z 121 ($[M-H]^-$) and m/z 265 ($[2M-2H+Na]^-$). The CDL temperature and voltage values were varied appropriately for BA experiments focused on studying the effect of these parameters on sampling efficiency and consequently, ion formation.

Flow injection analysis of the compounds was used as a quick and easy way to study pseudo-molecular ion formation by ESIMS. The pumps were operated isocratically at 0.1 mL/min with a mobile phase of 50/50 acetonitrile/water for work with substituted BA analytes and 1/99, 25/75, 50/50, and 75/25 acetonitrile/water for studies of BA in different mobile phase compositions. 200 μL injections were made at a flow rate of 0.1 mL/min for analytes prepared at 0.01 mM concentration. Assuming no band broadening, the sample injection band was infused into the interface for two minutes. In this time, an equilibrium, or quasi-equilibrium, was established in the source chamber. The response was a plateau. The average maximum of this response plateau was the relative ionization efficiency for an analyte. Specific effects of FIA-ESIMS are studied in detail in Chapter 5.

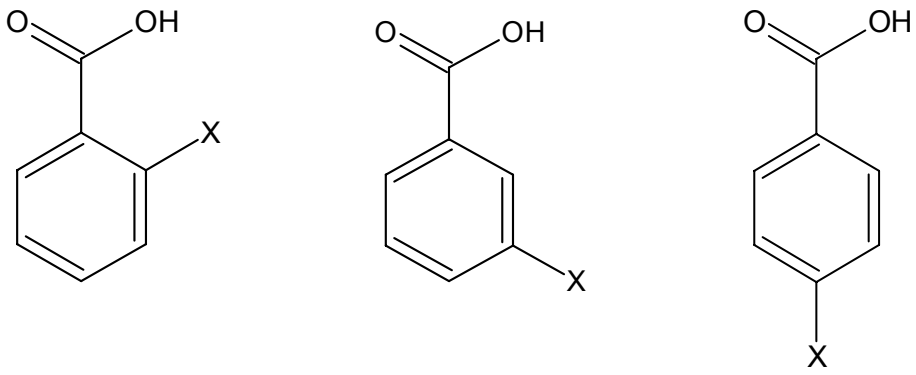

Figure 2.3.1 Structures of *ortho*-, *meta*-, and *para*- substituted benzoic acid analytes where X = Br, Cl, F, and NH_2. T-butyl BA is only available as a *para*-substituted standard.

2.4 Experiment 3: Concentration and pH Effects in FIA-ESIMS

Investigations of concentration and pH effects in ESIMS are of paramount importance due to the large variations in analyte types, amounts, and optimal ionization conditions when performing chromatographic separations with ESIMS detection in everyday use. Methods for pH modification are far from universal and often the use of different types of additives to achieve a desired chromatographic separation is commonplace. For example, in chromatographic separations, a method developed using acetic acid as a modifier may show very little difference from a similar method that employs formic acid. In ESIMS, this is rarely the case. Very small changes in solution conditions can have a marked effect on the type and intensity of the various pseudo-molecular ions formed.

For this experiment, *para*-amino benzoic acid (PABA), obtained from Sigma – Aldrich (St. Louis, MO), was used to investigate the effect of pH, type of pH modification, and concentration of analyte on the formation of a traditional deprotonated molecular ion ($[M-H]^-$) and a sodium bridged dimer ion ($[2M-2H+Na]^-$) in the negative ionization mode by FIA-ESIMS. Response was also investigated as a function of injection volume.

For reliable data, large injection volumes were necessary to obtain accurate ionization efficiencies by FIA-ESIMS. This hypothesis was investigated by studying the effect on response precision for five injection volumes (10, 20, 100, 200, and 400 μL). The value obtained for intensity of an ion was compared for each injection volume relative to the number of scans available in the ion chromatogram for averaging to obtain a mass spectrum. Scan-by-scan reproducibility was evaluated statistically. For the study

of linearity, five concentrations (0.01, 0.1, 0.5, 1.0, and 2.0 mM) of PABA were prepared. Each concentration was injected at each of the five injection volumes. Six repetitions of each sample set, prepared in standard auto-sampler vials, were infused for analysis.

Experiments involving the study of pH effects on PABA were performed in two ways. The first pH experiment involved the preparation of four aqueous pH modifiers as indicated by the Handbook of Chemistry and Physics.[119] These solutions contained a high concentration of acids, bases, and buffers to achieve the desired pH. Table 2.4.1 describes the solution composition used to achieve the desired pH. For comparison of ionization results due to pH modification, a second sample set was modified by using common LC-MS modifiers. The modifiers chosen were acetic acid (HOAc) (Fisher Scientific, Fair Lawn, NJ), formic acid (FA) (Aldrich, Milwaukee, WI), triethylamine (TEA) (Sigma, St. Louis, MO), and ammonium acetate (NH_4OAc) (Lancaster, Pelham, NJ). Each modifier was present with analyte in the sample solution at 0.5 mM concentration. Table 2.4.2 lists pK_a values and measured pH values for these modifiers and modified solutions, respectively. The pH of each system, including 0.5 mM PABA and 50% acetonitrile were measured with an Accumet pH Meter 900 (Fisher Scientific, Pelham, NJ).

Table 2.4.1 Solution pH modifications made according to the Handbook of Chemistry and Physics.[119]

Solution	pH (aq)	Composition (in 100 mL)	pH (mix)
A	3.0	50 mL 0.1 M KHP + 22.3 mL 0.1 M HCl	3.7
B	5.0	50 mL 0.1 M KHP + 22.6 mL 0.1 M NaOH	7.0
C	8.0	50 mL 0.025 M borax + 20.5 mL 0.1 M HCl	7.9
D	10.0	50 mL 0.05 M $Na_2(CO_3)$ + 10.7 mL 0.1 M NaOH	11.1

pH(aq) denotes the quoted value of 100 mL of aqueous modifier made in the manner described under composition. pH(mix) denotes the final pH of the system upon addition of 0.5 mM PABA and dilution with 50% acetonitrile. KHP is potassium hydrogen phthalate.

Table 2.4.2 pK_a and measured pH values for modifiers and solutions commonly used in LC-MS and tested in this study.

Solution	pK_a	pH(mix)
0.5 mM HOAc	4.74	3.9
0.5 mM FA	3.75	3.4
0.5 mM TEA	10.78	10.6
0.5 mM NH_4OAc	NA	6.9

pH(mix) denotes the measured pH of the solution containing 0.5 mM PABA and diluted with 50% acetonitrile.

CHAPTER 3

Experiment 1: Common Acidic Pharmaceuticals

3.1 Introduction

An experimental finding for the analysis of pseudo-molecular ion formation for common acidic pharmaceuticals by ESIMS has been published by Schug and McNair.[10] These results showed the formation of a deprotonated molecular ion ($[M-H]^-$), a sodium-bridged dimer ion ($[2M-2H+Na]^-$), and in some cases a deprotonated dimer ion ($[2M-H]^-$) for a series of anti-inflammatory pharmaceuticals. The observation of a $[2M-2H+Na]^-$ ion formed by aromatic carboxylic acids had not been reported previously and justified further investigation of the factors influencing the formation of this pseudo-molecular ion species.

Ibuprofen, carprofen, ketoprofen, naproxen, flurbiprofen, and fenoprofen are well known anti-inflammatory pharmaceuticals which contain phenylacetic acid functionality, yet differ slightly in substituent arrangement and functionality.[120] The structures of these compounds were shown previously in Figure 2.2.1. The acidic moiety allows these model compounds to be efficiently ionized in the negative ionization mode by ESI. Positive mode ionization is possible in strong acidic media if a molecule contains functionality that will readily associate a positively charged species; however positive ion abundances observed here were either negligible or too small to be informative under the conditions of this study. All of the work presented here was performed in the negative ionization mode.

The purpose of this work was to optimize the generation of specific pseudo-molecular ions by studying the effect of common LC mobile phase additives on spectral

intensity. Three acidic and three basic mobile phase modifiers were studied. These were: formic acid (FA); acetic acid (HOAc); trifluoroacetic acid (TFA); ammonium acetate (NH_4OAc); ammonium carbonate ($(NH_4)_2\ CO_3$); and triethylamine (TEA). Table 3.1.1 lists the pH (or pK_a) for each modified solution based on additive chosen. Each additive was mixed 1:1 at three different concentrations (20, 10, 5 mM) with each analyte in an auto-sampler vial. Analysis was performed via flow injection with no LC column.

Table 3.1.1 Common LC-MS additives used in experiment 1.

Additive	pH (pKa)
Triethylamine	11
Ammonium carbonate	9
Ammonium acetate	6.8
Acetic acid	(4.74)
Formic acid	(3.75)
Trifluoroacetic acid	2.5

Approximate pH (or pK_a) values are listed where available for solutions at 10 mM concentration.

3.2 Results

The pseudo-molecular ions chosen for this study were based on the major ions obtained during the analyses. The results for each analyte are addressed sequentially, noting both differences and similarities for ionization of these molecules, in the following sections. It is obvious from the data that trends exist with the addition of certain modifiers.

It is also apparent that the presence of differing functionality in the model compounds accounts for differences in the most intense pseudo-molecular ion formed. Table 3.2.1 lists the conditions used to obtain the most intense ion observed for each analyte. Table 3.2.2 lists the calculated log P and pK_a values for the six test analytes. Since ESI is largely affected by the solution phase characteristics of the system and the analyte, acid/base interactions and solvation energy are two important parameters controlling ionization efficiency. Correlations between these values, approximated by pK_a and log P respectively, and relative intensities of pseudo-molecular ion responses may be useful for extrapolating dominant trends in the data. The reported values were calculated using the ACDlabs SpecManager software package.

Table 3.2.1 Most intense base ion observed for the six anti-inflammatory pharmaceuticals.

Analyte	Most Intense Ion	Conditions	Int. / 10^5
Ibuprofen	$[M-H]^-$	20 mM TEA	24
Carprofen	$[2M-H]^-$	5 mM TEA	15
Naproxen	$[M-H]^-$	20 mM TEA	5
Ketoprofen	$[M-H]^-$	5 mM $(NH_4)_2CO3$	11
Flurbiprofen	$[2M-2H+Na]^-$	5 mM FA	7.5
Fenoprofen	$[M-H]^-$	5 mM HOAc	11

Results listed along with the condition necessary to obtain the given ion intensity for the most intense pseudo-molecular ion observed as well as confirmation of other pseudo-molecular ions observed.

Table 3.2.2 Calculated pK_a and log P values for the six ibuprofen derivative test analytes.

Analyte	pKa	log P
Ibuprofen	4.41	3.72 ± 0.23
Carprofen	4.39	4.03 ± 0.29
Naproxen	4.40	3.00 ± 0.24
Ketoprofen	4.23	2.81 ± 0.33
Flurbiprofen	4.14	4.12 ± 0.37
Fenoprofen	4.20	3.84 ± 0.33

Values were obtained from the ACDlabs SpecManager software package.

3.2a Ibuprofen

Ibuprofen is a simple molecule that lacks heteroatoms other than a carboxylic acid group. The ESI mass spectrum showed an intense molecular ion and a moderately intense dimer adduct with sodium. No simple homogeneous dimer ion was observed. The formation of an intense molecular ion is due to the molecule's affinity for a hydrophobic medium. Lacking a high degree of polarity, ibuprofen will migrate to the surface of an aqueous droplet faster than the other analytes due to its higher degree of hydrophobicity. This results in increased ionization efficiency relative to the other model compounds and subsequently, a more intense molecular ion signal. Figure 3.2.1 shows the mass spectrum corresponding to the ionization of ibuprofen in the absence of any mobile phase modifiers. Figure 3.2.2 shows the Hartree-Fock *ab initio* geometry optimization for the deprotonated molecular ion at the 3-21G basis level. All modifiers, except TEA, suppressed the formation of the molecular ion ($[M-H]^-$). As is the case with all analytes, TFA suppressed the formation of all ibuprofen negative ions, especially at

higher concentrations. This was due to the high acidity of TFA (pH = 2.5 at 10 mM concentration) which hindered deprotonation of acidic analytes.

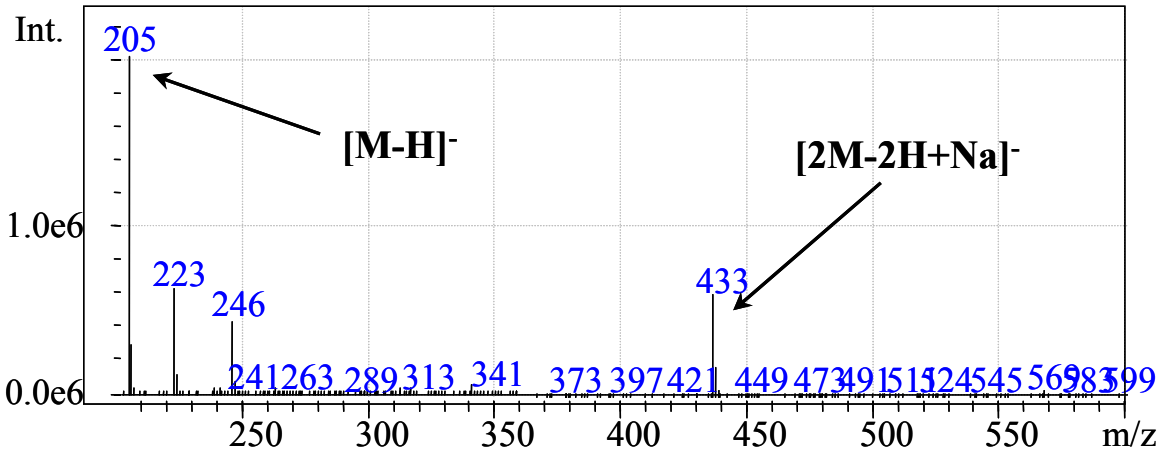

Figure 3.2.1 Flow injection ESI mass spectrum of ibuprofen in a 50/50 water/acetonitrile mobile phase with no modifiers in the negative ionization mode. The masses of interest for ibuprofen in this study were m/z 205 ($[M-H]^-$) and 433 ($[2M-2H+Na]^-$). Ibuprofen did not form dimers under any condition tested. The responses due to m/z 223 and 246 have been assigned as $[M-H+H_2O]^-$ and $[M-H+ACN]^-$, respectively.

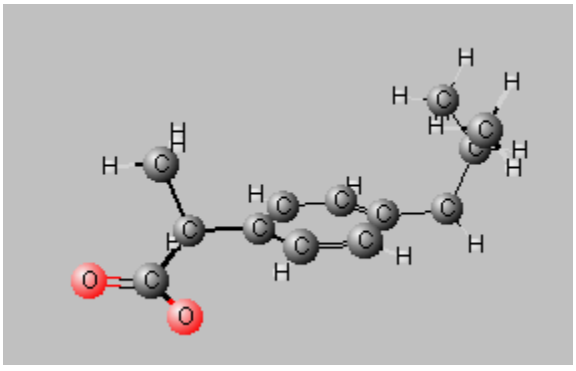

Figure 3.2.2 Geometry optimized structure of the deprotonated ibuprofen molecular ion at the 3-21G basis level using Hartree-Fock *ab initio* simulations.

Ibuprofen did not form dimers under the conditions tested here. This was due to the lack of hydrogen bonding sites and low polarity functionality. Ibuprofen did form a dimer adduct with sodium ($[2M-2H+Na]^-$), especially in neutral solution, but the intensity of this signal was diminished upon addition of any of the six tested additives. Figure 3.2.3 shows the geometry optimized structure for the $[2M-2H+Na]^-$ pseudo-molecular ion of ibuprofen. Only in the presence of NH_4OAc and FA was the dimer adduct ion still observable at high modifier concentration. Figure 3.2.4 is a graph of response of $[2M-2H+Na]^-$ ion in the presence of the six additives.

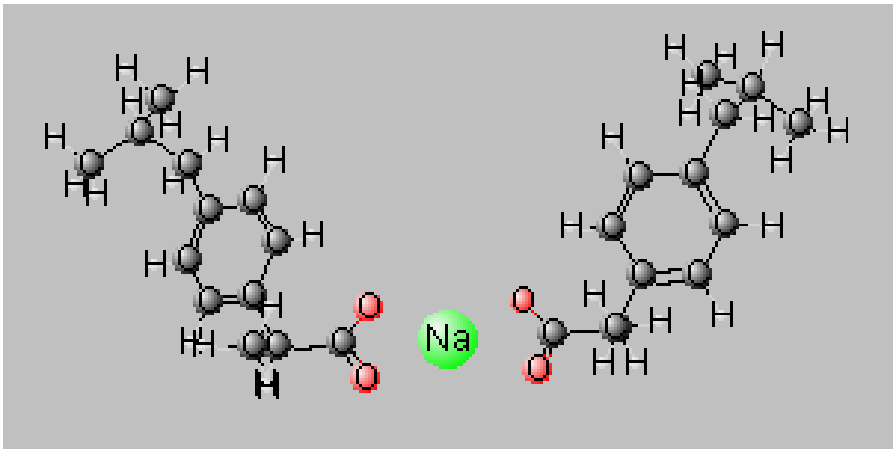

Figure 3.2.3 Hartree-Fock *ab initio* geometry optimized structure for the sodium-bridged dimer ion of ibuprofen at the 3-21G basis level.

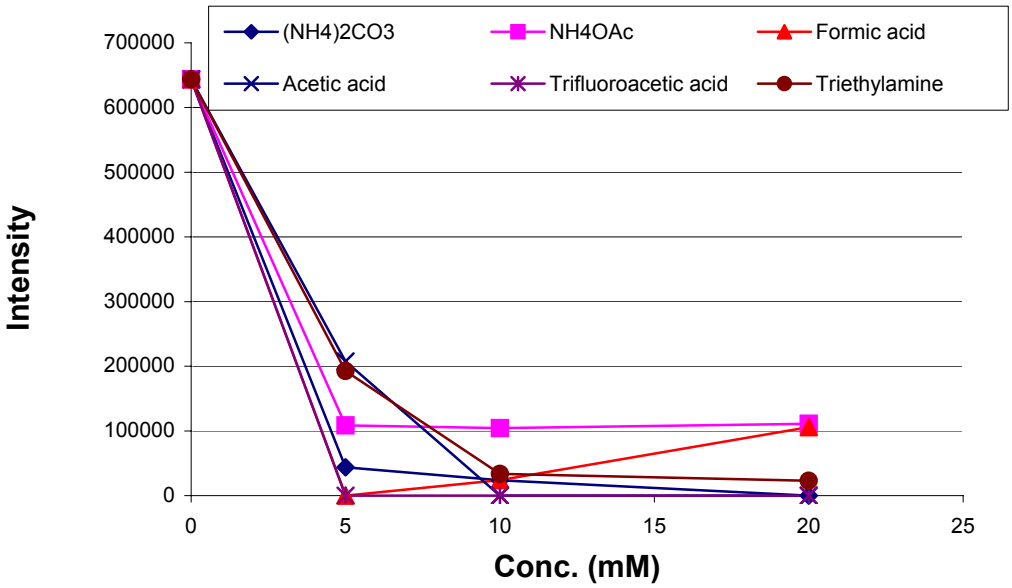

Figure 3.2.4 Effect of mobile phase modifiers on abundance of $[2M-2H+Na]^-$ for ibuprofen. Points shown at 0 mM concentration imply a 50/50 acetonitrile/water system with no additives present.

3.2b Carprofen

Carprofen is one of the more interesting molecules studied in this experiment. It contains an amine functionality that allows for hydrogen bonding between two carprofen molecules. As a result, carprofen formed an intense dimer ion ($[2M-H]^-$), as well as an intense $[2M-2H+Na]^-$ ion and a moderately intense $[M-H]^-$ ion when no modifier was present. The molecular ion was diminished in the presence of all additives except TEA. *Ab initio* geometry optimized structures at the 3-21G level are shown for the deprotonated molecular ion in Figure 3.2.5; for the hydrogen bonded dimer ion in Figure 3.2.6; and for the sodium-bridged dimer adduct ion in Figure 3.2.7.

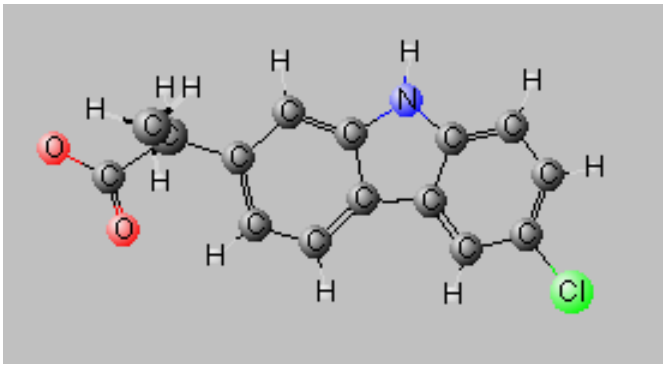

Figure 3.2.5 Geometry optimized structure of $[M-H]^-$ ion of carprofen. Atom size is shown at 50% of relative actual size.

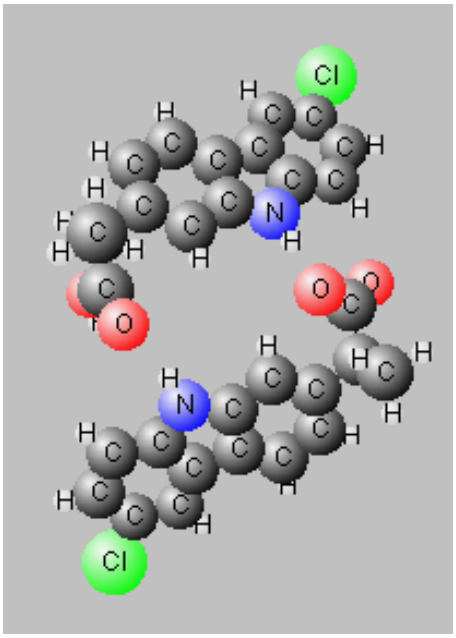

Figure 3.2.6 Geometry optimized structure of $[2M-H]^-$ ion of carprofen. Atoms shown here are depicted as scale to their actual size.

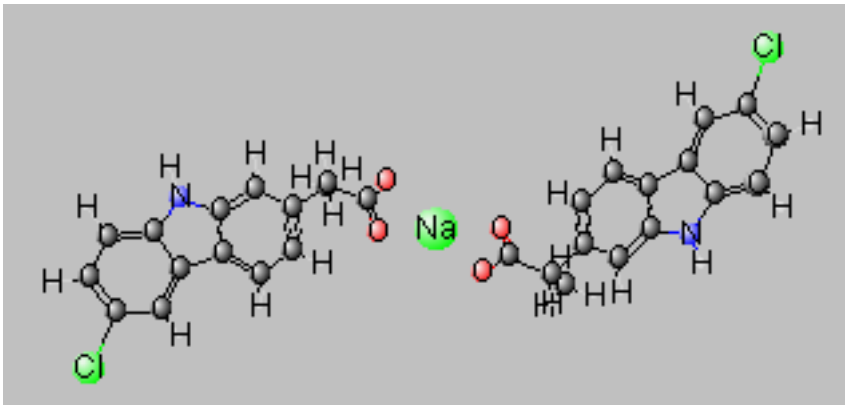

Figure 3.2.7 Geometry optimized structure of $[2M-2H+Na]^-$ ion of carprofen.

Figure 3.2.8 shows the effect of all of the additives on formation of $[2M-2H+Na]^-$ for carprofen. NH_4OAc greatly suppressed ionization of carprofen for all three ions monitored. The $[2M-2H+Na]^-$ ion still remained prominent in high concentrations of FA and HOAc. Figure 3.2.9 shows the effect of all additives on carprofen dimer ($[2M-H]^-$) ion formation. At low concentrations, TEA and HOAc had the least effect on dimer ion formation, whereas all other additives caused the dimer ion to decrease with increasing concentration. The intensity of the dimer ion was enhanced by the increased hydrophobicity of the hydrogen-bound species. It is well known that the surface activity of a dimer species is greater than that of a monomer.[116]

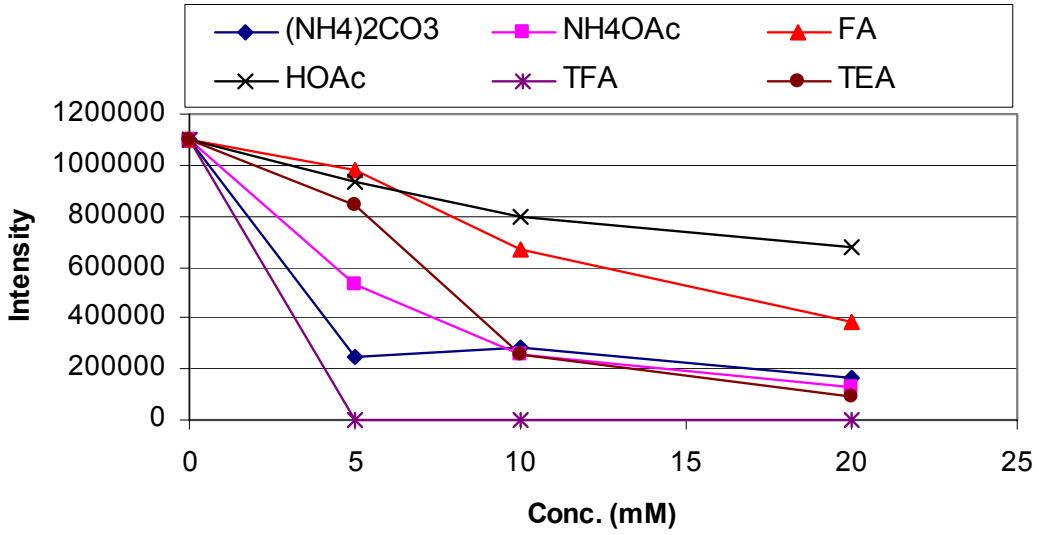

Figure 3.2.8 Effect of additives on abundance of $[2M-2H+Na]^-$ for carprofen.

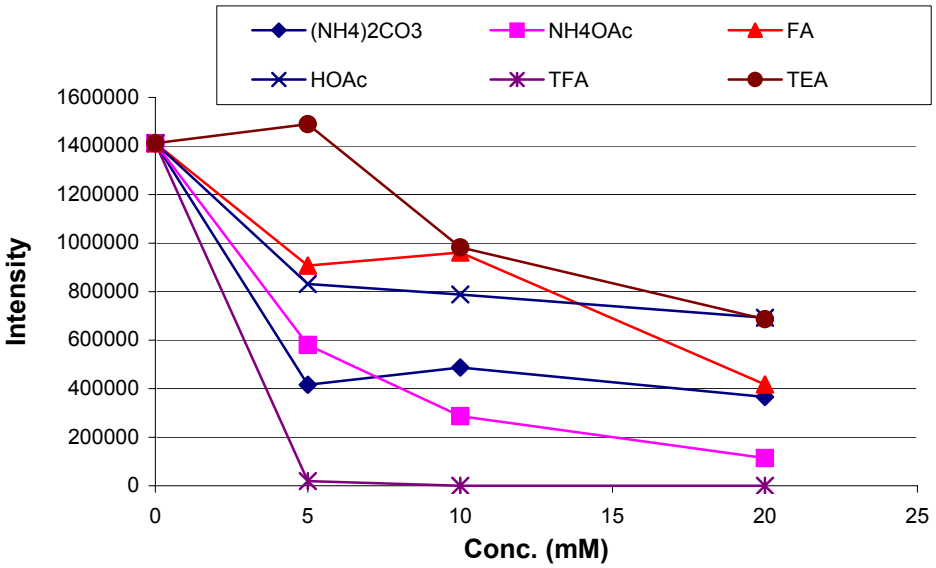

Figure 3.2.9 Effect of additives on abundance of $[2M-H]^-$ for carprofen.

3.2c Ketoprofen

Ketoprofen is an aromatic ketone attached to phenyl acetic acid. Ketoprofen formed all of the three pseudo-molecular ions of interest. The bridging carbonyl between the benzene rings gives the molecule a weak hydrogen bonding site. Consequently, a small response for the dimer ion ($[2M-H]^-$) was observed in the ESI spectra in the absence of modifiers. The presence of any additive except HOAc caused the dimer ion to rapidly diminish with increasing modifier concentration. Ketoprofen produced an intense $[M-H]^-$ signal and a moderate $[2M-2H+Na]^-$ signal in the absence of modifiers. The intensity of the molecular ion was increased in the presence of NH_4OAc, $(NH_4)_2CO_3$, TEA, and HOAc. The molecular ion disappeared when TFA and FA were present. This can be explained by ion suppression of the acidic analyte in the presence of acidic media, however the increase in response in the presence of HOAc indicates 'wrong-way-round' ionization[121] (negative ion formation in acidic media). Figure 3.2.10 shows the effect of the presence of modifiers on the observed intensity for $[M-H]^-$.

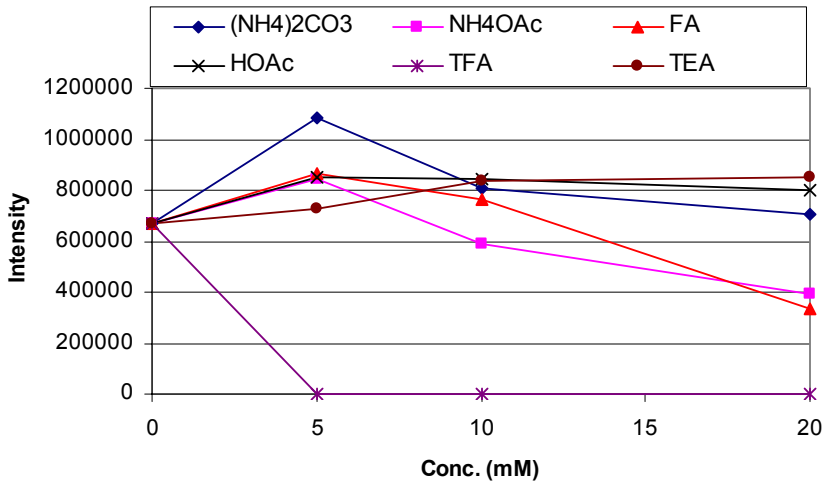

Figure 3.2.10 Effect of additives on formation of $[M-H]^-$ by ketoprofen.

The intensity of the sodium-bridged dimer ion form was also affected by the presence of modifiers. The $[2M-2H+Na]^-$ ion signal was enhanced four times by HOAc; four times by FA at low concentrations; and two to three-fold by NH_4OAc. The $[2M-2H+Na]^-$ ion was moderately suppressed in the presence of $(NH_4)_2CO_3$, and was completely suppressed when TFA or TEA was present. Figure 3.2.11 is the Hartree-Fock *ab initio* geometry optimized structure of $[2M-2H+Na]^-$ for ketoprofen at the 3-21G basis level.

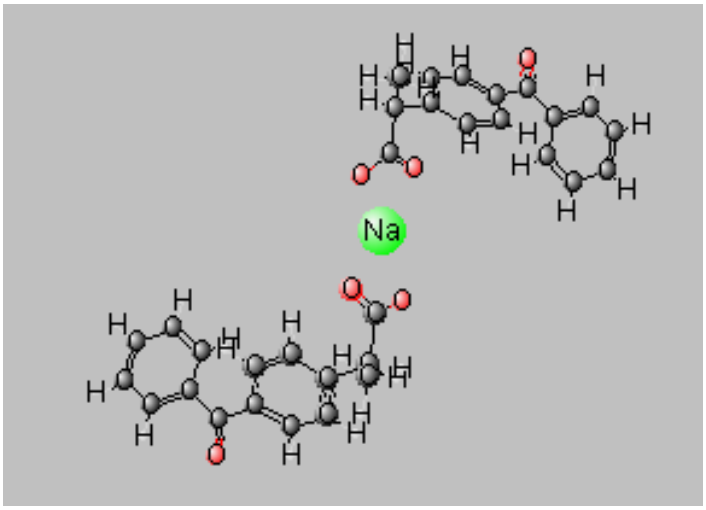

Figure 3.2.11 Geometry optimized structure for the sodium-bridged dimer pseudo-molecular ion of ketoprofen.

3.2d Naproxen

Naproxen is composed of a naphthalene ring, an acetic acid moiety, and a terminal methoxy substituent. Overall, compared to the other model compounds, naproxen represented a middle of the road functionality with moderate affinity for sodium. Naproxen formed $[M-H]^-$ (base peak) and $[2M-2H+Na]^-$ ions under a variety of conditions, but no dimer ions. Figure 3.2.12 shows the *ab initio* structure of deprotonated

naphthalene calculated at the 3-21G basis level. Naproxen lacks the necessary functionality to form hydrogen-bonded dimer complexes.

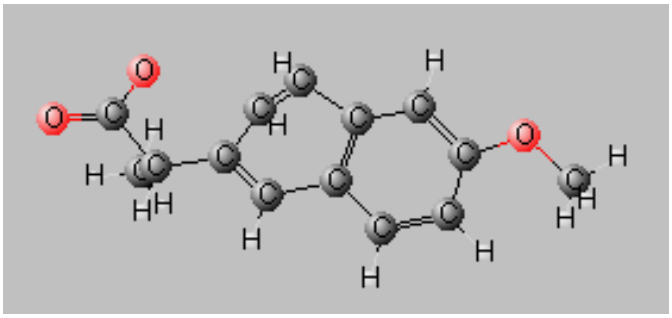

Figure 3.2.12 Geometry optimized structure of $[M-H]^-$ ion for naproxen.

Signal intensity of the $[M-H]^-$ was enhanced two-fold by the addition of 20 mM TEA and moderately enhanced by small amounts of $(NH_4)_2CO_3$ and NH_4OAc. The molecular ion signal remained largely unaffected by the addition of HOAc. Therefore molecular ion response of naproxen was enhanced in basic media, but also persisted, though slightly diminished, in acidic media such as acetic acid. Figure 3.2.13 depicts the effect of additives on formation of naproxen $[M-H]^-$ ion. Figure 3.2.14 shows the response of $[2M-2H+Na]^-$ for naproxen in the presence of the six additives. Differences in ionization of naproxen relative to the other analytes were attributed to its relatively inactive methoxy functionality and rigid naphthalene ring structure.

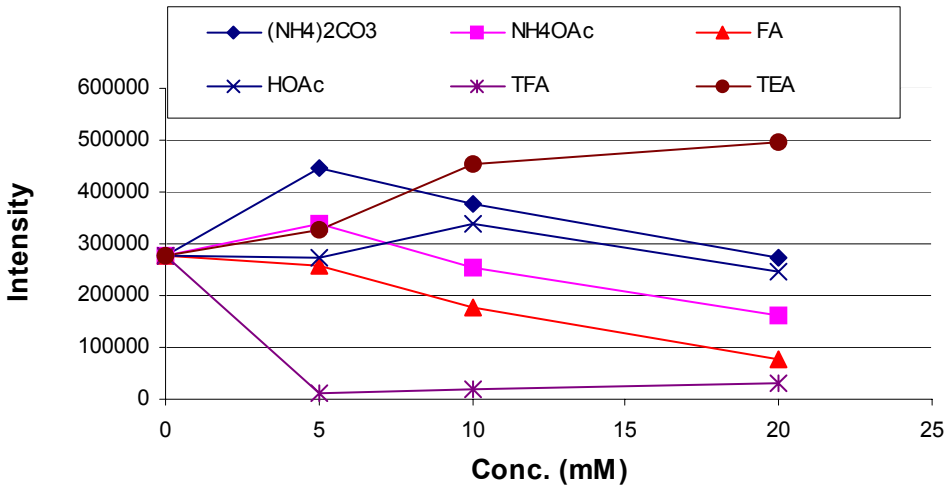

Figure 3.2.13 Effect of additives on the abundance of the $[M-H]^-$ ion for naproxen.

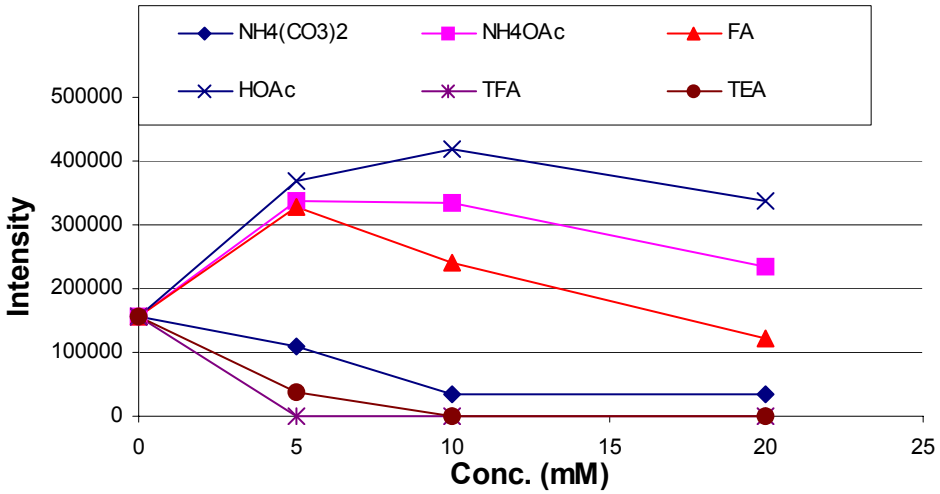

Figure 3.2.14 Effect of additives on response of $[2M-2H+Na]^-$ for naproxen.

3.2e Flurbiprofen

Under all conditions tested, flurbiprofen formed $[2M-2H+Na]^-$ as the base peak. The *ab initio* geometry optimized structure of this ion is shown in figure 3.2.15. No response was observed for either the molecular ion, $[M-H]^-$, or the dimer ion, $[2M-H]^-$.

This molecule is composed of an acetic acid functional unit bonded to an aromatic ring with an electronegative fluorine substituent bonded *meta*- and another benzene *para*- to the acid group. Intensity of the adduct ion was slightly increased at low concentrations of HOAc, NH_4OAc, and FA. The signal was diminished in the presence of TFA, $(NH_4)_2CO_3$, and TEA, but was still the base peak.

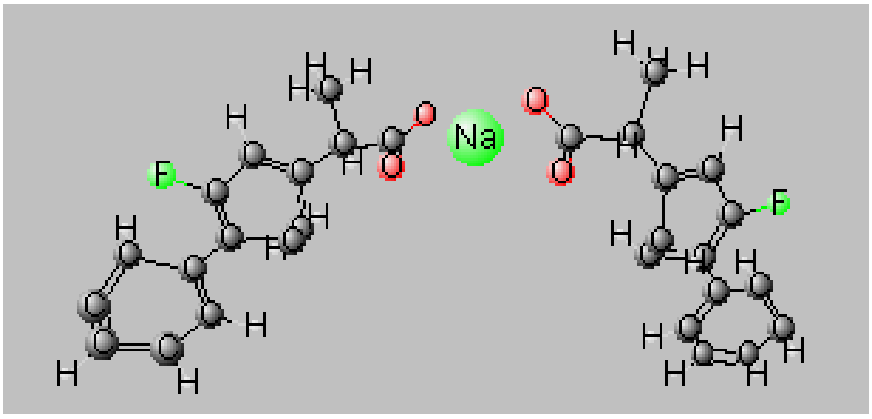

Figure 3.2.15 Geometry optimized structure of the $[2M-2H+Na]^-$ ion for flurbiprofen.

The inductive effect of the *meta*-fluorine in flurbiprofen pulls electrons away from the acid moiety and creates a more acidic analyte. The pK_a of flurbiprofen is 4.14, the most acidic of all test probes studied in this experiment. The electronegativity of the fluorine atom placement creates a highly polar molecule which readily coordinates sodium. This is supported by the complete absence of a molecular ion in the mass spectra. Figure 3.2.16 is the mass spectra of flurbiprofen in the presence of 5 mM formic acid.

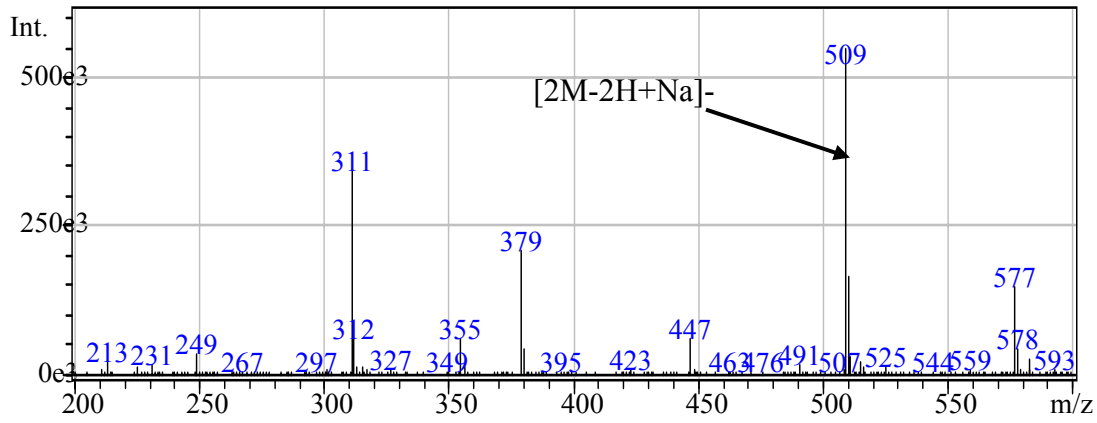

Figure 3.2.16 Direct injection ESI mass spectrum of flurbiprofen (m.w.=244) in the presence of 5 mM formic acid. Possible peaks of interest for flurbiprofen were: $[M-H]^-$, m/z = 243; $[2M-H]^-$, m/z = 487; $[2M-2H+Na]^-$, m/z = 509. Only m/z 509 corresponding to the adduct ion was present. Other spectral peaks have not been assigned, but show an interesting pattern ($[M-H+68]^-$, m/z = 311; $[M-H+2(68)]^-$, m/z = 379; $[M-H+3(68)]^-$, m/z = 447; $[2M-2H+Na+68]^-$, m/z = 577), and are assumed to be due to the presence of formic acid. The molecular weight of sodium formate is 68 amu.

3.2f Fenoprofen

Fenoprofen is a phenoxy phenyl acetic acid. Fenoprofen did not form dimers with itself under any conditions tested due to its lack of hydrogen-bonding sites. With no additives present, the ESI of this analyte produced an intense $[M-H]^-$ signal and a moderate $[2M-2H+Na]^-$ signal. Figure 3.2.17 shows the Hartree-Fock *ab initio* geometry optimized structure of deprotonated fenoprofen at the 3-21G basis level. Addition of NH_4OAc, HOAc, and FA increased the abundance of both ions. These ion enhancements were most pronounced at low concentrations of additive. In the presence of $(NH_4)_2CO_3$ and TEA, the signal for the molecular ion was effectively unchanged and the signal for the adduct ion was significantly diminished. TFA suppressed all ionization, even at low

concentrations. Figure 3.2.18 shows the effect of all additives on the $[2M-2H+Na]^-$ ion formation.

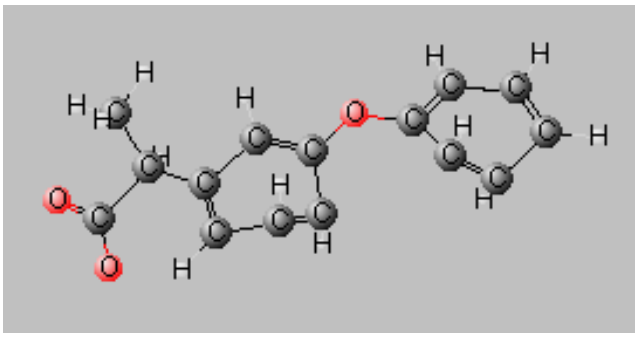

Figure 3.2.17 Geometry optimized structure for the $[M-H]^-$ ion of fenoprofen

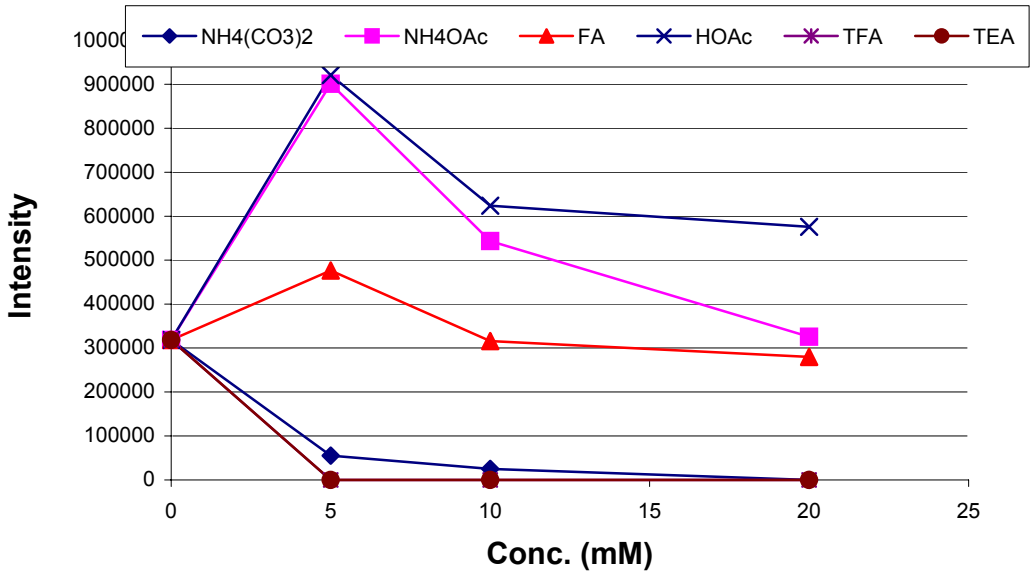

Figure 3.2.18 Effect of additives on $[2M-2H+Na]^-$ of fenoprofen.

3.3 Discussion

This experiment showed investigation of the formation of pseudo-molecular ions by negative ionization mode ESIMS in the presence of various common LC-MS additives. Results have shown that two or three common ion forms were observed for these six acidic analytes. Table 3.3.1 shows the specific ion forms observed for each ibuprofen derivative in the negative ionization mode. The ion forms corresponded to a deprotonated molecular ion ($[M-H]^-$), a sodium-bridged dimer ion pair ($[2M-2H+Na]^-$), and in some cases, a homogeneous dimer ion ($[2M-H]^-$). The effects of the additives on relative intensities of these ion forms could be attributed mainly to solution-phase behavior of the species present. In some cases, gas-phase interactions may have been present and therefore should be considered.

Table 3.3.1 Observation of specific pseudo-molecular ion species for ibuprofen derivatives during negative ionization mode FIA-ESIMS.

Analyte	$[M-H]^-$?	$[2M-H]^-$?	$[2M-2H+Na]^-$?
Ibuprofen	yes*	no	yes
Carprofen	yes	yes*	yes
Naproxen	yes*	no	yes
Ketoprofen	yes*	yes	yes
Flurbiprofen	no	no	yes*
Fenoprofen	yes*	no	yes

*Denotes base ion in mass spectra observed in a 50/50 acetonitrile/water solution system with no modifiers present.

Four of the six model compounds formed negative molecular ions ($[M-H]^-$) as the base peak in the spectra. The presence of acidic functionality on the analytes facilitated formation of a deprotonated molecular ion, especially in basic media. The differences in relative intensity and type of pseudo-molecular ion observed, as displayed in Tables 3.2.1 and 3.3.1, were attributed to functionality in the remaining structure of the molecules. The affinity of each analyte for the hydrophobic gas phase, approximated in this study by calculated log P values, has an effect on relative ionization efficiency. However, log P values calculated for the ionic species here vary little and may not have been an adequate estimation of hydrophobicity, especially in relation to a solution system that is 50% organic. Ibuprofen showed the most intense response due to its hydrophobic nature, and thus, high affinity for the gas phase relative to the other model compounds.

The observation of an increased or decreased $[M-H]^-$ ion response in the presence of modifiers could be attributed to solution phase chemistry where ionization was facilitated or hindered depending on the pH of the modifier used. An acidic analyte in basic media is expected to be ionized, presumably increasing the negative ion abundance in the mass spectra. This effect was seen when TEA was present, as depicted by Figure 3.3.1, which shows the effect of TEA on the deprotonated molecular ion of the six test probes.

When the molecules are present in acidic media where the pH of the solution is less than the pK_a of the molecule, one would expect ion suppression to take place. The observation of molecular ion peaks under these conditions suggested 'wrong-way-round' ionization was possible for these relatively small molecules. This phenomenon has been previously reported for larger molecules by Fenselau and coworkers[121] and for amino

acids by Boyd and coworkers.[122] Still, it was notable that ionization in acidic media to produce negatively charged molecular ions was possible.

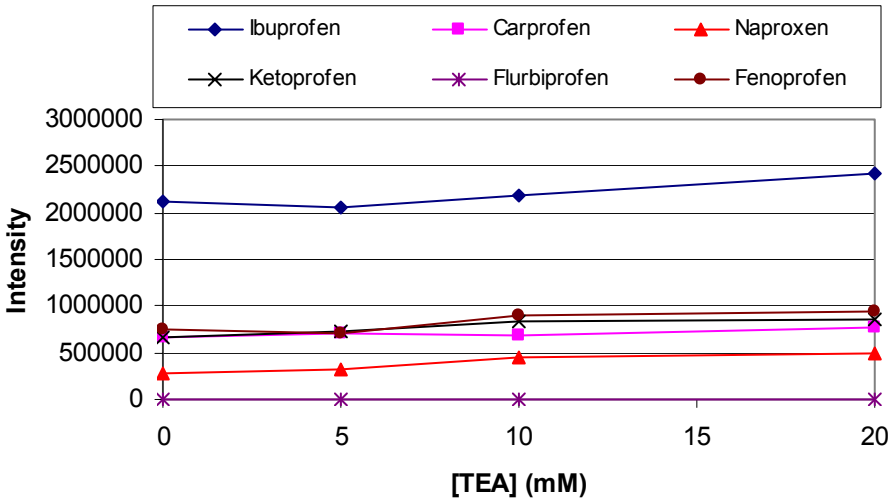

Figure 3.3.1 Effect of TEA on abundance of $[M-H]^-$ for the six acidic pharmaceuticals.

Most interesting was the formation of a sodium-bridged dimer ion pair ($[2M-2H+Na]^-$) for all of the model compounds studied. This ion species had not been previously reported in the literature. In the case of flurbiprofen spectra, the sodium-bridged dimer ion was the base peak. Complex formation between species in the system may occur in several places during the ESI process: solution-phase; gas-phase; or the point of transfer from solution-phase to gas-phase. In solution, sodium ion is known to form clusters with solvents to lower the free energy barrier for ion evaporation.[123] The Gibbs free energy for ion evaporation of a sodium-water cluster ion is approximately 40 kcal/mol more favorable than for the naked sodium ion. In the case of the ibuprofen derivatives, sodium-bridged dimer ion formation is likely a result of solution-phase

electrostatic interactions. The fact that the most abundant signal for the dimer ion pair is attributed to two *deprotonated* analytes and a sodium ion suggested that ionic interactions in solution phase are the cause of complex formation. However, alkali metals ions such as K^+ and Na^+ are known to form strongly bonded complexes to polar groups in the gas-phase during ESI.[8] Future studies on the effect of the MS inlet voltage on sodium-bridged dimer ion pair formation may provide useful information for distinguishing between formation of the sodium-bridged dimer ion in solution versus gas-phase. If an increase in MS inlet voltage leads to an increase in the signal for the $[2M-2H+Na]^-$ ion, then it can be inferred that collisions in the gas-phase are responsible for the formation of the adduct due to increased gas-phase collisions. Studies investigating the effect of concentration of analytes and additives present may also shed some light on this matter.

Geometry optimized structures of the sodium-bridged dimer ions simulated using Gaussian98 software with Hartree-Fock *ab initio* algorithms corresponding to the 3-21G level of basis showed a structure with the deprotonated carboxylic acid groups localized around a sodium ion to be the most favorable arrangement of the complex ion. Multiple arrangements were compared for simple benzoic acid sodium-bridged dimer ions to find the arrangement of the monomers about sodium which corresponded to the lowest energy. These results are discussed in the next chapter.

The fact that TEA inhibited the formation of sodium-bridged dimer ion species indicated a competing interaction between the analyte and TEA for background sodium ions. This effect could be rationalized in one of two ways depending on the point of formation (solution vs. gas-phase). If the formation of a sodium-bridged dimer ion was a solution phase phenomenon, the decrease in response due to TEA could be attributed to

steric effects which can deter binding of two carprofen ions by a sodium ion in the presence of the large alkyl amine modifier. If formation of $[2M-2H+Na]^-$ was a gas-phase phenomenon, the decrease in ion intensity could be attributed to the high proton affinity of TEA, which decreased the amount of sodium ion available for complex formation by the analyte ions. Only carprofen showed an appreciable signal for the alkali-bridged dimer ion in the presence of TEA.

The fact that the adduct ion enhancement was pronounced for ketoprofen in the presence of some additives suggests that Na^+ may complex species by coordinating with the unshared electrons on the carbonyl group. Sodium has been shown to coordinate between two carbonyl groups in a single compound, such as succinamide and glycylglycine[112], as well as to favorably bind two acetone molecules in a positively charged sodium-bridged dimer complex.[124] The pseudo-molecular ion may also be formed through dimer ion-pair interactions, where the Na^+ cation is bound between the two deprotonated ketoprofen carboxylic acid moieties. The latter case is most likely due to the mass observed (two *deprotonated* analyte ions plus sodium ion) of the dimer adduct between two deprotonated analyte molecules and Na^+. The point of contact predicted with *ab initio* calculations supports the formation of a complex with sodium through the deprotonated acid moieties.

Two of the molecules, carprofen and ketoprofen, formed homogeneous dimer ions ($[2M-H]^-$) due to the presence of hydrogen bonding sites in their structure. Association of the dimer species was most likely a product of intermolecular solution-phase interactions. These hydrogen bonded dimer ions were more surface active than their monomer counterparts and the strengths of the hydrogen bonds were strengthened upon

transition from solution to gas phase. As stated previously, the energy imparted by the ESI interface was insufficient to break these complexes prior to sampling by the mass spectrometer. Carprofen, with both an acid and an aromatic amine functionality, generated a dimer ($[2M-H]^-$) as the base peak. Hydrogen bonding was evidenced in the *ab initio* generated structure for the dimer ion by the increased bond length of the amine and carboxyl groups in the dimer relative to the unbound monomer species. This effect is detailed in Figure 3.3.2.

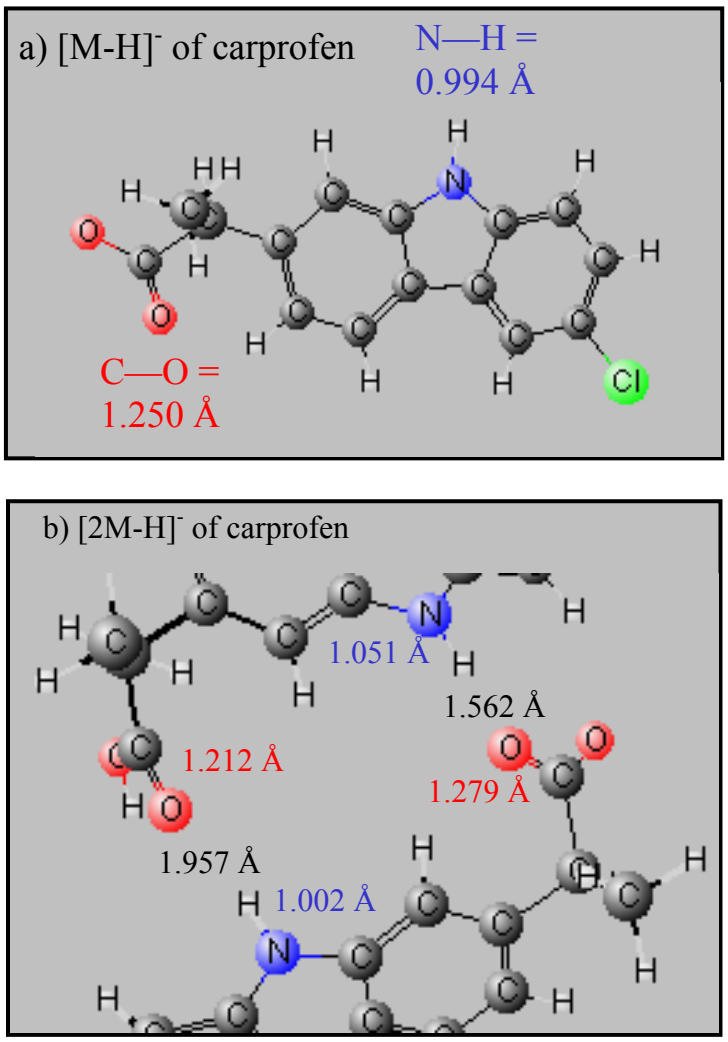

Figure 3.3.2 Hartree-Fock *ab initio* simulation of hydrogen bonding in the homogeneous dimer ion of carprofen. Hydrogen-bonding is evidenced by the increase in bond lengths of the amine and carboxyl group in the dimer relative to the deprotonated monomer. Part a) shows the bond lengths in the deprotonated molecular ion and part b) shows a magnified view of the region of hydrogen bonding approach in the dimer ion ($[2M-H]^-$).

The effect of additives on ESI of the analytes in the negative ionization mode can be summarized through the examination of trends in ion formation when the additives are present. A few specific trends are worth mentioning to summarize the results of this experiment. As previously stated, the presence of TFA suppressed all ionization of all of the analytes. Some modifiers, like TEA and ammonium carbonate, promoted the formation of molecular ion and diminished the response of adduct ion. When analytes in solution were transferred into the gas phase with TEA present, either the steric character or the high proton affinity of TEA inhibited the formation of sodium adduct species. As a result the intensity of the adduct ion decreased. Conversely, the presence of modifiers containing the acetate anion, such as NH_4OAc and HOAc, created an increase in signal for negative adduct ion species for a majority of the analytes. Acetic acid and formic acid, in particular, promoted formation of adduct ions at low concentration for all analytes except carprofen and flurbiprofen. The increase in the number adducts formed in the presence of HOAc and FA was likely due to increased sodium ions in the system from impurities in the modifiers. Adduct formation by carprofen in the presence of HOAc or FA was actually decreased. The mechanism of these phenomena was not clear. This may be explained by the relative surface activity and higher concentration of the acetate ion relative to the polar, hydrophilic carprofen molecule. The effect of $(NH_4)_2CO_3$ varied depending on the analyte, but generally inhibited formation of adduct ion as well as molecular ion.

Results of this experiment showed that the effect of various modifiers on the formation of pseudo-molecular ions was not easily surmised. Subsequent experiments served to build on the trends observed here, but focused on less complex sets of test

analytes where relative differences in response for the various ion forms could be related directly to specific substituents. Such investigations would be used to draw conclusions that were applicable to ESIMS investigations of acidic analytes. This work is directly applicable to fields where acidic analytes are encountered and is not limited to but includes biological, medical, and environmental analyses. However, those real-solution matrices may be composed of a large variety of co-analytes, such as salts and impurities. Therefore, one must careful to examine how these co-analytes affect the outcome of the mass spectral results. Separation strategies become paramount in such situations.

CHAPTER 4

Experiment 2: Substituted Benzoic Acids

4.1 Introduction

Benzoic acid (BA) and substituted benzoic acids were studied by flow injection analysis in the negative ionization mode using electrospray ionization mass spectrometry. This experiment dealt with functionally less complex molecules than those investigated in Chapter 3. Halide-substituted molecules were investigated to deduce the effect of electron-withdrawing substituents (bromo-, chloro-, and fluoro-) and ring position (*ortho*-, *meta*-, and *para*-) on the response of a deprotonated molecular ion ($[M-H]^-$) and a sodium-bridged dimer ion ($[2M-2H+Na]^-$). Amino-substituted benzoic acids were analyzed to study the effect of an additional ionizable group on the molecule and *para*-t-butyl-BA was analyzed to study the effect of increased hydrophobicity, as they relate to the formation of pseudo-molecular ions. Figure 2.3.1 depicts the structures of the analytes.

Also included in this study were a series of experiments characterizing the response of unsubstituted BA under various instrument conditions. Varying the percent acetonitrile in an acetonitrile/water system allowed an indirect study of ionization of BA relating to droplet formation, specifically the effect of the solvent dielectric on sodium-bridged dimer ion formation and the surface activity of BA in molecular ion formation. Interface conditions between the LC and MS were also studied; specifically the voltage and temperature of the curved desolvation line (CDL). The effect of the CDL voltage is akin to in-source collision induced dissociation, where a higher voltage will influence ionization of molecules in the gas-phase by initiating a greater number of collision

reactions. Often, this parameter may be used to study fragmentation of molecules; however the ion selectivity of in-source collision induced reactions is poor in comparison to modern tandem MS instrumentation. The CDL temperature was also varied to study the effect on ion formation. The heat applied to the CDL serves to decluster analyte/solvent clusters sampled from the gas phase. Thermally labile species are susceptible to decomposition when the CDL temperature is too high and inefficient declustering of gas-phase species (low ionization) can result if the CDL temperature is too low.

The effect of instrument parameters on unsubstituted BA ion formation served as a basis for establishing trends related to substituent effects as well as a means to characterize optimum operating conditions for ionization of aromatic acids. Results from these experiments served as building blocks for elucidating pseudo-molecular ion formation for species with higher functionality, such as the ibuprofen derivatives previously studied.[10] Comparison of ionization trends to tabulated and calculated solution-phase and gas-phase physical chemical data were used to deduce the point of formation of particular pseudo-molecular ions (solution phase versus gas phase) as well as the relative importance of each physical parameter in influencing negative mode ionization of aromatic acids. Hartree-Fock *ab initio* geometry optimization simulations were performed to investigate structural arrangements of the pseudo-molecular ions.

4.2 Results

The first set of experiments studied the effect of mobile phase composition and ESI source parameters on the formation of unsubstituted benzoic acid pseudo-molecular ions. For this study, 40 samples of benzoic acid were prepared at eight concentrations in the presence of five different mobile phase compositions. Benzoic acid was prepared at 0.05, 0.01, 0.005, 0.001, 0.0005, 0.0001, $1x10^{-5}$, and $1x10^{-6}$ mM concentration levels in each mobile phase: 1/99; 25/75; 50/50; 75/25; and 99/1 acetonitrile/water. Each sample was run at normal LC-MS tune parameters (CDL temperature = 250 °C, CDL voltage = -25 V). In addition, each sample was analyzed with CDL voltages of -10, -70, -120, and -180 V. The CDL temperatures investigated were 200, 250, and 300 °C. The results of these experiments are shown in Figures 4.2.1 and 4.2.2.

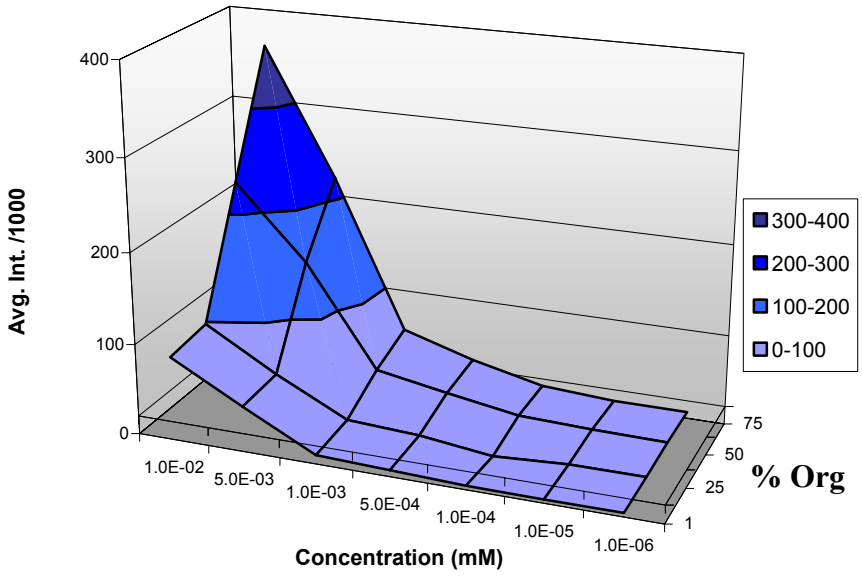

Figure 4.2.1 Plot relating response of benzoic acid molecular ion ($[M-H]^-$) to percent organic (acetonitrile in an acetonitrile/water system) as a function of concentration. Note in this figure that concentration *increases* from right to left for ease of visualizing the data.

Figure 4.2.1 shows the response of benzoic acid at different concentrations in the presence of changing mobile phase composition. As expected, ionization efficiency increased dramatically with an increase in percent organic mobile phase. A high percentage of organic allowed for the formation of smaller droplets due to decreased surface tension. This increased the ionization efficiency, and allowed a greater number of ions to evaporate into the gas phase. The results for 99% acetonitrile were not included here due to the erratic response observed at this high organic concentration. Though intensity increased as percent organic increases, a certain amount of water must be present to provide adequate conduction in the droplets. Conduction is provided by the high dielectric of water, which makes charge flow by providing separation between ionic species. At the other extreme, poor response was observed at low concentration of organic due to the large droplets formed by the high surface tension of water. Also hindering ionization was the low vapor pressure of water relative to acetonitrile, which made droplet evaporation more difficult with a low percentage of organic in the system. These studies show that there exist optimum conditions for ionization of BA in acetonitrile/water solution systems. The results suggest a lower limit of detection of BA in a mobile phase containing a high percentage of organic.

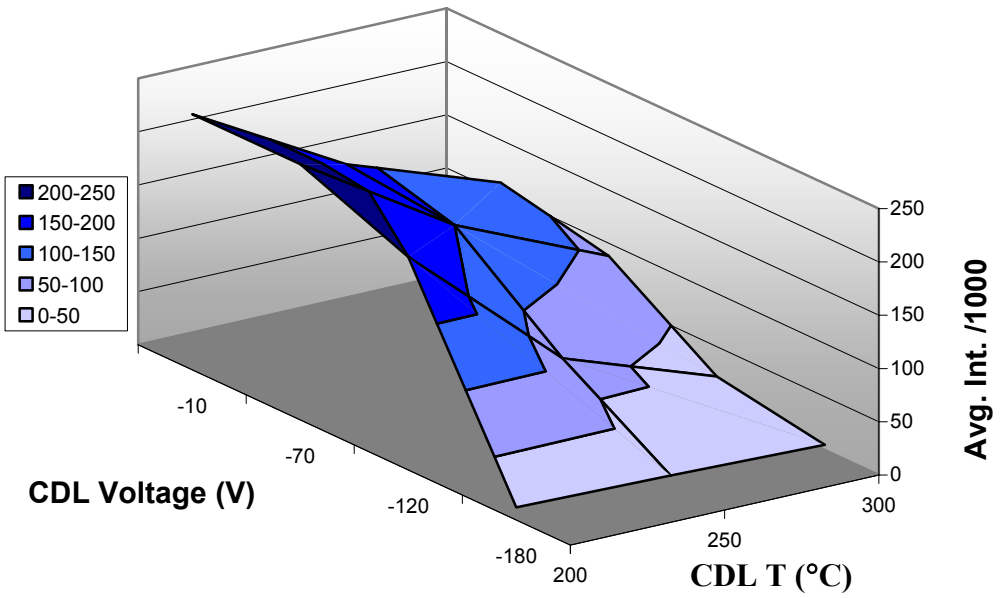

Figure 4.2.2 The effect of CDL voltage and temperature on the response of benzoic acid molecular ion ($[M-H]^-$). Benzoic acid is present here at 0.01 mM concentration.

Figure 4.2.2 shows the effect of MS inlet parameters on the response of BA deprotonated molecular ion. For this study, 0.01 mM BA was analyzed while changing CDL voltages and temperatures. The graph depicts the thermal lability of BA in response to increasing CDL temperature. Signal was diminished by almost a factor of two at 300 °C versus 200 °C. Also shown is the lack of stability of the $[M-H]^-$ ion with respect to increased collisional interactions at high CDL voltages. Signal decreased dramatically above -100 V and went to zero when the CDL voltage was set to -180 V. This study showed the relative stability of the BA deprotonated molecular ion with respect to temperature and collisional decomposition and provided guidelines for increasing ionization efficiency.

As a comparison, the same plot was made for the response of the sodium-bridged dimer ion pair in Figure 4.2.3. Notable was the exceptional stability of the $[2M-2H+Na]^-$

ion in the presence of higher temperatures and voltages. The stability of the sodium-bridged dimer ion pair explained observation of sodium-bridged dimer ion pairs in LC-ESIMS of aromatic acids under a variety of conditions.

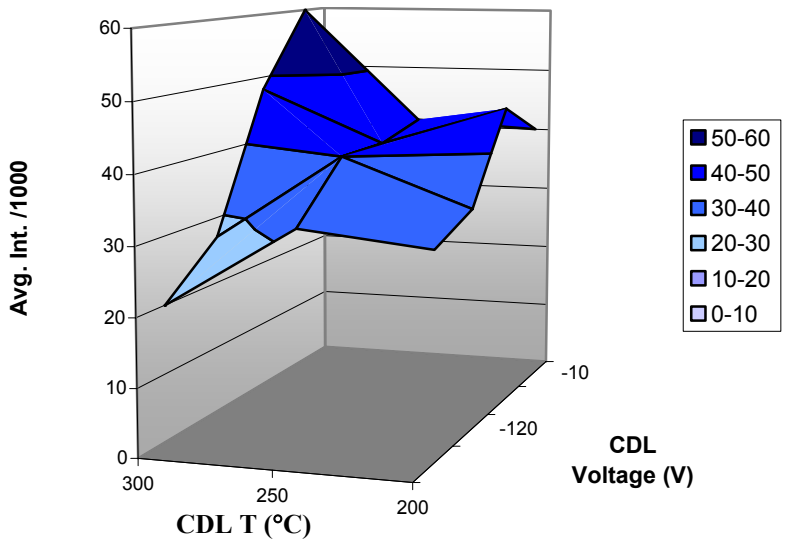

Figure 4.2.3 Effect of CDL voltage and temperature on response of the sodium-bridged dimer ion for benzoic acid. The response of this pseudo-molecular ion was greatest at CDL temperature = 300 °C and CDL voltage = -10 V.

Hartree-Fock *ab initio* calculations were used to model the structures of the $[M-H]^-$ and $[2M-2H+Na]^-$ pseudo-molecular ions of BA. These are shown in Figures 4.2.4 and 4.2.5, respectively. The deprotonated molecular ion is planar and when combined with sodium and another deprotonated BA molecule to form the sodium-bridged dimer complex ion, the most stable orientation calculated was an electrostatic interaction where sodium coordinated with the carboxyl oxygens in a perpendicular arrangement. Figure 4.2.6 shows three views of the alternate generated structure for the sodium-bridged dimer ion pair by *ab initio* Hartree-Fock calculations at the 3-21G level of basis. The Hartree-

Fock energy calculated for this structure is 0.02637 Hartree less stable than the calculated Hartree-Fock energy associated with the more stable arrangement depicted in Figure 4.2.5.

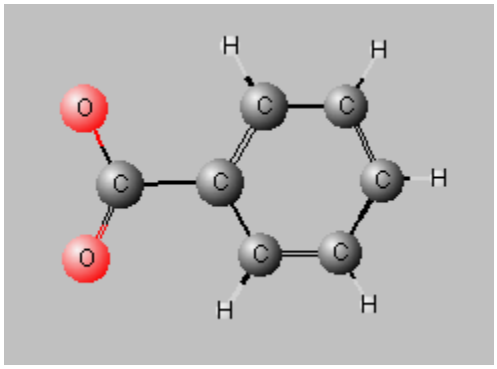

Figure 4.2.4 Deprotonated molecular ion of benzoic acid modeled with Hartree-Fock *ab initio* calculations at the 3-21G level of basis. Atoms are shown at 50% of their relative actual size.

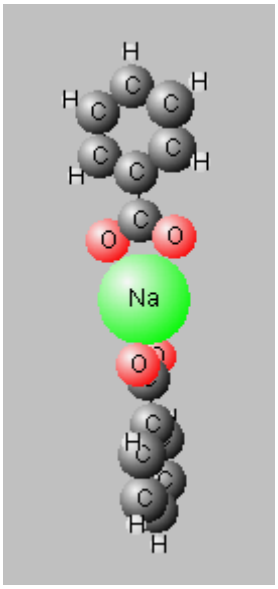

Figure 4.2.5 Most stable sodium-bridged dimer ion complex of benzoic acid modeled by Gaussian98 Hartree-Fock *ab initio* calculations at the 3-21G level of basis. Atoms are shown at 100% of their relative actual size.

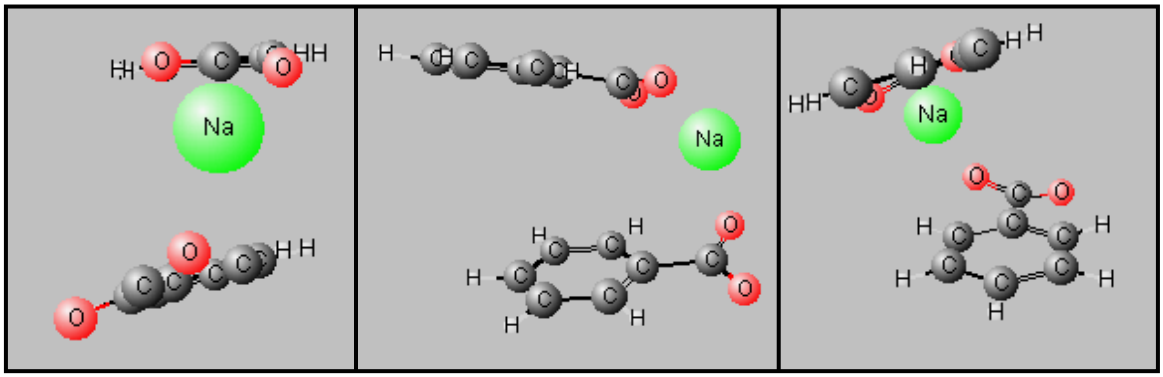

Figure 4.2.6 Three views of an alternate $[2M-2H+Na]^-$ ion form calculated by Hartree-Fock *ab initio* simulations at the 3-21G level of basis.

The next set of experiments was designed to study the effects of substituents on pseudo-molecular ion formation. Calculated solution phase data (ACDlabs SpecManager) are shown in Table 4.2.1. The values show the relative effect of each substituent on the acidity and hydrophobicity of the modified benzoic acid. Addition of electronegative groups makes the molecule more acidic and slightly more hydrophobic relative to benzoic acid. Intuitively, the addition of an electron-withdrawing group would make a molecule more ionic (e.g. less hydrophobic), however the calculated log P values show that a halide substituent actually increases the phase affinity of the molecule for a hydrophobic phase. This was further supported by the increased ionization efficiency for the halide BA molecules due to higher hydrophobic phase partitioning activity relative to unsubstituted BA. In the case of the halide-substituted BA analytes, the calculated hydrophobicity of each analyte had a better correlation with intensity than did the calculated acid/base character.

Table 4.2.1 Solution phase data for benzoic acid and substituted benzoic acid model compounds.

Analyte	pKa*	log P*
Benzoic Acid (BA)	4.2	1.89
para-F BA	4.14	2.07
para-Cl BA	3.97	2.65
para-Br BA	3.97	2.86
meta-F BA	3.86	2.16
meta-Br BA	3.81	2.71
meta-Cl BA	3.38	2.9
ortho-F BA	3.27	1.86
ortho-Cl BA	2.97	2.04
ortho-Br BA	2.85	2.15
ortho-amino BA	4.94	1.21
meta-amino BA	4.75	0.78
para-amino BA	4.86	0.001
para-t-butyl BA	4.4	3.58

Values calculated from Advanced Chemistry Development, Inc. Spec Manager (ACD labs, Toronto, Ontario, Canada).

Figure 4.2.7 shows the response of $[M-H]^-$ for the halide substituted benzoic acids. An increase in log P caused an increase in the ionization of the molecular ion. This was expected, since the molecule will have a higher affinity for the hydrophobic gas phase relative to an aqueous liquid droplet. The analyte will diffuse faster to the droplet/air interface, due to its lower affinity for the liquid droplet, thus increasing efficiency for ion evaporation. In all cases, the *meta*- position was the most active for promoting ionization. The mechanism responsible for increased efficiency of *meta*-halide substituted BA analytes is unclear. It could be speculated that substitution in the *meta*- position causes a more favorable orientation of the analyte at the droplet surface for ion evaporation.

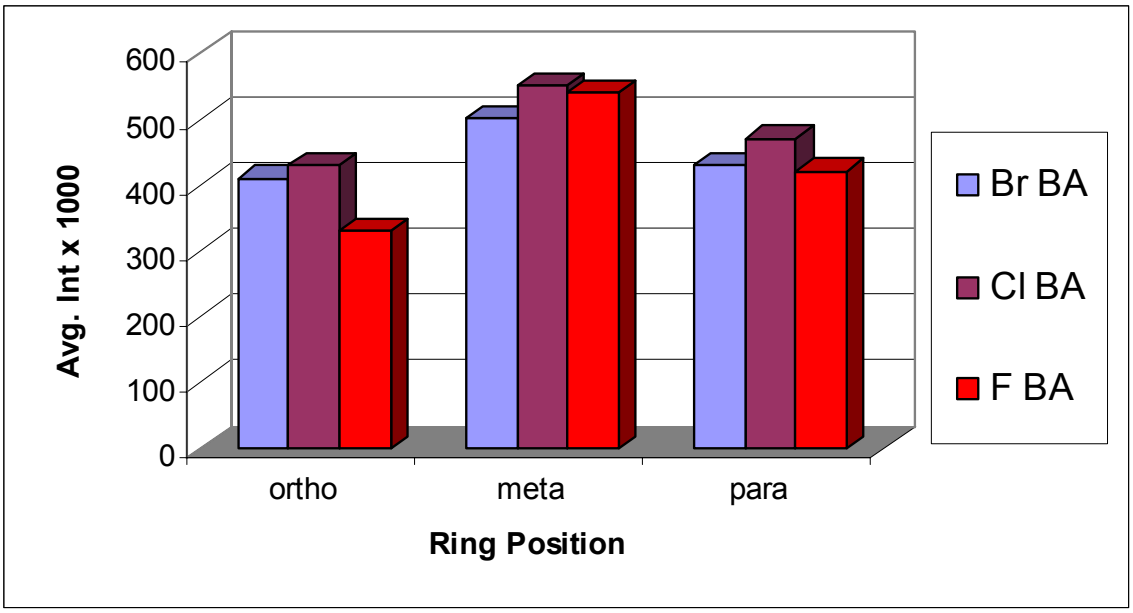

Figure 4.2.7 Response of $[M-H]^-$ for 0.01 mM halide-substituted benzoic acid model compounds in 50/50 acetonitrile/water. For these molecules, the *meta*- position appears to be the most active for enhancing the ESIMS response.

Figure 4.2.8 shows the geometry optimized structures of the halide-substituted benzoic acid molecules. All *meta*- and *para*- substituted species were planar, whereas ortho-substituted species showed a steric influence which skewed the carboxylic acid group out of the plane. The degree of steric interaction was dependent on the size of the halide atom and consequently, *ortho*-bromo BA showed the highest degree of steric strain in its most stable modeled configuration. Figure 4.2.9 illustrates the degree of steric strain in the *ortho*-halide substituted species.

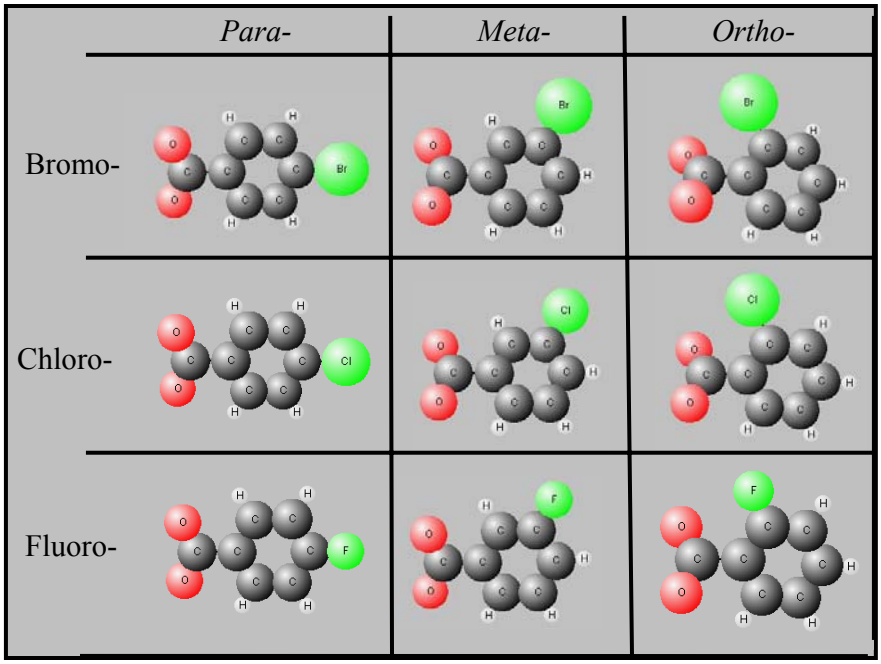

Figure 4.2.8 Hartree-Fock *ab initio* simulations for the deprotonated molecular ion of halide-substituted benzoic acid molecules. Atoms are shown at 100% actual size relative to each other.

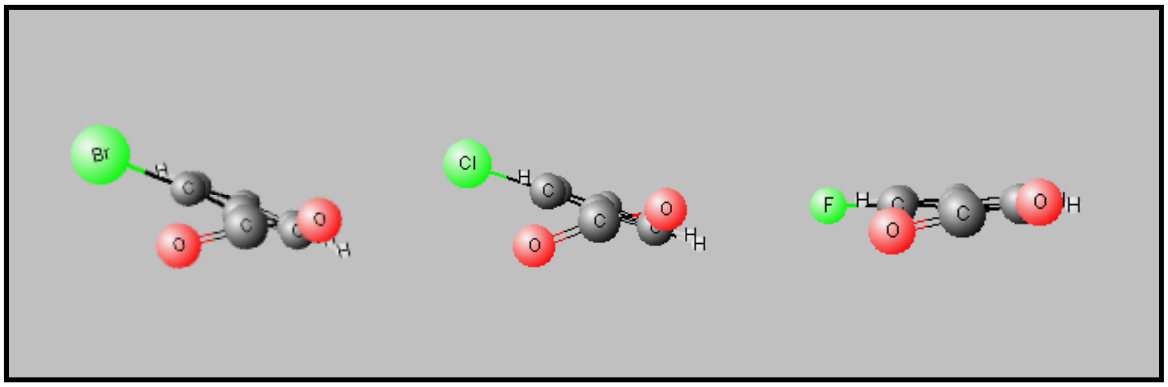

Figure 4.2.9 Steric interaction caused by halide-substituted benzoic acids in the *ortho*-position. These models depict the most stable configuration of the ion according to Hartree-Fock *ab initio* simulations at the 3-21G level of basis. Atoms are shown at 50% of their relative actual size.

Figure 4.2.10 shows the response of the dimer ion pair ($[2M-2H+Na]^-$) for the halide-substituted benzoic acids. These data correlated best with changes in pK_a associated with electronegative groups. Molecules with lower pK_a (higher acidity) values formed higher intensity dimer ion pair ions relative to BA. This was rationalized by the greater availability of coulombic sites for background Na^+ ion to associate with the deprotonated acid molecules. A greater amount of deprotonated species allows for more species to coordinate with sodium, thus increasing the observed $[2M-2H+Na]^-$ ion abundance. However, within a set of halide-substituted BA compounds (e.g. *ortho*-, *meta*-, and *para*-chloro BA), the intensity of $[2M-2H+Na]^-$ increased with pK_a. In other words, *meta*- and *para*-chloro BA have a higher intensity despite being less acidic. This trend holds for all of the halide-substituted BA models and may be explained by the steric hindrance in the *ortho*- position which interferes with the approach and complex formation by Na^+. The highly electronegative atom in the *ortho*- position limits the potential approach of a sodium ion. The sodium ion can be encapsulated by the deprotonated oxygen atoms when approaching opposite the halide group. Then, the nonlinear skew caused by the atoms in close proximity, lowers the stability of the complex. In other words, normal axial rotation of the oxygens about the sodium ion when the complex is formed becomes hindered with the halide in the *ortho*-position.

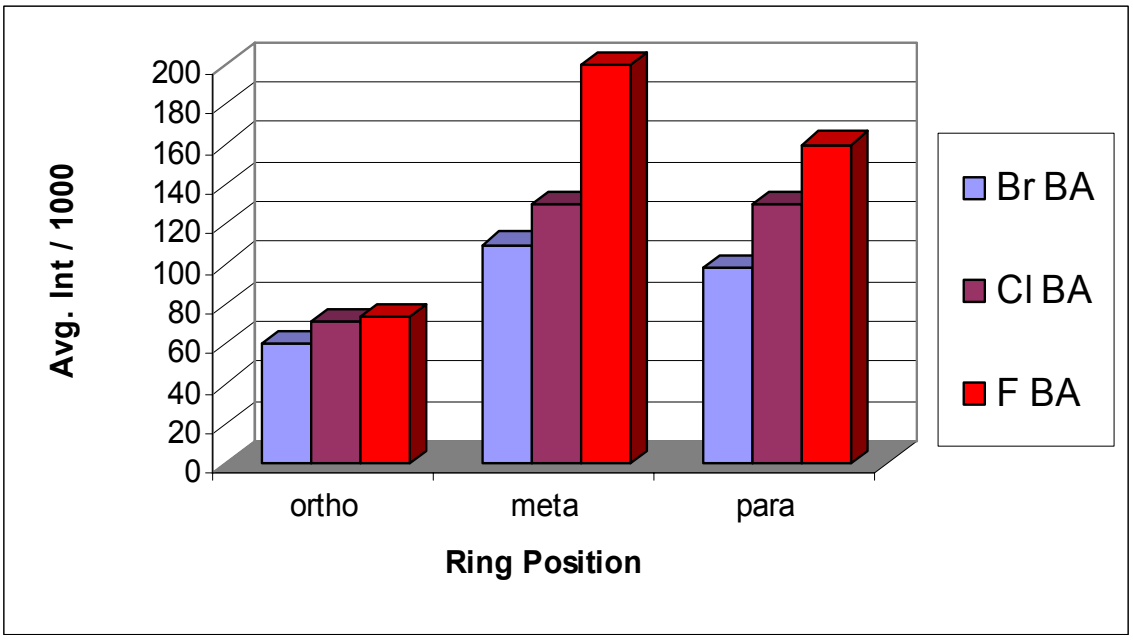

Figure 4.2.10 Response of $[2M-2H+Na]^-$ for 0.01 mM halide-substituted benzoic acid model compounds in 50/50 acetonitrile/water.

The simulated models for the sodium-bridged dimer ion complexes for the halide-substituted BA molecules showed that the most favorable interaction was induced when the monomers were placed perpendicular on-axis about the sodium. Strain induced by the *ortho*-subtituted species can be correlated with the experimental results where this species was observed with decreased response relative to the *meta*- and *para*- substituted species. Bromine induced the most strain and as such, had a lower response than *ortho*-chloro or *ortho*-fluoro substituted BA complexes with sodium. Figure 4.2.11 depicts the *ab initio* modeled structures of the sodium-bridged dimer ions for the *ortho*-halide substituted species. Figure 4.2.12 shows the structures modeled for the *meta*- and *para*-halide substituted sodium-bridged dimer ion complexes

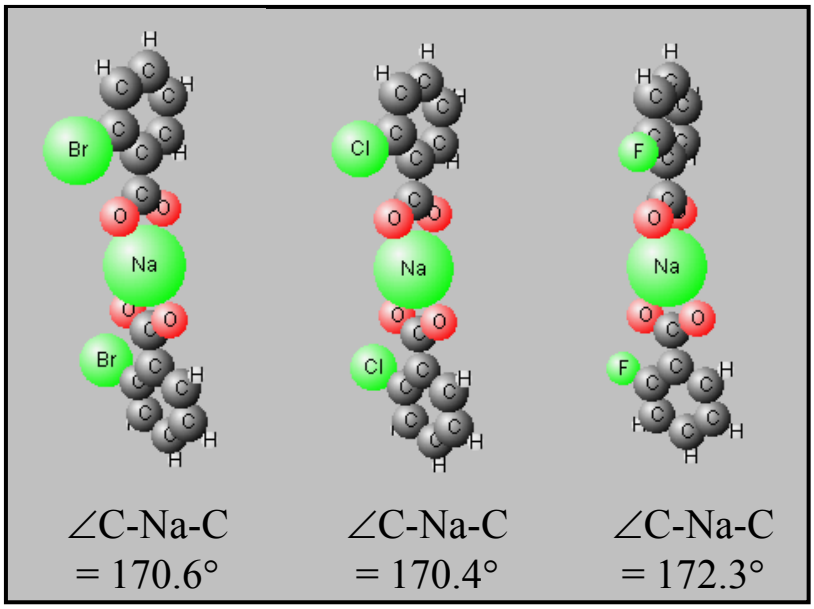

Figure 4.2.11 *Ab initio* Hartree-Fock structures modeled at the 3-21G level of basis for the *ortho*-halide substituted sodium-bridged dimer ion species. Calculated angles correspond to those between the terminal carbons in the complex and sodium.

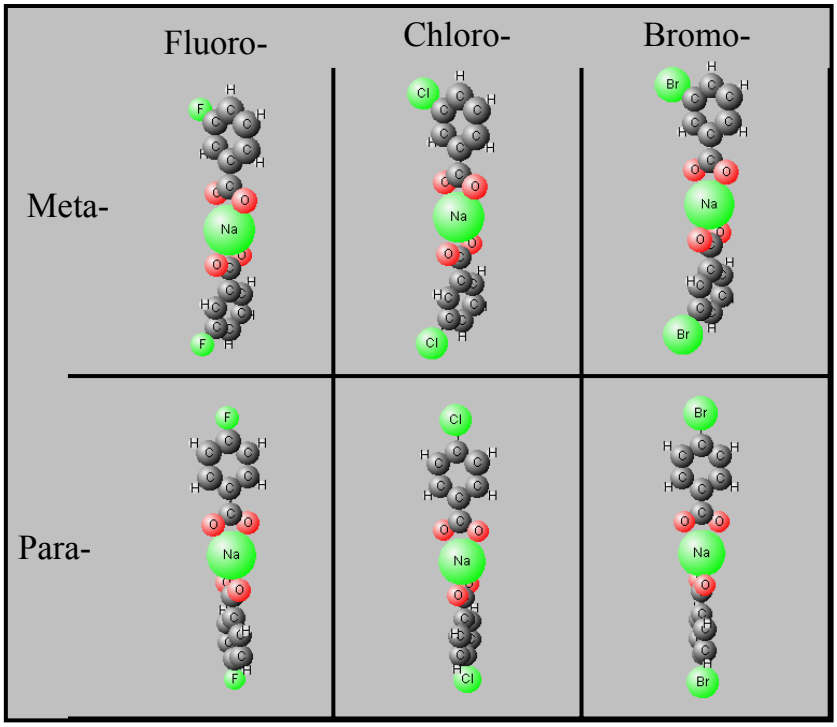

Figure 4.2.12 Modeled structures for *meta*- and *para*-halide substituted benzoic acid complexes performed by Hartree-Fock *ab initio* calculations at the 3-21G level of basis. Bond angles made between terminal carbons in the complex and sodium are essentially 180°.

Amino- and t-butyl-substituted benzoic acids were also analyzed under the same conditions as the halide-substituted compounds. T-butyl BA, with a much higher log P (3.58) was more hydrophobic. Consequently, with a higher affinity for the hydrophobic gas phase, the ion intensity for the molecular ion was enhanced nearly ten-fold compared to unsubstituted BA. Figure 4.2.13 shows the geometry optimized structure for t-butyl BA at the 6-31G(d) level of basis. The amino-BA data were not as easy to interpret. The amino substituent caused an increase in pK_a which should have increased dimer ion pair formation; however the effect of ring position on pK_a was minimal whereas its effect on dimer ion pair response was significant.

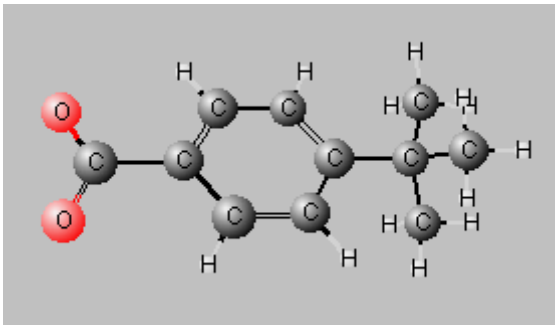

Figure 4.2.13 Hartree-Fock *ab initio* geometry optimized simulation for t-butyl benzoic acid at the 6-31G(d) level of basis. Atoms are shown at 50% of their relative actual size.

A greater effect of substituent position is shown for *ortho*-, *meta*-, and *para*-amino benzoic acid. As with the halide-substituted BA model compounds, the response of the amino-substituted molecular ion ($[M-H]^-$) follows the trend of log P values (e.g. *ortho*-amino BA has the highest log P value and the highest response whereas *para*-amino BA has the lowest log P value and the lowest response). Still, log P values for the amino-substituted species are very low due to the presence of multiple ionizable groups on the molecule. Figure 4.2.14 shows the geometry optimized structures of the amino-substituted BA $[M-H]^-$ pseudo-molecular ions.

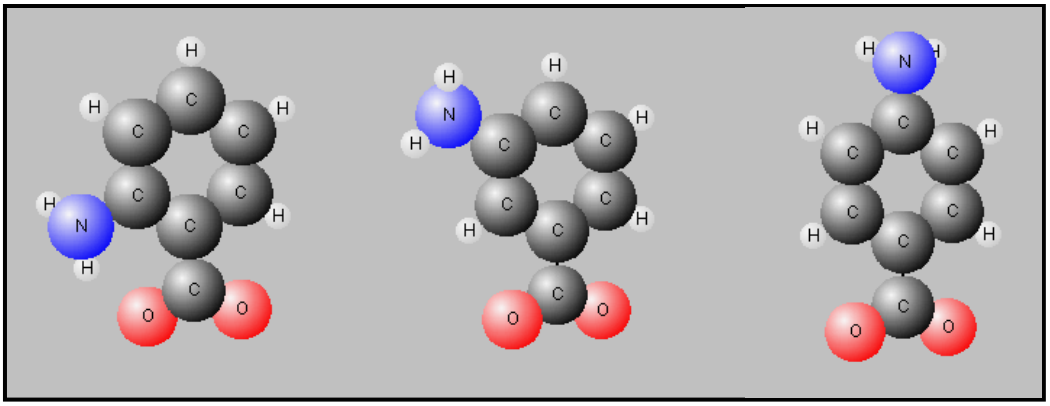

Figure 4.2.14 Hartree-Fock *ab initio* geometry optimized structures for *ortho*-, *meta*-, and *para*-amino BA [M-H]- pseudo-molecular ion forms at the 6-31G(d) level of basis.

The response of the sodium-bridged dimer ion pair for amino-substituted BA *did not* conform to the trend observed with halide-substituted BA where increased ionization was observed with increased pK_a. Instead, response of $[2M-2H+Na]^-$ was most intense for the *ortho*-amino substituted species and was least intense for the *para*-amino substituted species; the same trend that was observed for the deprotonated molecular ion. As a result, these data show that the increase in complexity of a molecule with increased functionality makes predictions of ionization response for pseudo-molecular ions from solution-phase data more difficult. Figure 4.2.15 shows the response for the molecular ion and the dimer ion pair of the amino-substituted species by FIA-ESIMS in the negative ionization mode.

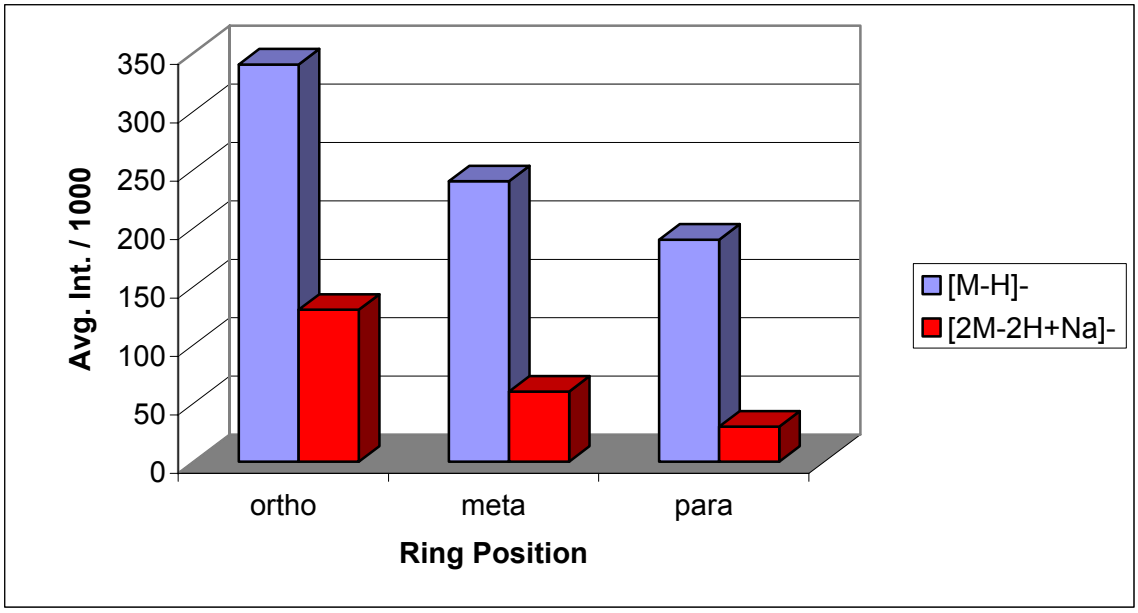

Figure 4.2.15 Electrospray ion response of the deprotonated molecular ion ($[M-H]^-$) and the sodium-bridged dimer ion ($[2M-2H+Na]^-$) for *ortho*-, *meta*-, and *para*-substituted amino benzoic acid analytes.

4.3 Discussion

Results presented here seek to correlate solution phase behavior calculated by theoretical methods to responses of pseudo-molecular ions formed by a simple set of substituted benzoic acid molecules. Calculated values of pK_a for the molecules represent the acid/base nature of the analytes. Values for log P were calculated and used as an approximation of the relative phase partitioning ability of the analyte. The solution phase system employed was a mixture of acetonitrile and water. The calculated solution phase values for pK_a and log P assume a completely aqueous liquid phase. Therefore, this information is useful only for relating qualitative trends in ionization.

Unsubstituted benzoic acid responses of $[M-H]^-$ showed a high degree of variation depending on the solution system (percent organic) and the instrumental parameters (CDL temperature and voltage) used. An increase in response was observed with increased percent organic, however some water must be present to increase the dielectric of the system and allow charge to flow. At low percentages of organic, ionization efficiency was hampered by the low vapor pressure and high surface tension of water which dominated the liquid phase, decreased the vapor pressure of the liquid phase and increased the size of the initial droplets formed. The response of benzoic acid decreased when high temperature and voltages were applied to the MS inlet line, owing to the thermal and collisional lability of the benzoic acid molecule. The responses for $[2M-2H+Na]^-$ were shown to be very stable with little variation when subjected to increased voltages and temperatures. The sodium-bridged dimer ion form showed little variation with solution composition, and increased only slightly with an increase in percent

organic. Figure 4.3.1 shows the effect of solution composition on benzoic acid pseudo-molecular ion responses.

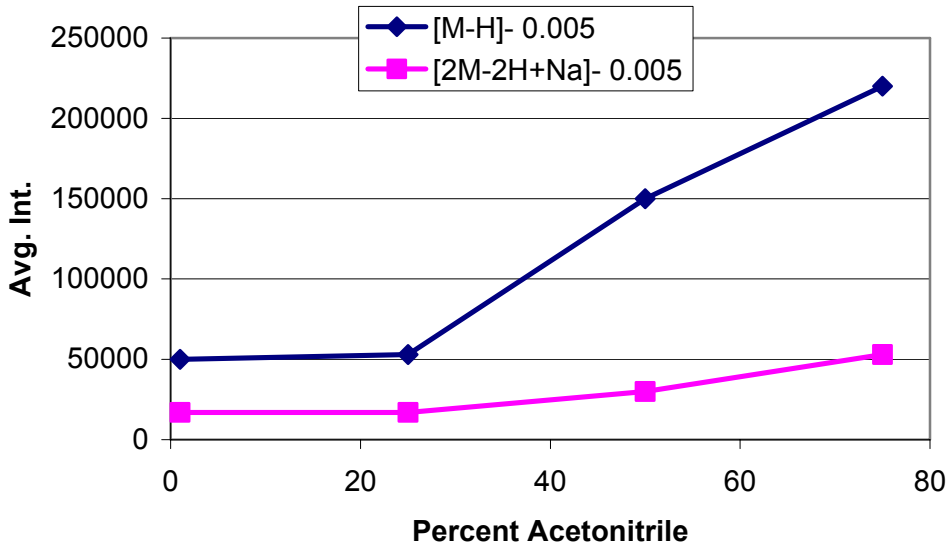

Figure 4.3.1 Effect of percent organic in solution on the intensity of the deprotonated molecular ion and sodium-bridged dimer ion for benzoic acid.

Incorporating halide substituents into the benzoic acid molecule changes the molecule's solution phase behavior. This change is approximated by calculated values for pK_a and log P of the analytes. Figure 4.3.2 shows: in part a), the change in intensity with change in pK_a values; and in part b), the change in response relative to the change in calculated log P values. Differences in ionization for the halide-substituted benzoic acids correlate better with log P values rather than pK_a values, meaning that the affinity for the hydrophobic gas phase induced by a higher degree of hydrophobicity, has a greater effect on ionization efficiency than the relative acid/base nature of the analyte.

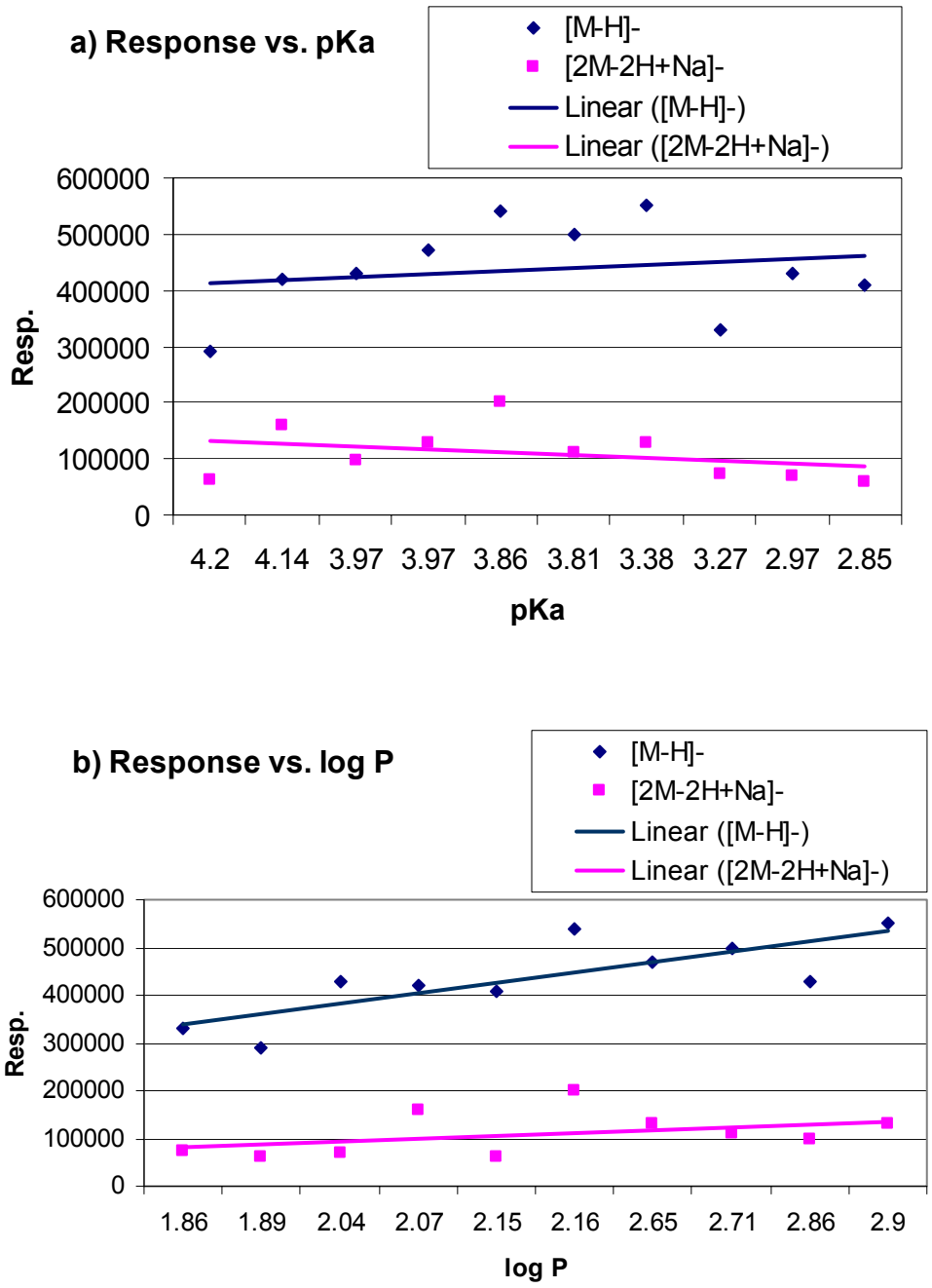

Figure 4.3.2 Effect of: a) pK_a; and b) log P on the ionization response for benzoic acid and halide substituted benzoic acids.

Relating pK_a and log P to the formation of sodium-bridged dimer ion does not appear to be straightforward. The response of $[2M-2H+Na]^-$ showed a higher degree of

variability and was almost independent of both of these solution parameters. Two important points must be considered. First, the calculated log P and pK_a values for the monomer species are certainly not the same as if corresponding values for the sodium-bridged dimer ions were calculated. Also, the relative differences between log P values for the $[2M-2H+Na]^-$ complexes are not expected to change much for different halide substituents. Secondly, the minimal effect of solution phase parameters on the sodium-bridged dimer ion responses could be evidence that these species are controlled by gas-phase processes, rather than solution-phase association.

While the substitution of the amine group at different positions on the aromatic ring had little effect on the acidity of the acid group, the observed trend for ionization response as a function of ring position was: *ortho-* > *meta-* > *para*-amino BA. This trend was observed for the response of both $[M-H]^-$ and $[2M-2H+Na]^-$ and correlates most readily with the trend of calculated log P values for the model compounds. When hydrophobicity of the molecule is drastically increased, through the substitution of a *para*-t-butyl group, there is a drastic increase in response in negative ionization mode ESIMS. The ionization efficiency of 4-t-butyl BA is approximately ten times greater than unsubstituted BA. A comparable example in the previous experiment (Chapter 3) is the increased ionization efficiency for deprotonated ibuprofen, due to the increased hydrophobicity imparted by its propyl alkane tail, relative to the other ibuprofen derivatives.

Though this experiment shows log P to be paramount in controlling the intensity of $[M-H]^-$, processes in the gas-phase should not be disregarded, especially when considering formation of $[2M-2H+Na]^-$. Table 4.3.1 lists gas-phase physical chemical

data for the proton affinity and gas-phase basicity of a few common molecules.[125] Although data for most of the molecules used in this study were not available, benzoic acid is included as well as the effect of electronegative substituents on these parameters for other species. The gas-phase basicity (GB) and proton affinity (PA) of a molecule characterizes its behavior in the gas-phase. Simply defined, the GB is $-\Delta G_{rxn}$ and the PA is $-\Delta H_{rxn}$ for a simple gas-phase protonation reaction: $M + H^+ \rightarrow MH^+$.[37]

Table 4.3.1 Gas-phase basicities and proton affinities for selected analytes.

Analyte	Gas-Phase Basicity (kcal/mol)	Proton Affinity (kcal/mol)
triethylamine	224.5	232.3
formaldehyde	221	229
aniline	202.5	209.5
3-iodo-aniline	201.1	208.9
4-chloro-aniline	201	208.6
3-bromo-aniline	200.3	208.1
4-fluoro-aniline	200.3	208.1
3-chloro-aniline	199.4	207.2
3-fluoro-aniline	199.2	207
benzaldehyde	192.4	200.2
4-chloro-benzaldehyde	192.4	200.2
4-fluoro-benzaldehyde	191.4	199.1
benzoic acid	*189.6*	*198.2*
3-fluoro-benzaldehyde	188.7	196.5
acetic acid	181.7	190.2
acetonitrile	*180.6*	*188.4*
ethanol	180.2	188.3
methanol	174.1	181.9
water	*159*	*166.5*
nitrogen gas	111	118.2

Values for benzoic acid, acetonitrile, and water are italicized. Values for the substituted benzoic acids were not available in the literature.[125]

The values in table 4.3.1 allow deductions concerning the relative gas-phase behavior of benzoic acid as well as the effect of halide substitution on shifts in values for GB and PA in a structurally similar model compound set (e.g. benzaldehyde, 4-chloro benzaldehyde, 4-bromo benzaldehyde, etc.). The first point to note is that the PA and the GB of benzoic acid is higher than both acetonitrile and water. If sodium-bridged dimer ion species are formed in the gas phase and if we assume that PA is applicable to association of species with sodium ion, then it follows that benzoic acid will have a greater affinity for sodium ion than both water and acetonitrile and adduct ions will be observed. This hypothesis is consistent with our observations.

The next point to note is the shift in GB and PA values with halide substitutions. Included in table 4.3.1 are values for aniline and aniline derivatives, as well as, benzaldehyde and benzaldehyde derivatives. In both cases, the PA and GB of halide-substituted species are slightly lower than the PA and GB of unsubstituted species. As a consequence, it is expected that halide-substitution would cause a decrease in the affinity for sodium ion in the gas-phase. This does not agree with the data observed in this study and suggests that either the point of association of sodium-bridged dimer ion is in the solution phase and is controlled by solution phase behavior or relative effects of halide substitution on benzoic acid derivatives do not follow the same trends observed for aniline and benzaldehyde derivatives. Other interactive forces, such as the increase in carbonyl charge density due to halide substitution leading to a higher degree of gas-phase association, may also be important. To differentiate between these effects, it would be necessary to perform a similar study to what is presented here, except using a model

compound set, such as benzaldehyde and halide-substituted benzaldehyde, where gas-phase physical chemical data is established.

Ab initio computer simulations may also prove useful in deducing the effect of halide substitution on the electronic structure of the benzoic acid derivatives. These calculations have not been previously reported in the literature. Table 4.3.2 shows the change in deprotonated carboxylic charge density with halide-substitution on benzoic acid calculated by Hartree-Fock *ab initio* calculations at the 6-31G(d) level of basis. It is evident that placement of an electron withdrawing group on the benzoic acid ring withdraws negative charge from the carboxylic oxygen atoms, resulting in a more acidic structure. In other words, a decrease in charge density lowers the affinity of the molecule for a proton. The effect of halide ring position on charge density has a less marked effect. Differences between calculated values may be too small to draw quantitative conclusions at this level of basis. Qualitatively, acidity of the molecule is increased as each halide is moved closer to the carboxylic acid (*ortho*- > *meta*- > *para*-). These data support the increase in response of the $[M-H]^-$ pseudo-molecular ion when halide substitution is incorporated into the structure relative to unsubstituted BA.

Differences in ionization relating to the formation of the $[2M-2H+Na]^-$ do not follow the trends established by *ab initio* calculations. Instead, it is assumed that steric interactions play a greater role in formation of the sodium-bridged dimer ion especially with respect to the decrease in response for *ortho*-, relative to *meta*- and *para*- substituted species. Response of *meta*- and *para*- substituted species are very similar as evidenced by the data shown previously in Figure 4.2.9. Figure 4.3.3 shows the results of charge

density placement about the atoms in a geometry optimized *ab initio* calculation by Gaussian98 for *meta*-fluoro benzoic acid.

Table 4.3.2 Deprotonated carboxylic acid charge density as a function of halide substitution calculated by the Hartree-Fock *ab initio* method at the 6-31G(d) level of basis.

Molecule	Charge density* COO^-
Benzoic Acid	-0.790
p-fluoro BA	-0.747
m-fluoro BA	-0.742
o-fluoro BA	-0.735
p-chloro BA	-0.743
m-chloro BA	-0.741
o-chloro BA	-0.726
p-bromo BA	-0.742
m-bromo BA	-0.741
o-bromo BA	-0.723

*Data presented as an average of the charges calculated for both oxygens on the deprotonated carboxylic acid group.

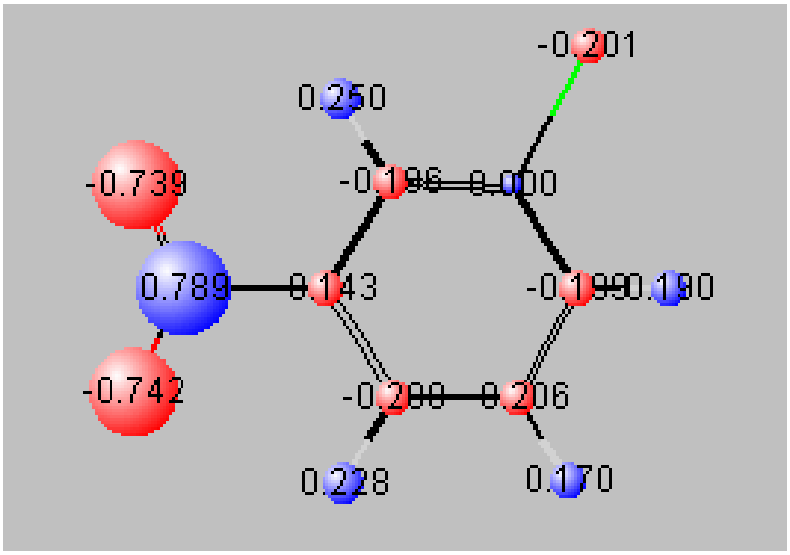

Figure 4.3.3 Placement of charge density about the atoms in *meta*-fluoro benzoic acid according to *ab initio* calculations performed by Gaussian98 with the 6-31G(d) basis set.

CHAPTER 5

Experiment 3: pH and Concentration Effects in FIA-ESIMS

5.1 Introduction

Due to the effect of solution environment on pseudo-molecular ion form and the recent finding of the recurrence of a sodium-bridged dimer ion complex formed by aromatic acid analytes in negative ionization mode ESIMS[10], an evaluation of the effect of pH and concentration on ionization efficiency was a logical extension of this research. Results from this experiment were used to correlate hypotheses derived in preceding experiments, specifically related to the formation and behavior of the $[2M-2H+Na]^-$ ion complex.

This work demonstrated the effect of injection volume, concentration, and pH on the pseudo-molecular ion formation for para-amino-benzoic acid (PABA) during FIA-ESIMS. All samples were monitored in both the positive and the negative ionization modes. PABA is a small aromatic acid that is known to form a molecular ion ($[M-H]^-$, m/z = 136) and a sodium bridged dimer pseudo-molecular ion ($[2M-2H+Na]^-$, m/z = 295), both in the negative ionization mode.[10] The presence of amine functionality was expected to facilitate ionization in positive ionization mode ESIMS as well. Experiments presented here were designed to monitor changes in pseudo-molecular ion intensity due to changes in the following solution and instrumental parameters: 1) five different injection volumes; 2) five PABA concentrations; and 3) four pH values. The pH of the sample solutions were adjusted in two ways to comprise a study of routine solution pH adjustment as recommended by the Handbook of Chemistry and Physics[119] versus pH adjustment common to routine LC-MS method development. Simple statistical analyses

are presented for comparing data from each sample set. Specific attention was made to the precision of ion response data relative to the shape of the ion chromatogram.

Done properly, FIA-ESIMS can be a convenient tool for both simplistic and complex investigations. Analysis times are generally short (minutes), instrumental settings can be easily adjusted for optimum operation, and relevant ionization efficiencies can be monitored for a variety of analyte systems. The technique allows for investigation of interactions of species in the gas phase and in the solution phase. Selectivity and molecular recognition experiments can be easily devised by simply mixing analytes and selectivity agents in a solution for flow injection. The drawbacks of the technique are: matrices and samples which are complex and require separation cannot be analyzed because all species in the sample are ionized simultaneously; sample preparation of multiple solution compositions can be time-consuming and cumbersome; and relative comparison investigations require that instrumental parameters remain constant between given data sets.

The use of FIA in analytical research had rarely been investigated in detail, according to the literature. The use of FIA for ESIMS research was often addressed indirectly. Many studies incorporate small injection volumes for scouting purposes,[11, 126-128] but if reliable qualitative and quantitative data are desired, the sample must be introduced in a manner so as to achieve quasi-equilibrium in the spray chamber.[31,35] It was critical to use large injection volumes or continuous infusion of samples to observe true ionization efficiencies as evidenced by the appearance of a plateau region (constant intensity) in the mass spectrum. Introduction of a broad band of sample solution and sampling the mass spectral data in the middle of the plateau (around the peak centroid)

region ensured the results would not be influenced by mixing with the flowing mobile phase and that a sufficient number of scans could be taken across the mass spectrum for accurate and reproducible results. The mobile phase acted simply as a carrier of the sample band since no chromatographic separation phase was present to provide mixing.

5.2 Results

Separate experiments were performed to evaluate the change in response of PABA pseudo-molecular ions in positive and negative ionization mode FIA-ESIMS due to injection volume, analyte concentration, and pH of solution. Each experiment is addressed individually below.

5.2a Injection Volume and Analyte Concentration

Five injection volumes (10, 20, 100, 200, and 400 μL) and five analyte concentrations (0.01, 0.1, 0.5, 1.0, and 2.0 mM) were investigated to assess the effect on pseudo-molecular ion response for PABA. Figure 5.2.1 shows the relative response for the total ion chromatogram (TIC) obtained at each injection volume with the analyte present at 0.5 mM concentration in a 50/50 acetonitrile/water solution system with no modifiers. The appearance of a plateau, or quasi-equilibrium, region showed a constant response was obtained when large injection volumes were employed. This indicated the applicability of ESIMS as a concentration-sensitive detector at this analyte concentration. It has been shown previously that this behavior is dependent on the analyte concentration.[129] Our results are consistent with this assessment by Henion and coworkers.

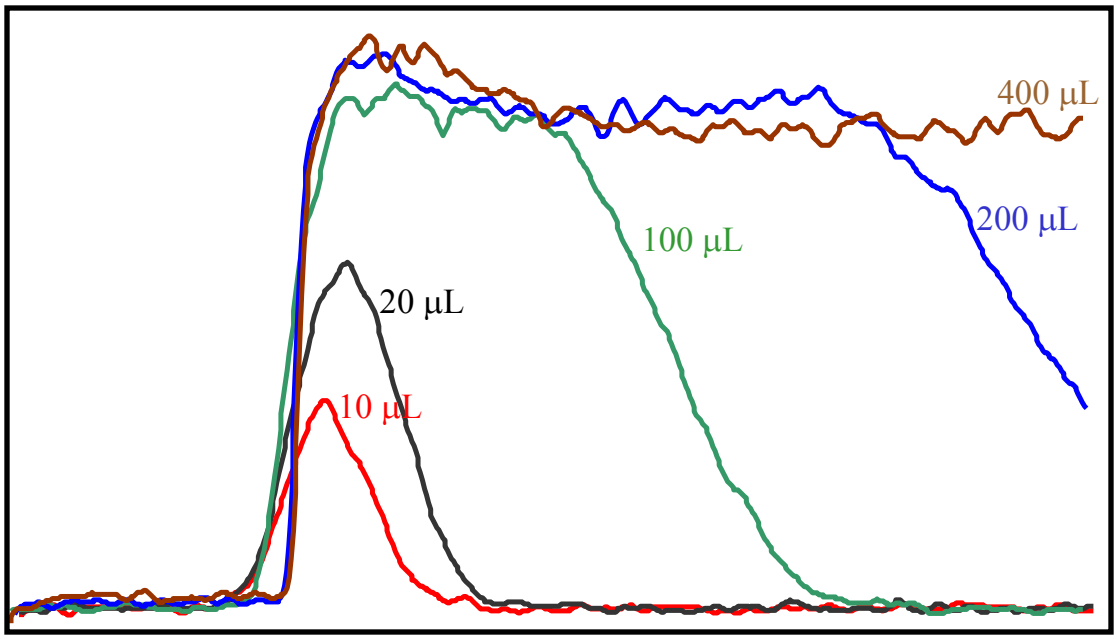

Figure 5.2.1 Flow injection profiles for the total ion chromatogram of 0.5 mM PABA at five injection volumes in the negative ionization mode.

Statistical assessment of the scan region can give information for the most reproducible selection of ions. Figure 5.2.2 and Table 5.2.1 detail the results, including scan-by-scan reproducibility, for two pseudo-molecular ions, $[M-H]^-$ (m/z = 136) and $[2M-2H+Na]^-$ (m/z = 295) (where M = PABA) across the 5 injection volumes for 0.5 mM PABA. The data is presented for the average of the scans incorporated in the region between the centroid minus 25% and plus 25% of the total scan number (denoted as $Scan\#_{50\%}$, with a relative standard deviation $RSD_{50\%}$). For example, if a response in the total ion chromatogram (TIC) was composed of 1000 individual scans, then $Scan\#_{50\%}$ would correspond to the spectral average between scan 250 and scan 750 in the TIC and $RSD_{50\%}$ would correspond to the relative standard deviation for the response of a particular m/z in that region. This procedure was used to simulate the sampling of the ion chromatogram to obtain a typical mass spectrum average of the intensities of ions. When

a plateau ion chromatogram response was observed (≥100 μL injection volume), the average of the scans across the heart of the plateau region (centroid ± ~5% scans) (denoted as $Scan\#_{plat}$, RSD_{plat}) was taken for comparison of precision of ion intensity relative to that for a normal peak ($Scan\#_{50\%}$) average spectrum. It is shown in Figure 5.2.2 that the precision of pseudo-molecular ion response for scan-by-scan averaging was greatly improved with increased injection volume. Added constraint in the selection of a constant intensity scan region, as shown in table 4b) with values for Int_{plat} and RSD_{plat}, further increased the accuracy of measurements obtained through spectral averaging. These results indicated the necessity to inject large sample bands or to use continuous infusion to achieve constant response for accurate qualitative and quantitative measurement of true ionization efficiencies by FIA-ESIMS.

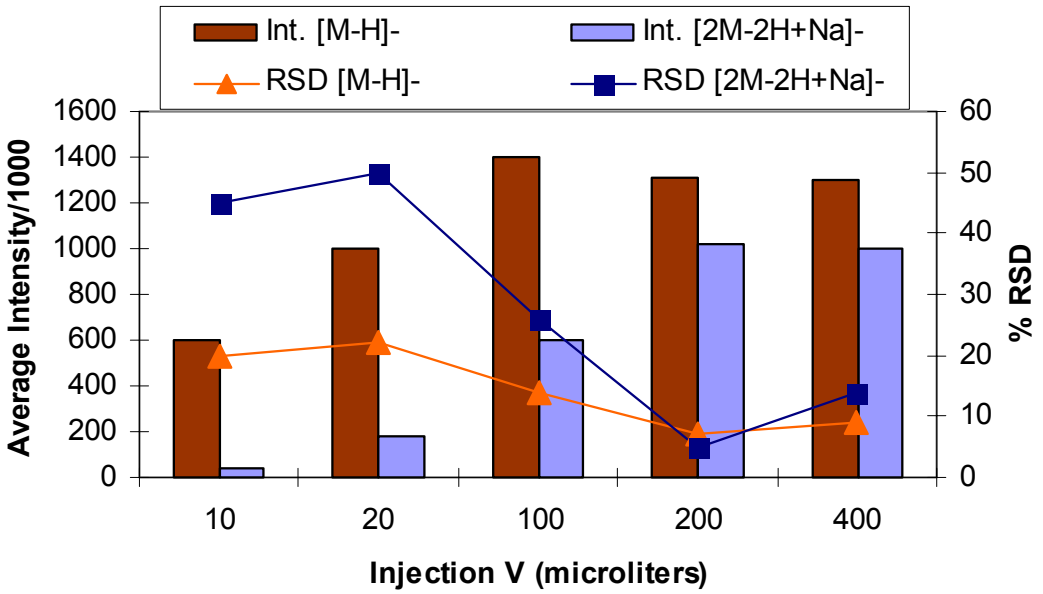

Figure 5.2.2 Average intensity and percent RSD of $[M-H]^-$ and $[2M-2H+Na]^-$ pseudo-molecular ion response as a function of injection volume. Bars correspond to values of average intensity on the left y-axis and lines correspond to values of percent RSD on the right y-axis. PABA was present at 0.5 mM concentration.

Table 5.2.1 Scan-by-scan reproducibility for FIA-ESIMS as a function of injection volume and number of scans averaged to generate a mass spectrum.

a)Scan Centroid ± 25%

			[M-H]-		[2M-2H+Na]-	
$V_{inj.}(\mu L)$	$Scan\#_{Tot}$	$Scan\#_{50\%}$	$Int_{50\%}/1000$	$\%RSD_{50\%}$	$Int_{50\%}/1000$	$\%RSD_{50\%}$
10	134	67	600	20	40	45
20	150	75	1000	22	180	50
100	308	154	1400	14	600	26
200	515	257	1310	7	1020	5
400	1001	500	1300	9	1000	14

b)Scan Centroid ± 5%

		[M-H]-		[2M-2H+Na]-	
$V_{inj.}(\mu L)$	$Scan\#_{plat}$	$Int._{plat}/1000$	$\%RSD_{plat}$	$Int._{plat}/1000$	$\%RSD_{plat}$
100	32	1450	4	700	16
200	35	1300	8	1030	5
400	50	1170	6	1030	5

$V_{inj.}$ denotes the injection volume in microliters. Int denotes the average intensity for the across the designated scan range. RSD is the relative standard deviation for the intensity in the designated scan range. $Scan\#_{Tot}$ denotes the total number of scans across the entire peak. Subscript '50%' denotes the region incorporated by the centroid ± 25% of the scans in the ion chromatogram and subscript 'plat' denotes scans taken from the heart of the ion chromatogram scan region (centroid ± ~5%) where applicable. Part a shows the data for 50% of the peak, while part b shows the data for scans across the heart of the plateau region, where a plateau region is observed. These results show an increased precision for measuring ionization efficiencies from large volume injections (part a) and with a constrained scan range (part b).

Positive mode ionization of PABA did not produce a stable response. Figure 5.2.3 shows typical FIA-ESIMS profiles obtained for PABA in the positive and the negative ionization mode. The pK_a of the analyte calculated by ACD labs SpecManager Software (Advanced Chemistry Development, Toronto, Ontario, Canada) was 4.9 ± 0.1 for the neutral form and 2.5 ± 0.1 for protonation of the amine. For a 50/50 acetonitrile/water solution system (pH ~ 6.5), deprotonated PABA is expected to be the dominant molecule form. Because of the solution system employed, a positive ion was not observed. According to the pK data, a solution pH approaching a value of one would be necessary to promote protonation of the amine group and consequently, a positive PABA ion. Such an approach for detection of this analyte was not practical, especially when considering the pH limits of most commercial LC columns (pH 3 – 10). The positive molecular ion of PABA ($[M+H]^+$) was rarely observed when positive ionization mode was employed. Positive ion results were therefore omitted from this work. The shape of the FIA-ESIMS TIC also indicated erratic, irreproducible, and immeasurable ionization response for PABA in positive ionization mode, as shown in figure 5.2.3b. In this case, the profile of the TIC response for large volume FIA-ESIMS provided a good diagnostic tool to assess ionization stability.

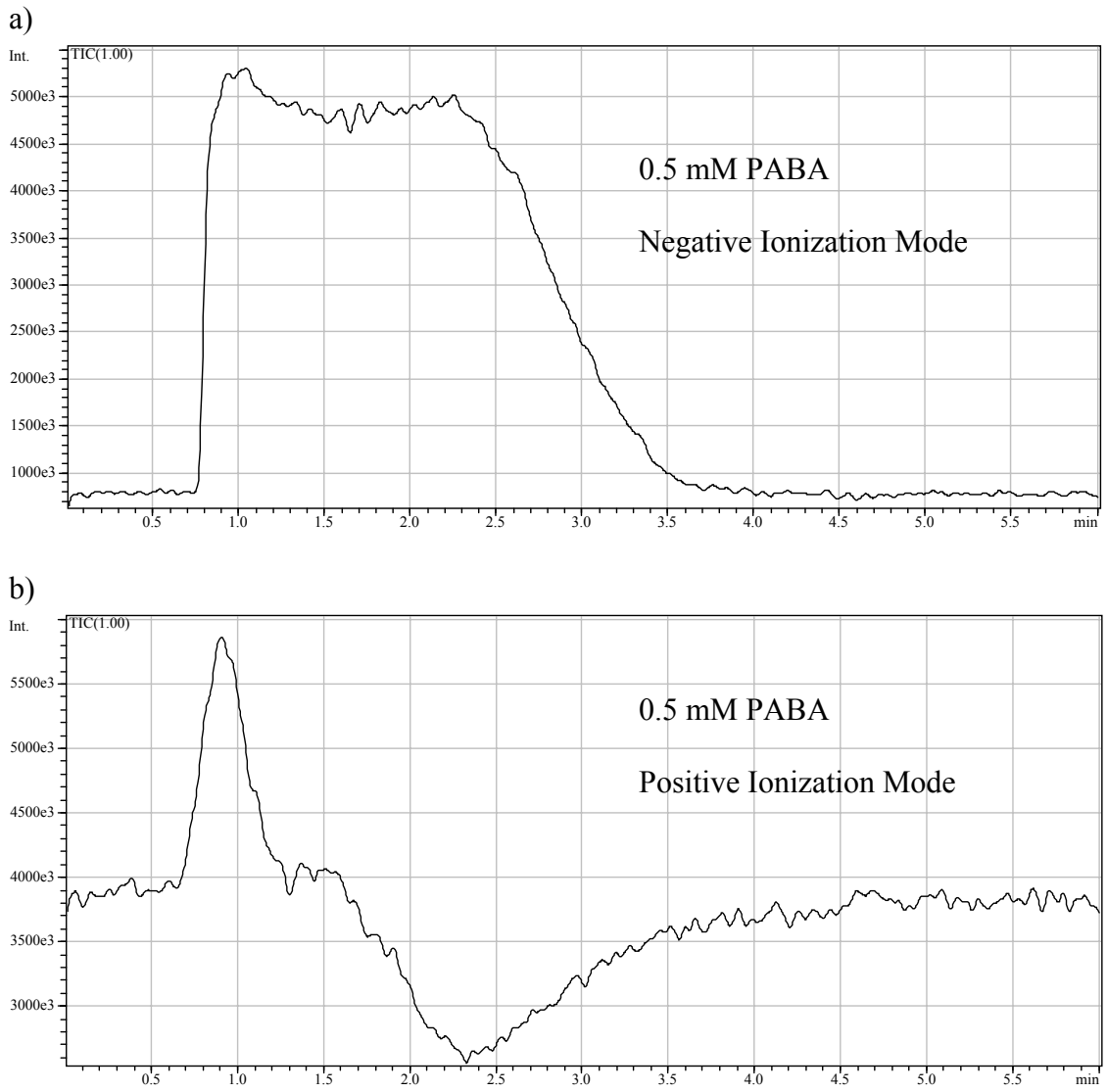

Figure 5.2.3 FIA-ESIMS profile for: a) negative; and b) positive ionization modes analysis of 0.5 mM PABA in the presence of 50/50 acetonitrile/water (pH ~ 6) with a 200 μL injection.

Five concentrations of PABA were used to investigate the linearity of response for the molecular ion ($[M-H]^-$) and the sodium-bridged dimer ion ($[2M-2H+Na]^-$) in 50/50 acetonitrile/water. Each concentration was analyzed at five different injection volumes. Results presented are averages of the scans across the heart of the plateau.

Figures 5.2.4a and b show the linearity of response for the pseudo-molecular ions for each of the five injection volumes. The poor linearity of $[M-H]^-$ throughout the concentration range investigated could be attributed to the dominance of $[2M-2H+Na]^-$ in the mass spectra at high concentrations. This sodium-bridged dimer adduct appeared to deplete the response of the deprotonated molecular ion. Also, for $[2M-2H+Na]^-$ response plots, the R^2 value of the 200 and 400 μL injections were 0.9886 and 0.9959, respectively, while R^2 for 10 μL was 0.9357 and for 20 μL was 0.9119. This meant that large injection volumes favored improved linearity for the $[2M-2H+Na]^-$ ion species. It also showed that this ion form was the dominant product in the electrospray ionization process for this system, as demonstrated by the predominance of the sodium-bridged dimer ion species over the deprotonated ion species at high concentrations. For trace analysis, the limit of detection of $[M-H]^-$ was lower than that of $[2M-2H+Na]^-$, as evidenced by the lack of response for the sodium bridged dimer ion when 0.01 mM PABA was analyzed.

a)

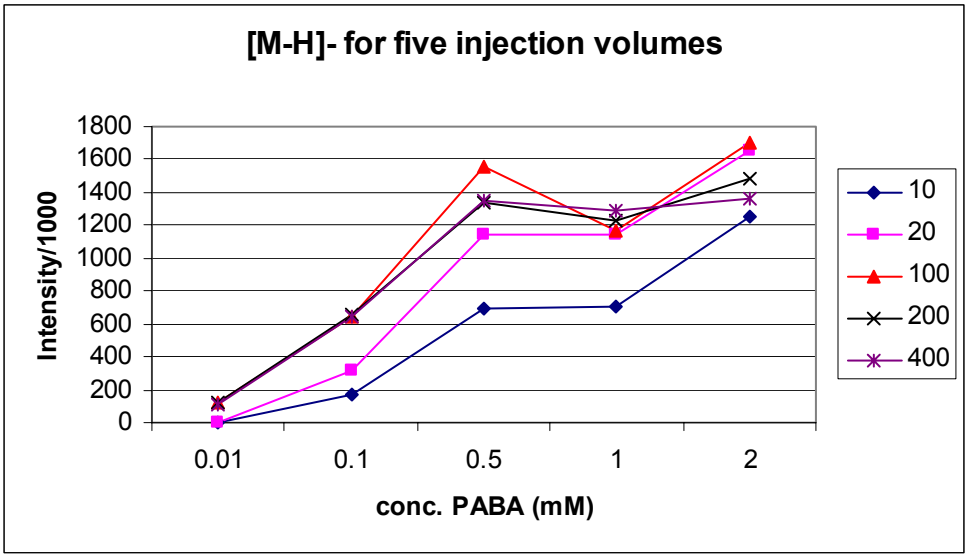

b)

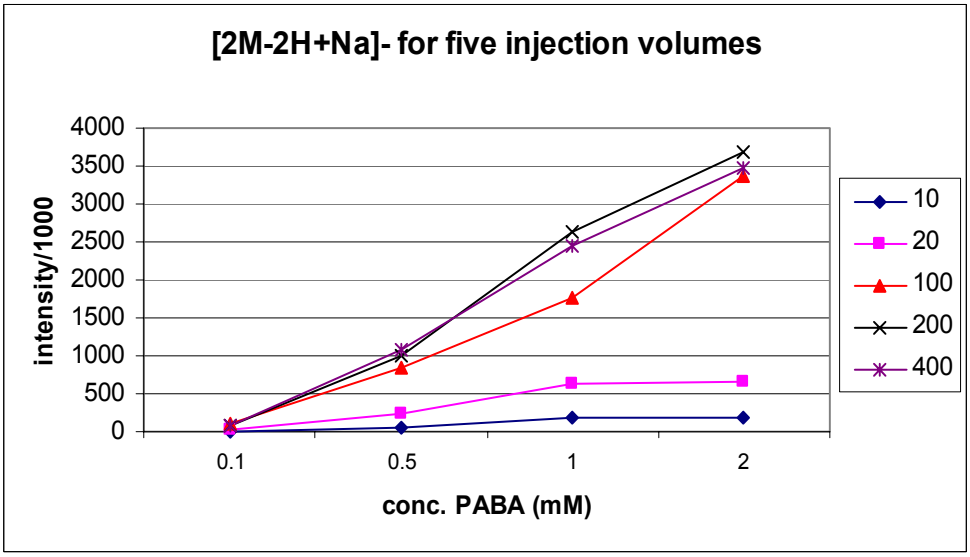

Figure 5.2.4 Pseudo-molecular ion response for PABA in 50/50 acetonitrile/water at five injection volumes and five concentrations. Part a) is $[M-H]^-$ ion response and part b) is $[2M-2H+Na]^-$ ion response. Response of $[2M-2H+Na]^-$ at 0.01 M PABA was not observed and therefore not included.

Figure 5.2.5 (a-d) shows the response of PABA versus injection volume for five different concentrations. Analyte response became essentially constant above 100 µL injection volume which indicated a saturated or quasi-equilibrium condition was present. Another indication of saturation was the tailing observed in the TIC. At the end of the plateau region, as the signal began to decrease, sample was no longer being infused into the spray chamber. The ions detected in this tailing region were those remaining in the spray chamber. It was evident that strong analyte concentration and injection volume effects were observed above 0.5 mM concentration and 100 µL injection volume. At higher concentrations and larger injection volumes, the response of $[2M-2H+Na]^-$ began to dominate the mass spectra as the base peak.

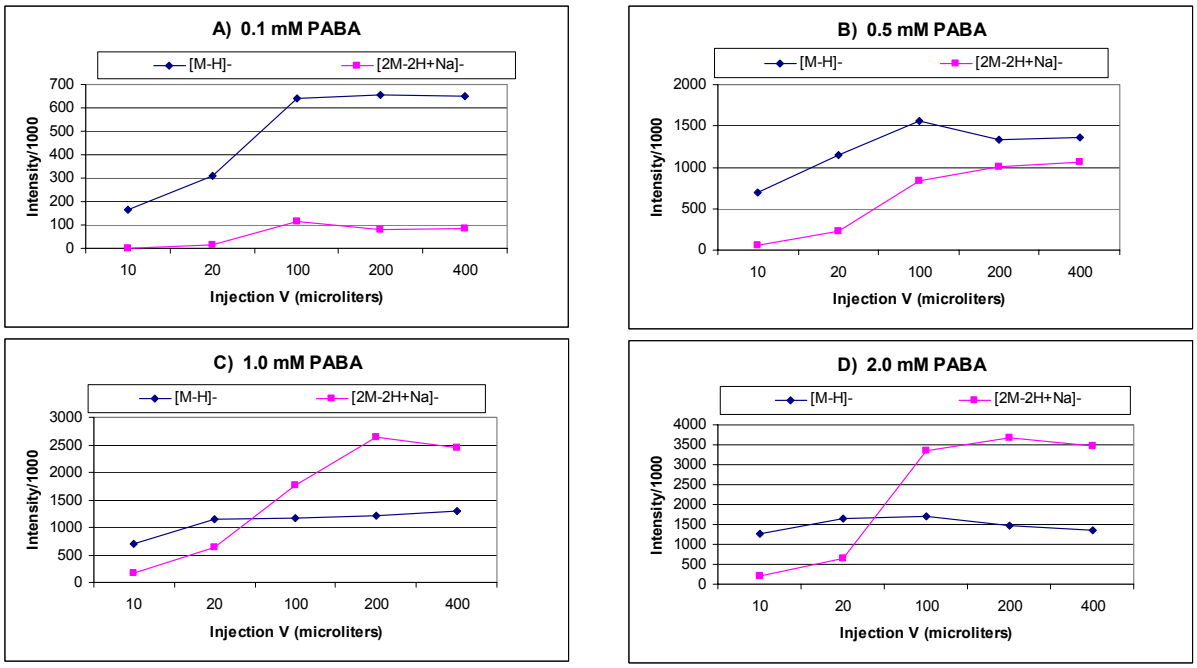

Figure 5.2.5 Parts A-D represent the pseudo-molecular ion response for PABA at 0.1, 0.5, 1.0, and 2.0 mM, respectively.

5.2b pH Effects

In this study, two contrasting methodologies for pH adjustment were employed to study the effect of each on ionization of 0.5 mM PABA during FIA-ESIMS. For use in the first part of this pH study, Table 2.4.1 (given previously in chapter 2) shows the solution composition used to achieve a desired pH as outlined by the Handbook of Chemistry and Physics.[119] These solutions were made up of high concentrations of acids, bases, and buffers to achieve the desired pH. The concentration and type of salts used were expected to suppress ionization of PABA during the ESI process, even though the overall pH value may have been favorable to promote ionization of the acid group. Because the modifiers were present in much larger amounts than the analyte, relatively few sites were available on the droplet surface for efficient analyte ionization. This effect is well known and has been detailed by Kebarle and coworkers.[16,19] Essentially, a large quantity of additives in the ESI system will compete with analytes for desorption sites at the droplet surface, thus lowering the number of desorption sites and decreasing analyte ion sensitivity.

The second method for pH modification employed the use of common LC-MS modifiers, namely acetic acid (HOAc), formic acid (FA), triethylamine (TEA), and ammonium acetate (NH_4OAc). These were prepared in 50/50 acetonitrile/water solutions at the same concentration as the analyte, 0.5 mM. Because of their compatibility with LC-MS, these modifiers are well known to be preferable to less volatile systems for pH modification. In addition, they were expected to have marked effects on pseudo-molecular ion formation of PABA.[10] Additives such as TEA inhibited formation of the sodium bridged dimer ion pair, and effectively increased the deprotonated molecular ion

response. Additives such as FA, HOAc, and NH_4OAc have been shown to promote formation of the $[2M-2H+Na]^-$ ion form relative to the $[M-H]^-$ ion form.

For effective protonation of the amine functionality (pK = 2.5) of PABA, pH values near 1.0 would be necessary to promote adequate ionization in the positive ionization mode. The lowest pH values studied was approximately 3.0 and therefore not low enough to promote a positive ion form. Higher pH values favored formation of a deprotonated molecule by loss of hydrogen from the carboxylic acid group which led to an enhanced signal in the negative ionization mode. Negative ionization mode was expected to be the method of choice for analyzing molecules with an acidic functionality regardless of other substitutions because of the mild solution conditions necessary to facilitate deprotonation of the acid.

Table 5.2.2 lists the results for ionization of PABA in the presence of the high concentration pH modifiers used in the first part of this study. Solutions A, B, and C (see table 2.4.1) greatly suppressed ionization for both pseudo-molecular ions monitored, relative to data observed without additives present. In all cases, the base peak was not a peak of interest. Solution D, pH 10, was the only system that showed an appreciable signal for $[M-H]^-$ of PABA. These results supported the expected ion suppression for using complex pH modifier systems at high concentration. No response was observed in the positive ionization mode.

Table 5.2.2 Ionization response for PABA in the presence of bulky pH modifiers.

Solution	pH	Int [M-H]-	Int. [2M-2H+Na]-	base peak
A	3	0	0	165
B	5	150000	0	165
C	8	130000	0	249, 156
D	10	850000	50000	136

Only for solution D is an ion of interest observed as the base ion (m/z = 136) with appreciable intensity. The compositions of solutions A-D were defined in table 2.4.1.

Figure 5.2.6 depicts the effect of the four common LC-MS mobile phase modifiers on formation of $[M-H]^-$ and $[2M-2H+Na]^-$ for PABA. As expected based on previous experiments,[10] very different effects were observed with respect to type of pseudo-molecular ion formed in the ionization process. HOAc, FA, and NH_4OAc promoted the formation of the sodium-bridged dimer ion over the deprotonated molecular ion. Conversely, TEA suppressed formation of the sodium-bridged dimer ion in favor of the deprotonated molecular ion. NH_4OAc also contains an ammonium cation which can scavenge sodium ions in the gas-phase. However, the results suggest that either it has a lower proton affinity than TEA or the acetate anion plays a role in promoting the formation of the sodium-bridged dimer ion due to the presence of a $[M-H]^-$ response relative to when HOAc or FA are present.

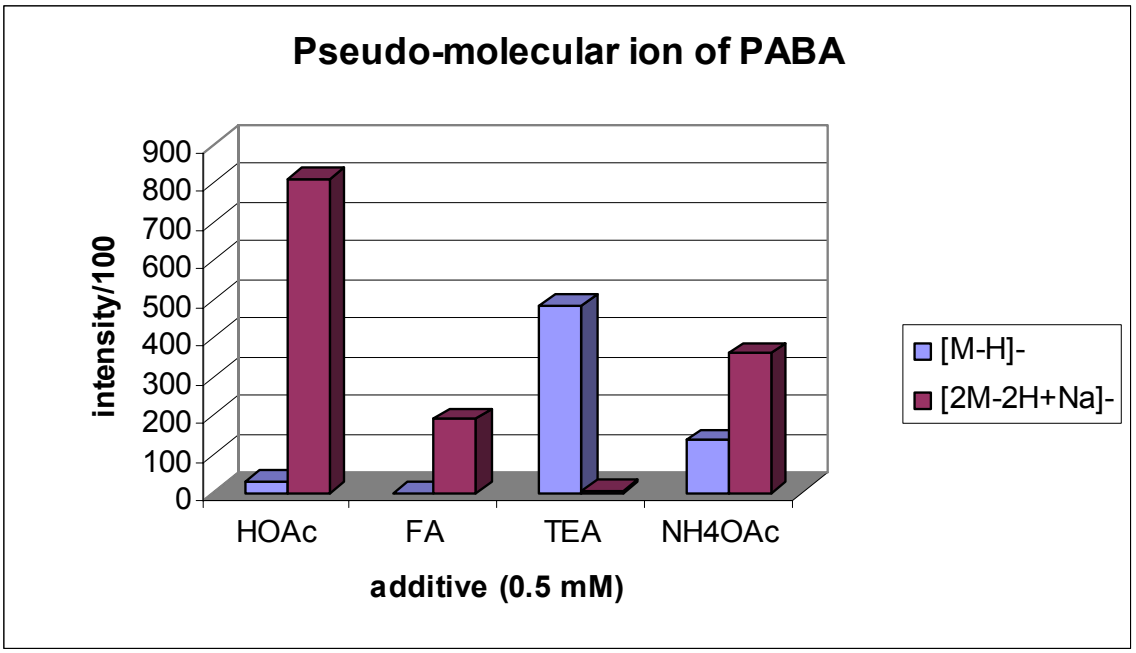

Figure 5.2.6 Pseudo-molecular ion response of PABA in the presence of common LC-MS pH modifiers. Results indicated HOAc, FA, and NH_4OAc promoted the formation of the sodium-bridged dimer ion ($[2M-2H+Na]^-$), while TEA promoted formation of the traditional deprotonated molecular ion ($[M-H]^-$).

5.3 Discussion

These results showed that at high concentrations, when a saturated condition was achieved in the spray chamber, a greater number of sodium bridged dimer ions were formed. This indicated that the pseudo-molecular ion $[2M-2H+Na]^-$ was most likely a result of increased gas-phase collisions due to a greater number of species available to form complexes. It can be hypothesized therefore that sodium-bridged dimer ions are a result of gas-phase processes and their formation is controlled by gas-phase dynamics.

If gas-phase dynamics governed the formation of $[2M-2H+Na]^-$ as hypothesized from the injection volume and concentration experimental results listed above, then the response difference caused by the presence of TEA, relative to other modifiers, could be reasoned by the high proton affinity of the gas-phase amine. TEA is known to readily adduct to molecules in positive ionization mode through gas-phase collisions. This could be demonstrated by adjusting the MS inlet voltage to promote gas-phase collisional processes.[35] If we assume proton affinity could be used as an estimate of sodium affinity, due to the single charge nature of the cations, TEA could be expected to scavenge sodium ions in the gas-phase environment, thus lowering their availability to deprotonated PABA for association into a dimer complex.

CHAPTER 6

OTHER EXPERIMENTS

6.1 Addition of Alkali Acetate Salts to Ibuprofen Derivatives

Following the observation of sodium-bridged dimer ions in the analyses of ibuprofen derivatives (Chapter 3), experiments were performed to investigate the relative binding of other alkali metal salts to these analyte test probes. Many other researchers have investigated the binding of alkali metal cations to a variety of molecule types, such as calixarenes, benzene derivatives, peptides, and amino acids. These analyses were largely performed in the positive ionization mode. No work has been reported in the literature for the formation of pseudo-molecular ions by added alkali metal salts in the negative ionization mode for aromatic acids.

Studies reported here were performed by addition of one of four alkali acetate salts (LiOAc, NaOAc, KOAc, and CsOAc) to solutions containing each of the six ibuprofen derivatives (carprofen, ibuprofen, ketoprofen, naproxen, fenoprofen, and flurbiprofen). Analyses were performed via flow injection analysis electrospray ionization mass spectrometry in the negative ionization mode using the normal tune parameters given previously in Chapter 2. Alkali acetate salts were mixed at three concentrations (0.1, 1.0, and 2.5 mM) with each ibuprofen derivative in 50/50 acetonitrile/water. Pseudo-molecular ion responses were measured by the mass spectrometer in scan mode.

Previous studies have established, with exception of very few cases, that adduction of alkali metal cations to molecules is most intense for smaller cations (Li^+) compared to larger cations (Cs^+), due to the greater charge density and smaller steric

interaction of the smaller cations. As a result, the observed pseudo-molecular ion formation response was expected to follow the trend $Li^+ > Na^+ > K^+ > Cs^+$.

Indeed, this was the case, and studies performed with alkali metal salts at 2.5 mM concentration showed a high degree of aggregation about the ibuprofen derivative molecules. The greatest amount of aggregation was observed in the presence of lithium containing acetate salt. Figure 6.1.1 shows the mass spectral response of carprofen in the presence of 2.5 mM LiOAc. Up to five aggregate ions ($[M-H+xLiOAc]^-$ (x = 1-5)) were observed in this analysis. Also notable is the change in the bridged dimer ion form, from a sodium-bridged dimer ion without any acetate salt present to a lithium-bridged dimer ion when LiOAc was added.

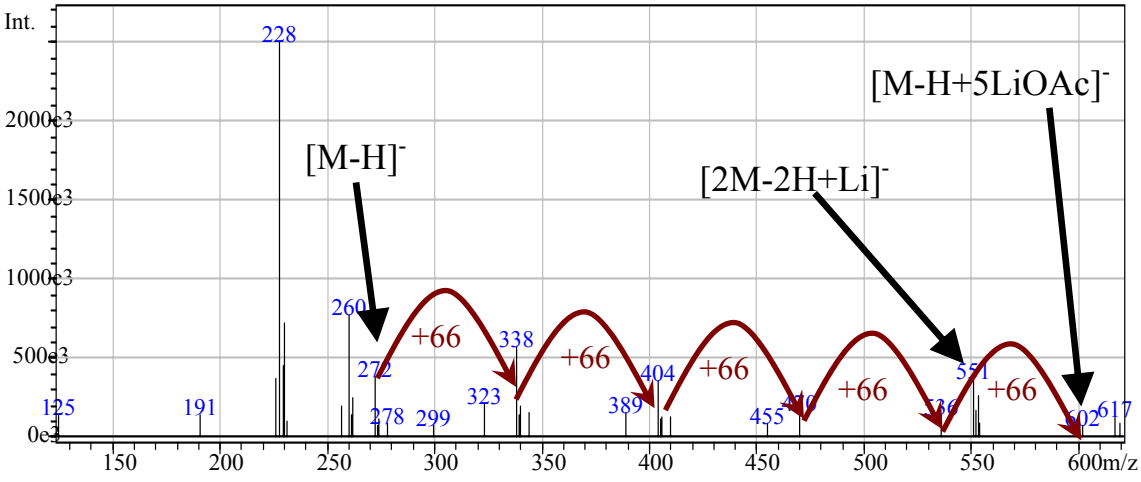

Figure 6.1.1 Aggregate pseudo-molecular ion formation by carprofen in the presence of 2.5 mM LiOAc. Subsequent aggregates were denoted by +66 amu, the molecular weight of LiOAc. Also apparent was the lack of ion response for $[2M-2H+Na]^-$, which had been replaced by $[2M-2H+Li]^-$. The base peak in this spectra at m/z = 228, corresponded to the loss of the carboxylic acid group $[M-COOH]^-$ by carprofen.

At a glance, this did not show impressive analytical merit, due to the decreased deprotonated molecular ion signal relative to analyses when no salts were present. However, in the case of flurbiprofen, which showed no response for $[M-H]^-$, the addition of acetate salt did provide a vehicle for sensitive detection of this analyte as a deprotonated molecular ion salt aggregate ($[M-H+LiOAc]^-$). Figure 6.1.2 shows a mass spectrum of flurbiprofen in the presence of 2.5 mM LiOAc. As observed previously for carprofen, the lithium cation also displaced sodium in the bridged dimer ion form.

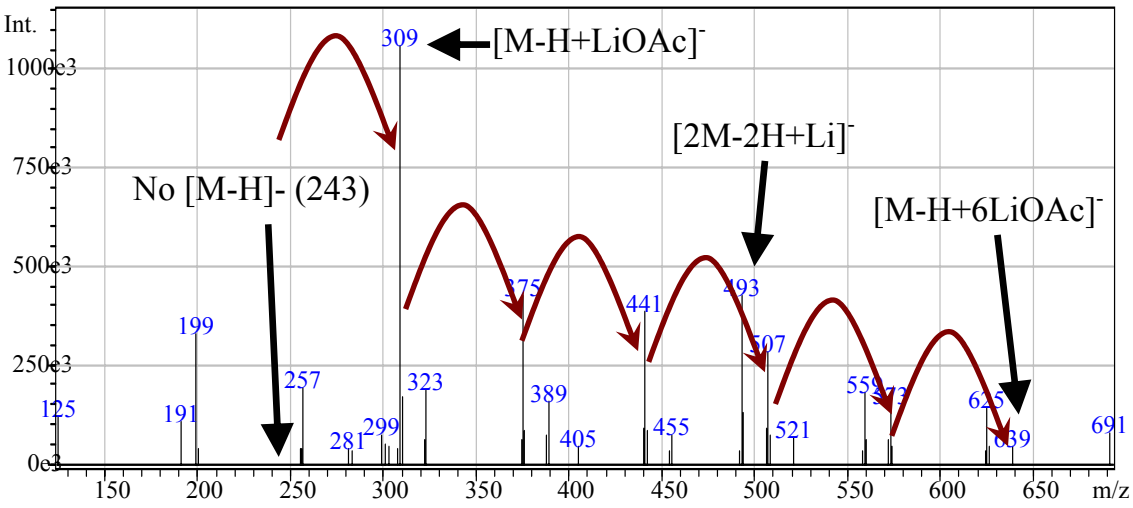

Figure 6.1.2 Pseudo-molecular ion formation by flurbiprofen in the presence of 2.5 mM LiOAc. The base peak in this spectrum was $[M-H+LiOAc]^-$. Arrows indicate subsequent aggregates of LiOAc (+66 amu).

Aggregation by addition of alkali metal acetate salts other than LiOAc showed a decrease in aggregation number with increasing cation size. Table 6.1.1 lists the ionic radii of the alkali metal cations investigated in this experiment. Figure 6.1.3 is a graph of the aggregation number observed for three ibuprofen derivatives (flurbiprofen, carprofen, and ketoprofen) as a function of the ionic radius of the cations.

Table 6.1.1 Ionic radii for alkali metal cations investigated in this experiment.[130]

Cation	Ionic Radius (pm)
Li^+	58
Na^+	102
K^+	138
Cs^+	170

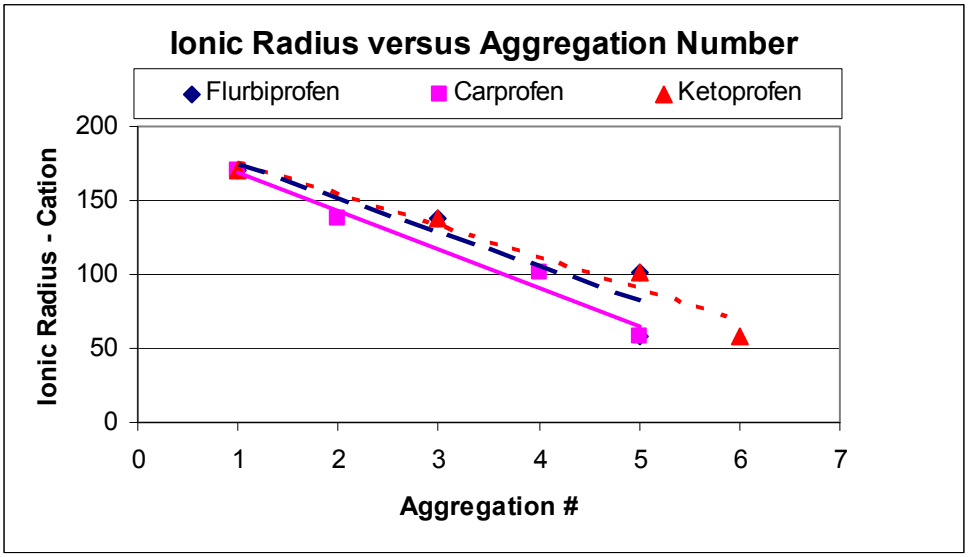

Figure 6.1.3 Aggregation of alkali metal salts as a function of ionic radius of the cation. Aggregates refer to the addition of nXOAc (n = 1 to 6, X = Li, Na, K, Cs) to the deprotonated pseudo-molecular ion of the respective ibuprofen derivative. All alkali metal salts were present at 2.5 mM concentration. The hatched line (– –)corresponds to the flurbiprofen trend line, the solid line corresponds to the carprofen trend line, and the dotted line (- - - -) corresponds to the ketoprofen trend line.

Concentration effects on ionization response were apparent with addition of alkali metal salts. An increase in the concentration of additive species is known to decrease the

relative ionization efficiency of the analyte of interest due to the limited number of sites on the droplet surfaces during ionization. This effect could be seen with the addition of LiOAc in three concentrations to separate solutions which contained carprofen and ketoprofen. Figure 6.1.4 shows the effect of added LiOAc on the response for the deprotonated molecular ion of the six ibuprofen derivatives. Though in some cases, addition of a small amount of LiOAc (0.1 mM) caused a slight increase in response for $[M-H]^-$, the overall effect was a decrease in signal.

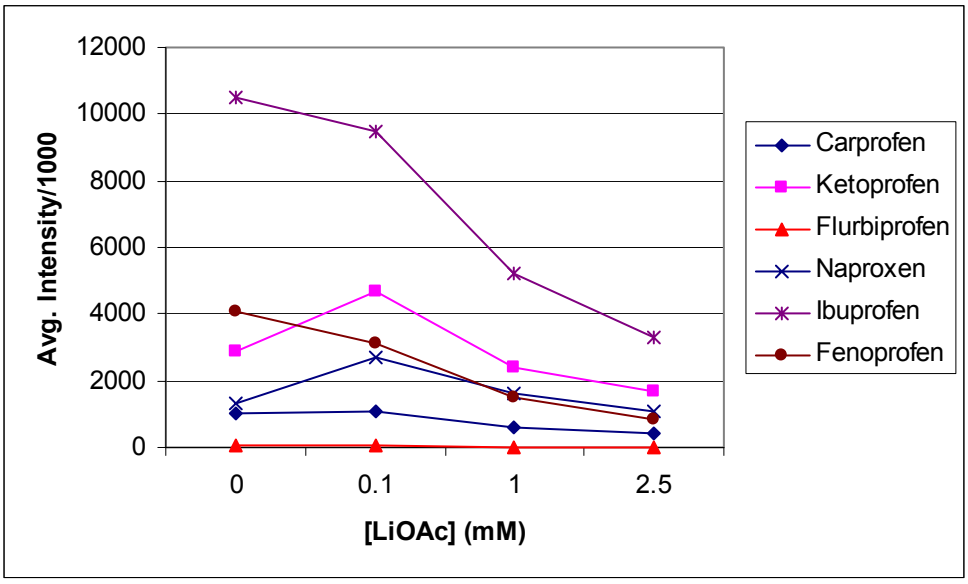

Figure 6.1.4 Effect of added LiOAc on the response of $[M-H]^-$ for six ibuprofen derivatives.

The effect of concentration of added alkali metal acetate salt on adduct ion relative intensity could also be demonstrated. Figure 6.1.5 shows the effect of added LiOAc on the response of $[M-H+LiOAc]^-$, $[2M-2H+Na]^-$, and $[2M-2H+Li]^-$ for carprofen

and ketoprofen. Lithium adducts began to dominate the mass spectra over sodium adducts at 0.1 mM added LiOAc.

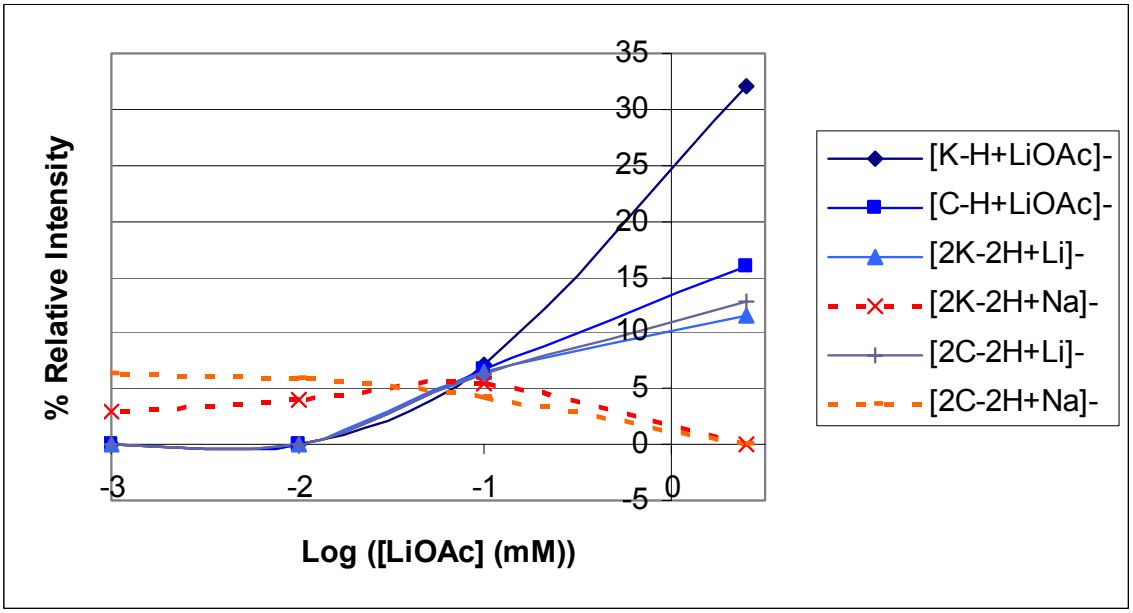

Figure 6.1.5 Relative intensity of sodium and lithium adducts with carprofen and ketoprofen as a function of added LiOAc. Solid lines correspond to lithium adducts and dashed lines correspond to sodium adducts. Carprofen (C) and ketoprofen (K) were present at 0.01 mM concentration.

Results consistent with those reported above were also observed when other alkali metal acetate salts were employed. The major difference between observed mass spectra was a lower degree of aggregation for acetate salts incorporating larger cations such as K^+ or Cs^+. However, these larger cations were still observed to displace background sodium in formation of a bridged dimer ion at higher (2.5 mM) concentrations. *Ab initio* geometry optimization simulations of bridged dimer ions with ibuprofen derivatives were not able to be performed due to time constraints; however Figure 6.1.6 shows the

formation of alkali metal-bridged dimer ion with benzoic acid for the purpose of visualizing the size difference between these cations. Distances between cation and neighboring oxygens are also offered as a measure of the strength of binding of each of these complexes.

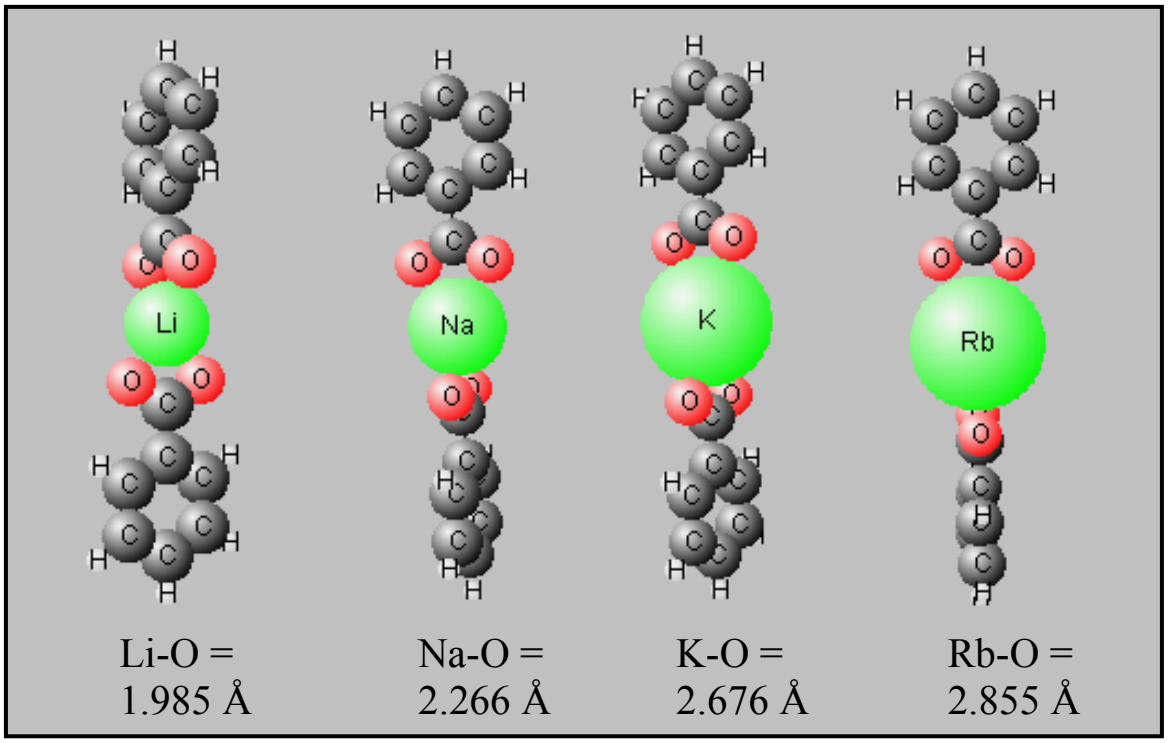

Figure 6.1.6 Hartree-Fock *ab initio* simulations of alkali metal-bridged dimer ions for benzoic acid at the 3-21G level of basis.

6.2 Analysis of Parabens

To investigate more fully the effect of surface activity on ionization response, a simple set of alkyl parabenzoate (paraben) test compounds were chosen. This set was comprised of methyl paraben, ethyl paraben, propyl paraben, and butyl paraben. The structures for these compounds are given in Figure 6.2.1. The increasing chain length on the paraben molecules caused an increase in surface activity in an evaporating droplet, and thus an increase in ionization response was expected in the order: butyl > propyl > ethyl > methyl paraben. Table 6.2.1 shows the respective log P values for these molecules calculated using the ACDlabs SpecManager software program.

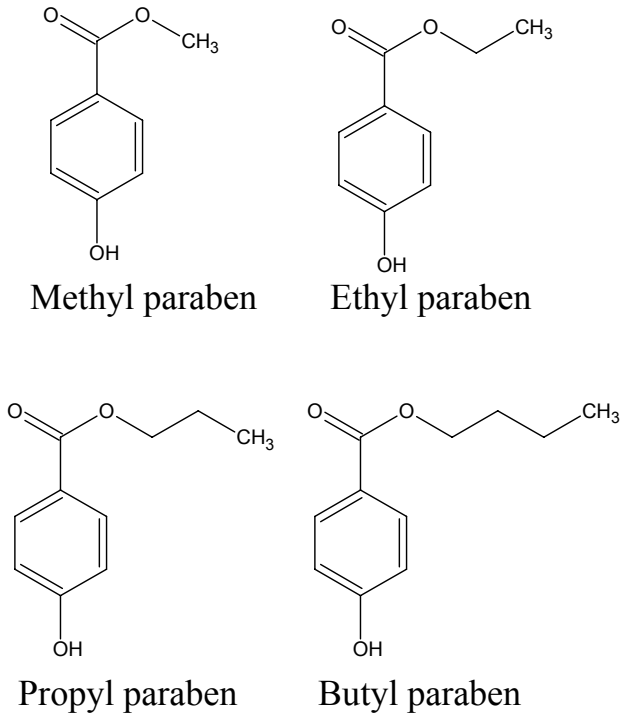

Figure 6.2.1 Structures of alkyl benzoate molecules.

Table 6.2.1 Calculated log P values for alkyl benzoate molecules.

Analyte	Log P
Methyl paraben	1.86 ± 0.22
Ethyl paraben	2.40 ± 0.22
Propyl paraben	2.93 ± 0.22
Butyl paraben	3.46 ± 0.22

Values calculated using ACDlabs SpecManager software program.

Good correlation of ionization intensity with hydrophobicity of the molecule was observed. Figure 6.2.2 shows: a) uniform response of 100 ppm mixture of the four alkyl parabens detected by UV at 254 nm; and b) increasing response in negative ionization mode ESIMS total ion chromatogram for the four alkyl parabens. In the case of each paraben, only the deprotonated molecular ion ($[M-H]^-$) was observed. Separations were performed with a C-18 (octadecylsilyl) column in gradient elution mode (figure 6.2.2) as well as in isocratic mode (not pictured) to determine the change in response due to changing percent organic in the ionized sample bands. No measurable change was observed. Detectors were placed in-line so that the outlet from the UV detector was coupled directly to the ESI interface. Figure 6.2.3 shows the correlation between ionization response and calculated log P values graphically. Figure 6.2.4 shows the Hartree-Fock *ab initio* geometry optimized structures for the deprotonated alkyl paraben analytes calculates using the 3-21G basis set.

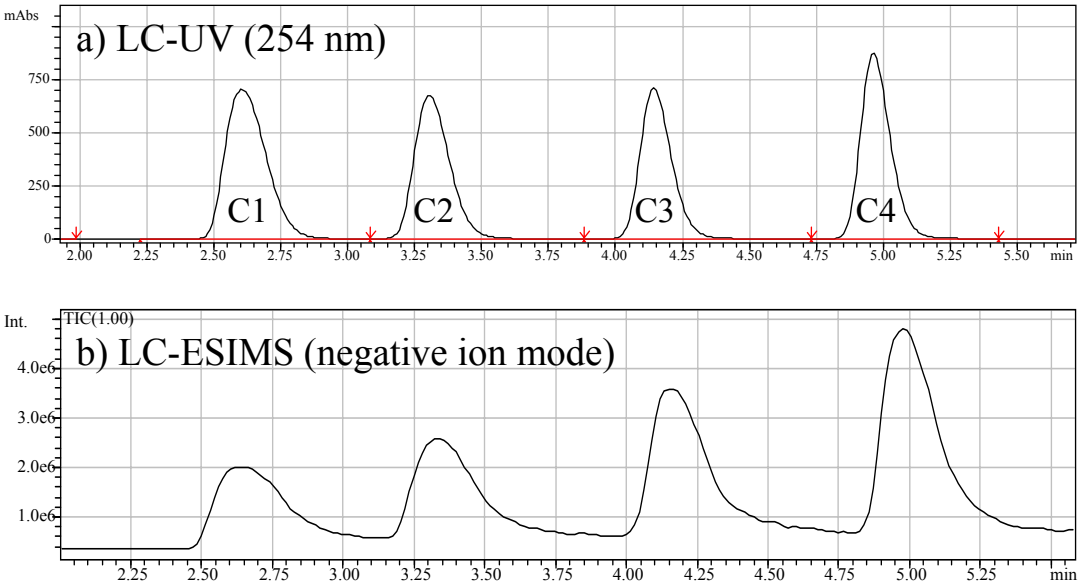

Figure 6.2.2 Gradient elution of four alkyl (C1 – C4) parabens detected by: a) UV at 254 nm; and b) negative ionization mode ESIMS. An increase in response is apparent with increasing alkyl chain length.

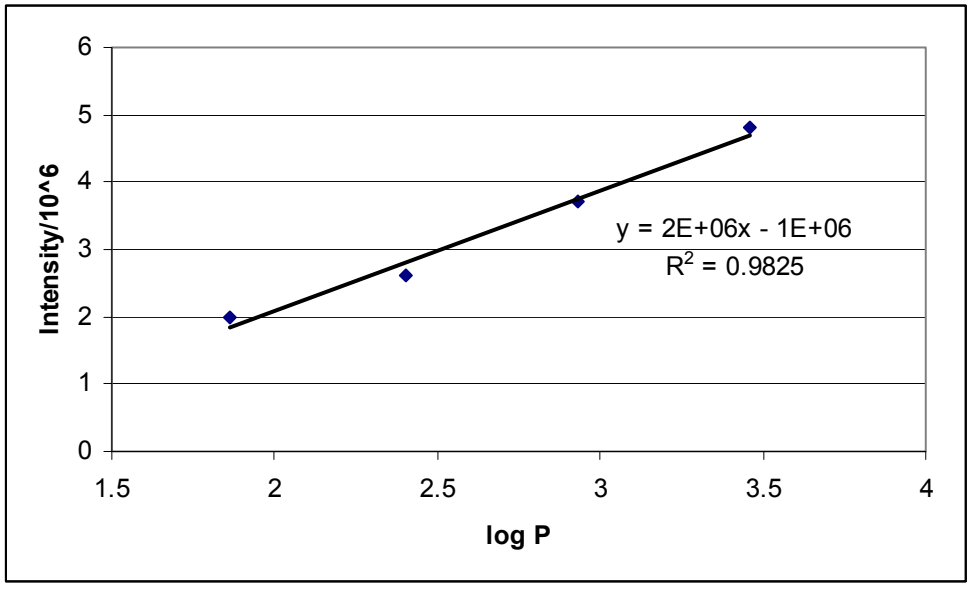

Figure 6.2.3 Ionization response as a function of calculated log P values for the separation of four alkyl paraben analytes.

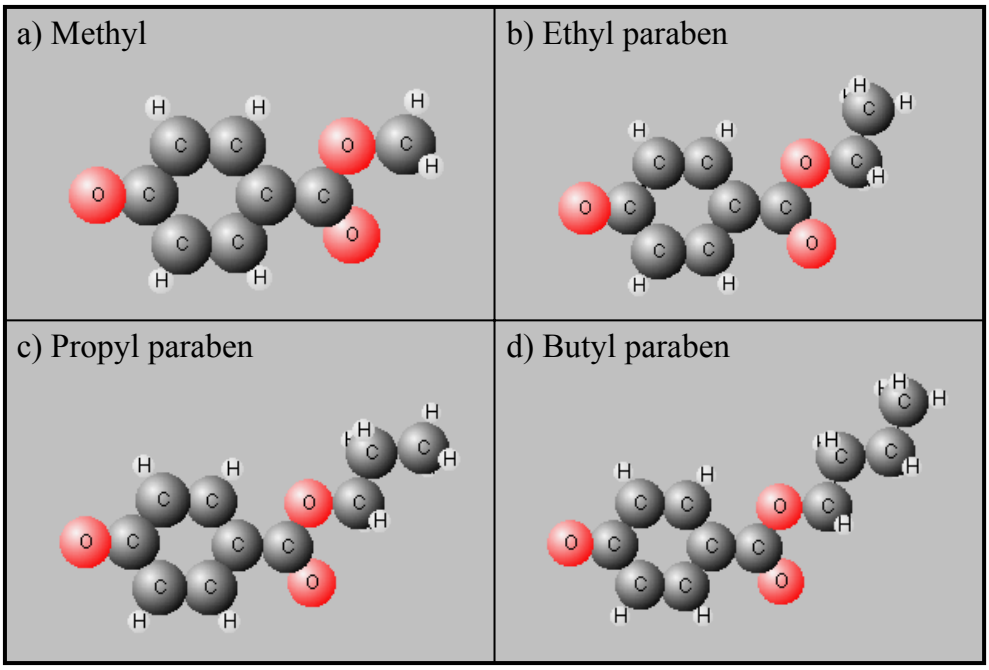

Figure 6.2.4 Hartree-Fock *ab initio* geometry optimized structures for the alkyl paraben deprotonated molecular ions at the 3-21G level of basis.

6.3 Positive Mode Ionization of PABA with Extreme pH Adjustment

To determine the relative sensitivity for analysis of aromatic acids by ESIMS in the positive ionization mode, PABA was mixed with a solution containing 50/50 acetonitrile/water and 5 mM $HClO_4$ as a strongly acidic pH modifier (pH ~ 2.0). With PABA present at 0.1 mM concentration, no signal for $[M+H]^+$ at m/z 138 was observed. When concentration of the analyte was increased to 0.25 mM, a small, but detectable signal for the protonated molecular ion could be seen. At 0.75 mM concentration, a respectable signal was obtained, but was not the base peak. Figure 6.3.1 shows a mass spectrum for the analysis of 0.75 mM PABA in the presence of 50/50 acetonitrile/water and 5mM $HClO_4$. This data shows conclusively: a) extreme pH adjustment, impractical for combination with chromatographic columns, is necessary to obtain a measurable ion signal for aromatic acids in the positive ionization mode; and b) the sensitivity associated with this approach is inferior to analyses of acidic analytes in the negative ionization mode.

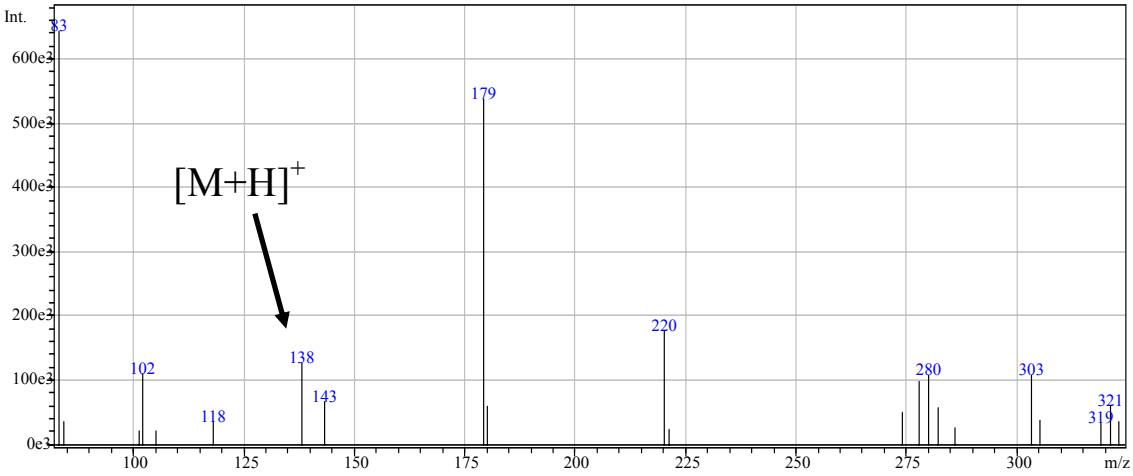

Figure 6.3.1 ESIMS mass spectrum of PABA in the positive ionization mode in the presence of 50/50 acetonitrile/water with 5 mM $HClO_4$ (pH ~ 2.0). $[M+H]^+$ corresponds to the response at m/z = 138. Ion responses at m/z = 179 and 220 are attributed to acetonitrile adducts $[M+H+ACN]^+$ and $[M+H+2ACN]^+$, respectively.

6.4 Analysis of Basis Set Selection in *ab initio* Simulations

Molecular modeling techniques, such as *ab initio* geometry optimization, have proven useful in elucidating structural arrangements of ions formed during ESIMS. Such techniques have been used extensively for the modeling of non-covalently bound complexes, particularly determination of points of attachment by metal ions on a molecule of interest. Due to the complex nature of these systems, calculations involving a large number of atomic species are often very time intensive.

Ab initio calculations performed for aromatic acid pseudo-molecular ions have been performed using the Gaussian98 software program.[118] These have been performed using relatively simple Pople-type split-valence basis sets, such as 3-21G and 6-31G(d). To increase the accuracy of these calculations, especially when considering non-covalent complex formation, more diffuse basis sets should be considered. Diffuse basis sets, such as 6-31+G(d), account for long-ranged interactions by including interaction potentials for electrons with radial distributions farther away from the nucleus of an atom. Such calculations were, logically, more expensive with respect to time.

Figure 6.4.1 and Table 6.4.1 show the difference in calculated parameters for the Hartree-Fock *ab initio* geometry optimization for $[2M-2H+Na]^-$ of benzoic acid. These results show that there was a significant difference in the distance between the complexed species and the assigned charge density distribution on the molecule calculated with different basis sets. This indicated the need to perform geometry optimization calculations at the higher level of basis when accurate quantitative data was desired.

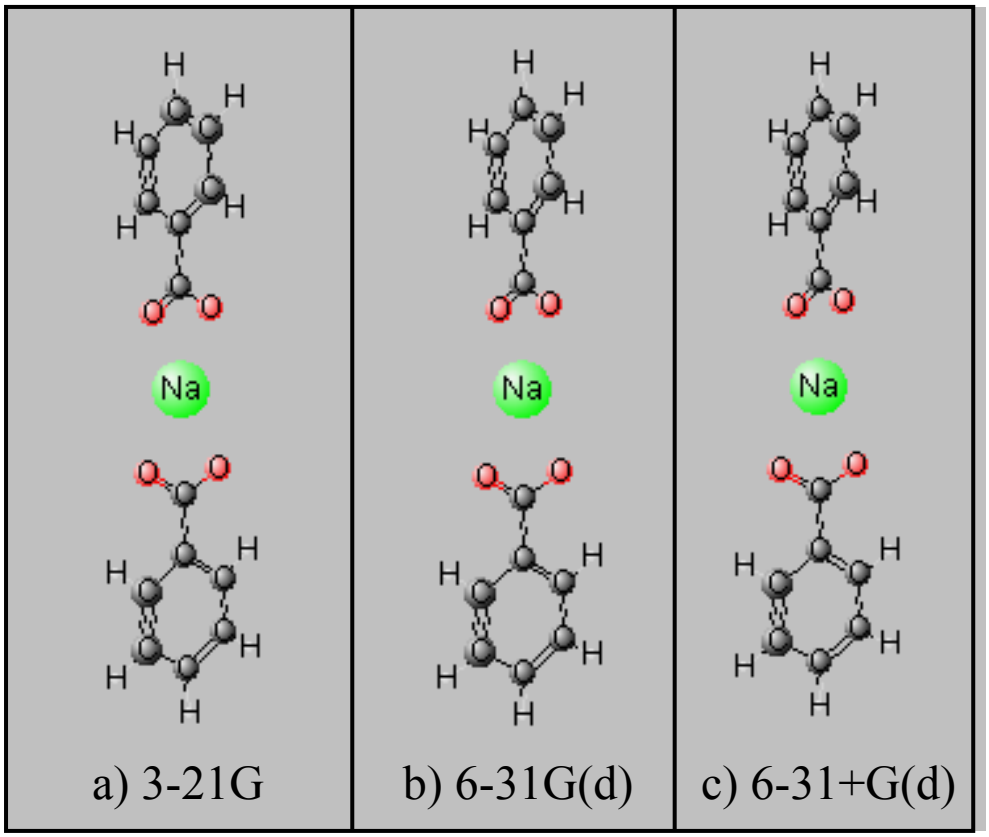

Figure 6.4.1 Hartree-Fock *ab initio* geometry optimization calculations for $[2M-2H+Na]^-$ of benzoic acid with three different basis sets: a) 3-21G; b) 6-31G(d); and c) 6-31+G(d).

Table 6.4.1 Calculated values for distance and charge density according to results of Hartree-Fock *ab initio* calculations with three basis sets.

	3-21G	6-31G(d)	6-31+G(d)
C--Na (Å)	2.556	2.612	2.633
q Na	+0.558	+0.605	+0.875

CHAPTER 7

CONCLUSIONS

"At daylight in the morning we discovered a bay, which appeared to be tolerably well sheltered from all winds, into which I resolved to go with the ship."

James Cook, 1770

When an opportunity arose to investigate a phenomenon of significant interest, of which to our knowledge no person had yet investigated, a joy of discovery overtook the reins of research. The work presented in this dissertation comprises a small portion of a field of study which appears to be without boundary. The capabilities provided by a powerful technique like ESIMS, does not come without its drawbacks. Understanding the processes governing those drawbacks dictates awareness and opens a wealth of new avenues for research. Our contribution to this understanding is the study of the pseudo-molecular ion response of aromatic acids in negative ionization mode ESIMS. A summary of this work as well as directions for future research are presented here.

Research began in earnest with a study of the formation of pseudo-molecular ions by a seemingly simple set of six test probes, all ibuprofen derivatives. Flow injection analysis in the negative ionization mode was used as a quick and efficient means for investigating the differences in ionization response between these analytes. Observation of ion responses in the mass spectra dictated focus on two to three prominent pseudo-molecular ion forms. These were a deprotonated molecular ion ($[M-H]^-$), a sodium-bridged dimer ion ($[2M-2H+Na]^-$), and in some cases, a homogeneous dimer ion ([2M-

H]$^-$). Observation of a sodium-bridged dimer ion had not been previously reported in the literature for analyses of acidic analytes.

Conclusions drawn from investigations involving ibuprofen derivatives served only to project more questions to be answered. Traditional deprotonated molecular ions for most organic acids could be readily observed in the negative ionization mode. This was demonstrated with the ibuprofen derivatives and confirmed to be consistent with following studies which incorporated benzoic acids and substituted benzoic acids. Little to no ion response was observed in the positive ionization mode. Homogeneous dimer ion formation was readily observed when hydrogen bonding groups were present in the aromatic acid structure. This was observed for the larger ketoprofen and carprofen molecules, but was not seen during analyses of the smaller, minimally functionalized benzoic acid derivatives. *Ab initio* studies were used to investigate the hydrogen-bound structure of these dimer ions. Changes in bond length for interacting atoms were used to show the presence the hydrogen bond. All of the studied aromatic acid analytes complexed with background sodium ion, an essentially ubiquitous species, to form stable sodium-bridged dimer ion pair adducts. Stabilities of these adducts were confirmed by in-source collision induced dissociation of the benzoic acid complex.

A dominant factor in electrospray ionization is known to be the surface activity of the analyte. Due to the partly aqueous nature of an evaporating droplet, and the hydrophobic phase boundary the droplet makes with the atmosphere in the spray chamber, log P values, the logarithm of the water/oil partition coefficient, were surmised to be a useful approximation of the hydrophobic nature of a given analyte. An analyte with a higher degree of hydrophobicity would have a greater affinity for the hydrophobic gas

phase relative to the aqueous liquid droplet. Correlations between log P values, calculated by ACDlabs SpecManager, and observed ion responses were shown to be weak. Qualitative correlations could be made only where a drastic degree of hydrophobicity change was evident in a molecule structure. Examples which favored the use of log P values for estimation of affinity for the hydrophobic gas phase were analyses of *para*-t-butyl benzoic acid (a ten-fold increase in $[M-H]^-$ ionization response relative to BA was attributed to the t-butyl group present) and the effect of increasing chain length in the analysis of alkyl parabenzoates. Problems associated with this approximated surface activity value were: a) the droplet itself was not completely aqueous and contained an organic component which changed with type and amount of organic present; and b) calculated log P values for aromatic acids varied little due to their common hydrophilic ionic component. Simulated calculations of pH dependent log P values, called log D, are available. However, to obtain a useful calculable measure of surface activity applicable to ESIMS analysis, the organic composition present in an evaporating droplet would have to be incorporated in the calculated value.

The formation of ionic species in solution is controlled by the dissociative/associative nature of the ionic moiety. In the case of acidic analytes, this is controlled by the acid dissociation constant, K_a. To investigate the contribution of K_a to ionization in negative ionization ESIMS, pK_a values were calculated using ACDlabs SpecManager. The values were compared with relative ionization efficiencies to establish whether or not correlation exists. If a correlation was present, molecules with lower pK_a (more acidic) would be expected to have a higher intensity response than a molecule with a higher pK_a (less acidic) in a given solution composition. Halide-

substituted benzoic acid molecules were studied to determine the effect of placement of an electron-withdrawing group on pseudo-molecular ion response relative to unsubstituted benzoic acid. Ion responses for the deprotonated molecular ion and the sodium-bridged dimer ion were determined to be essentially independent of calculated pK_a values.

Gaussian simulations showed a small degree of change in electron-withdrawing effect in calculated charge density of the deprotonated carboxyl oxygen atoms within a particular isomer set. *Ortho*-substitution showed the greatest degree of electron-withdrawal relative to substitution at other ring positions for a given halide according to *ab initio* geometry optimizations as well as the lowest calculated pK_a values from ACDlabs SpecManager. However, substitution in the *ortho*-position showed the lowest response compared to the other isomers. Substitution in the *meta*-position gave the highest $[M-H]^-$ response. In all cases, the response of the halide-substituted benzoic acid deprotonated molecular ion was greater than that of unsubstituted benzoic acid. Overall, this shows that the acidic nature, as quantified by charge density calculations and calculated pK_a values, was independent of ESIMS response in the negative ionization of aromatic acids. Rather, calculated values only served as a general indicator for pH adjustment to promote ionization of the acid group to form a deprotonated molecular ion.

All investigations performed with aromatic acid analytes also focused to a large degree on the observation of a sodium-bridged dimer ion in the mass spectra. This pseudo-molecular ion form was observed for all aromatic acid analytes tested. The ion species was most likely overlooked in publications in the literature due to the necessity of extending the scan range of the mass spectrometer to observe it. At the very least, it has

been shown here as a vehicle for sensitive detection of acidic molecules such as flurbiprofen, which do not form a traditional deprotonated molecular ion. Interactions between the deprotonated monomer ions and sodium cation were determined to be primarily electrostatic in nature according to the arrangement of the carboxylic oxygens about sodium in the *ab initio* geometry optimized structures. Correlation between the decreased response and angular distortion in the geometry optimized structures of *ortho*-halide substituted species relative to *meta*- and *para*- substituted species showed steric interactions played a significant role in the stability of the sodium-bridged dimer ions.

An important detail debated in these experiments was the point of formation of the sodium-bridged dimer ion during the ionization process. Was $[2M-2H+Na]^-$ formed by associations in the solution phase or in the gas phase? The lack of correlation between ion intensity and solution phase parameters, log P and pK_a, suggested that the complex was a result of gas-phase processes. Other indications of this hypothesis have also been noted in this work. The intensity of the sodium-bridged dimer ion was enhanced in a condition where saturation of analyte was present in the spray chamber. Saturation was confirmed by observation of a plateau response in the total ion chromatogram. As the amount (concentration of analyte and FIA injection volume) of sample introduced into the spray chamber increased, the intensity of $[2M-2H+Na]^-$ became the dominant ion species in the mass spectra. This indicated an increase in response due to an increase in the number of gas-phase collisions. Studies of linearity of response of the $[M-H]^-$ and $[2M-2H+Na]^-$ showed the sodium-bridged dimer ion to be the dominant product of the ionization process at high (>1 mM) concentration of analyte. Also, detection by the mass spectrometer was essentially limited by the sampling efficiency of the CDL transfer line

to the high vacuum region. Tailing associated with the plateau response indicated a point where sample was no longer being infused and detected ions were those gas-phase species which remained in the spray chamber. This supported the increase of gas-phase collisions due to a long residence of ionized species prior to MS sampling and detection.

Another point which supported the gas-phase formation of the sodium-bridged dimer ion was realized in the presence of added solution-phase modifiers. The addition of triethylamine to the ionized mixture caused a dramatic shift in response towards the deprotonated monomer ion. This can be explained by the high proton affinity of TEA. When 5 mM concentration of TEA was added, all sodium ions were scavenged in the gas-phase, which in turn completely suppressed $[2M-2H+Na]^-$ formation for PABA. Addition of modifiers such as formic acid, acetic acid, and ammonium acetate increased the relative intensity of the sodium-bridged dimer ion. Two reasons for this effect can be offered: a) these three modifiers lacked gas-phase activity, relative to TEA and the analyte; and b) impurities in the added modifiers increased the amount of sodium present in the system.

Overall, modifiers and additives added to the system had a large effect on the detected pseudo-molecular ion form. The effect on ion form due to the presence of common mobile phase modifiers has been shown. Studies focused on the effect of concentration of additives showed that an increase in the number of species in the system led to an overall decrease of analyte ion signal. This effect is well known and is due to the competition for desorption sites on the droplet surface. Consequently, modification of the mobile phase for chromatographic separation purposes must be done at low concentrations to avoid ion suppression when ESIMS detection is employed. It has also

been shown that simple solution modification procedures with a minimal number of additives were preferred over complex pH buffer systems for efficient ionization. The use of high concentrations of additives with low volatility in liquid chromatography is a major hurdle when transferring methods to incorporate ESIMS detection.

Addition of alkali metal acetate salts in moderate (0.1 – 2.5 mM) concentrations has been shown to affect the observed mass spectra in several ways. For a series of added salts (LiOAc, NaOAc, KOAc, and CsOAc), a high degree of aggregation by salts with smaller cations (up to six LiOAc adducts) was observed with ibuprofen derivatives. Aggregation decreased as the size of the cation species increased due a decreased charge density and greater steric character of the larger cations. The added cations also caused a change in the observed bridged dimer ion species where background sodium was replaced by the added cation of the salt to form a different bridged dimer ion ($[2M-2H+X]^-$, where X = Li, Na, K, Cs, depending on the salt added). Addition of LiOAc (2.5 mM) allowed for sensitive detection of the flurbiprofen species as $[M-H+LiOAc]^-$ (base peak), where a deprotonated molecular ion was not observed.

Analytically, the use of flow injection analysis for optimization and study of pseudo-molecular ion formation has been show to be very useful. Information regarding the interaction of species in a common solution system can be rapidly assimilated by simply mixing analytes and additives of interest and infusing them into the ESI interface. When performed using large injection volumes or continuous infusion, FIA-ESIMS can be used to obtain accurate and reproducible ionization efficiencies. Small changes in instrumental settings can be assessed based on the observed changes in the mass spectra.

Lack of a constant response plateau in the ion chromatogram has been shown to be a good diagnostic tool for assessment of ionization response stability.

Few deductions can be made regarding the ESI mechanism responsible for the observation of pseudo-molecular ion formation of aromatic acids presented in this work. Ionization of small molecules has been speculated to more closely follow the ion evaporation model, relative to the charged residue model. The observation of a high degree of aggregation could be assessed as supporting data for the charged residue scheme. Most likely, a combination of the two schemes is responsible for the observed ion responses. Gas-phase processes complicate the assessment of the mechanism responsible for the transition of species from solution phase to gas phase.

The direction of future work can follow many paths, and consequently, could traverse a long timeline. The application of pseudo-molecular ion formation of acidic analytes is directly applicable to research focused in the environmental, pharmaceutical, and biochemical fields. Gas-phase and solution-phase molecular recognition processes involving acidic analytes, such as chiral recognition and receptor-binding processes, are direct extensions of the fundamental research presented in this dissertation.

To extend the knowledge base of relative formation of pseudo-molecular ions, especially bridged dimer ions formed by aromatic acids, a more detailed study of selectivity as it relates to analyte structure should be investigated. Quantitative determination of binding constants, as outlined in Chapter 1, can be accomplished through a variety of techniques, depending on the capabilities of available instrumentation. With a single quadrupole mass spectrometer, these determinations are limited to experiments designed to generate Scatchard plots to determine host:guest

selectivity or melting point curves to determine relative complex stability. Such investigations would be useful for quantifying the binding of various metals to the aromatic acid analytes. Tandem MS instrumentation would be necessary to perform detailed studies for dissociative processes of complexes formed during ESIMS. To better understand the contribution of gas-phase behavior to observed ion form, model compound sets, such as benzaldehyde and aniline derivatives, could be chosen for which gas-phase data is well known.

Ab initio computer simulations have proven to be useful for modeling structures of pseudo-molecular ions, particularly relating to generation of most stable geometry and elucidation of interactions present in non-covalent complexes. A logical extension of this work would be elucidation of energies calculated for complexed species compared to the monomers which compose the complex. For this to be accurate, specifically designed basis sets must be incorporated to account for inadequacies associated with the simple basis sets used here. Basis sets with more diffuse interaction potentials are necessary to account for long-ranged interactions. Also, basis set superposition error (BSSPE) must be accounted for. BSSPE can be explained qualitatively as the decline in flexibility of a basis set when fewer interacting electrons are incorporated into the calculation. This applies directly to the simulated energies of a non-covalent complex and comparison to simulated energies of the non-complexed species making up the complex. The use of more detailed interaction potentials logically leads to more time-intensive (expensive) calculations.

The data generated and presented here corresponds to pseudo-molecular ion formation in a simple solution system (acetonitrile/water) with few additives. To extend

the applicability of pseudo-molecular ion formation, investigations should be performed where ion form is monitored in the presence of a variety of aqueous/organic mixtures. Modification of pH can be achieved in a multitude of ways. Chromatographic separations in the reversed phase make use of a wide variety of organic components. All of these factors will change the observed mass spectra for a given analyte species. The number of ways to affect ion formation in ESIMS is daunting, however, careful systematic studies with tight control of variables is the key to understanding the underlying mechanisms involved in the formation of pseudo-molecular ions by ESIMS. A logical extension for elucidation of dominant factors controlling ionization of acidic analytes would be to perform principal component analysis of all the variables present. In this way, correlations between calculated analyte characteristics and observed pseudo-molecular ion intensities could be made to bridge experimental and theoretical data.

Simple aromatic acids, such as the substituted benzoic acid molecules studied in this dissertation, are generally only used as precursors to building molecules with higher functionality for a specific purpose. Extensions of this research are expected to be useful in the analysis of amino acids, particularly related to chiral complex formation and protein-peptide binding. Work with ibuprofen derivatives gives insight into the relative affinity of these molecules for background sodium. Sodium is present in most analytical systems and cannot easily be removed; however, sodium is also present in most physiological systems and is integral to transport of molecules across cell membranes. The affinities observed for ibuprofen derivatives may be related to activity in biological studies and are therefore useful for further study in this field. Acids are common to the environment around us. From food chemistry to acid rain to pharmaceutical development,

analyses involving acidic molecules can hardly be avoided. When ESIMS is employed as the method of analysis, awareness of the possible results is essential. This information contained in this dissertation makes a strong contribution to that awareness.

REFERENCES

[1] Cole, R.B. *J. Mass Spectrom*. **2000**, 35, 763-772.

[2] Voress, L. *Anal. Chem*. **1994**, 66, 481A.

[3] Daniel, J.M., Friess, S.D., Rajagopalan, S., Wendt, S., Zenobi, R. *Int. J. Mass Spectrom*. **2002**, 216, 1.

[4] Brodbelt, J.S. *Int. J. Mass Spectrom*. **2000**, 200, 57.

[5] Sawada, M. *Mass Spectrom. Rev*. **1997**, 16, 73.

[6] Dűlcks, T., Juraschek, R. *J. Aerosol Sci*. **1999**, 30, 927.

[7] Cacace, F., de Petris, G. *Int. J. Mass Spectrom*. **2000**, 194, 1.

[8] Schalley, C.A. *Int. J. Mass Spectrom*. **2000**, 194, 11.

[9] Zhou, S., Hamburger, M. *J. Chrom. A* **1996**, 755, 189.

[10] a) Schug, K., McNair, H.M. *J. Sep. Sci*. **2002**, 25,760. b) Schug, K., McNair, H.M. *J. Chrom. A* **2002**, Article in Press.

[11]Matsuura, K., Takashina, H. *J. Mass Spectrom*. **1998**, 33, 1199.

[12] Iribarne, J.V., Thomson, B.A. *J. Chem. Phys*. **1976**, 64, 2287.

[13] Thomson, B.A., Iribarne, J.V. *J. Chem. Phys*. **1979**, 71, 4451.

[14] Dole, M., Mack, L.L., Hines, R.L., Mobley, R.C., Ferguson, L.D., Alice, M.B. *J. Chem. Phys*. **1968**, 49, 2240.

[15] Bruins, A.P., Covey, J.R., Henion, J.D. *Anal. Chem*. **1987**, 59, 2642.

[16] Tang, L., Kebarle, P. *Anal. Chem.* **1991**, 63, 2709.

[17] Hiraoka, K. *Rapid Commun. Mass Spectrom*. **1992**, 6, 463.

[18] Voyksner, R.D. *Nature* **1992**, 356, 86.

[19] Tang, L., Kebarle, P. *Anal. Chem*. **1993**, 65, 3654.

[20] Fenn, J.B. *J. Am. Soc. Mass Spectrom*. **1993**, 4, 524.

[21] Zolotoy, N.B., Karpov, G.V. *Phys. Lett. A* **2000**, 273, 132.

[22] Hoxha, A., Collette, C., De Pauw, E., Leyh, B. *J. Phys. Chem. A* **2001**, 105, 7326.

[23] Covey, T.R., Lee, E.D., Bruins, A.P., Henion, J.D. *Anal. Chem*. **1986**, 58, 1451A.

[24] Smith, R.D., Loo, J.A., Edmonds, C.G., Barinaga, C.J., Udseth, H.R. *Anal. Chem*. **1990**, 62, 882.

[25] Hamdan, M., Curcuruto, O. *Int. J. Mass Spectrom. Ion Processes* **1991**, 108, 93.

[26] Henry, C. *Anal. Chem. News and Features* July 1, **1997**, 427A.

[27] Niessen, W.M.A. *J. Chrom. A* **1998**, 794, 407.

[28] Bruins, A.P. *J. Chrom A* **1998**, 794, 345.

[29] Kebarle, P. *J. Mass Spectrom*., **2000**, 35, 804-817.

[30] Brinkman, U.A.Th. *LabPlus Int*. April/May **2002**, 10.

[31] Sakairi, M., Yergey, A.L., Michael Siu, K.W., Yvec Le Blanc, J.C., Guevremont, R., Berman, S.S. *Anal. Sci.* **1991**, 7, 199.

[32] Schmelzeisen-Redeker, G., Bűtfering, L., Röllgen, F.W. *Int. J. Mass Spectrom. Ion Processes* **1989**, 90, 139.

[33] Röllgen, F.W., Bramer-Weger, E., Bűtfering, L. *J. De Physique* **1987**, 48, C6-253.

[34] Blair, S.M., Kempen, E.C., Brodbelt, J.S. *J. Am. Soc. Mass Spectrom*. **1998**, 9, 1049.

[35] Zhou, S., Hamburger, M. *Rapid Commun. Mass Spectrom*. **1995**, 9, 1516.

[36] Taylor, G.I. *Proc. Roy. Soc. A* **1964**, 280, 383.

[37] Lias, S.G., Bartmess, J.E. "Gas-Phase Ion Thermochemistry," http://webbook.nist.gov/chemistry/ion/.

[38] Bruins, A.P. "Mechanistic aspects of electrospray ionization," *J. Chrom. A*, **1998**, 794, 345-357.

[39] *Personal communication*, Robert Classon, LCMS Product Manager, Shimadzu Scientific Instruments, Columbia, MD, USA, 5/2001.

[40] Bose, G.M. *Recherches sur le cause et sur véritable théorie de l'-électricité*; Wittenberg, **1745**.

[41] Lord Rayleigh *Proc. Roy. Soc*. **1879**, 29, 71.

[42] Lord Rayleigh *Phil Mag.* **1882**, 14, 184.

[43] Zeleny, J. *Phys. Rev*. **1917**, 10, 1.

[44] Chapman, S. *Phys. Rev*. **1937**, 52, 184.

[45] Chapman, S. *Phys. Rev*. **1938**, 54, 520.

[46] Chapman, S. *Phys. Rev*. **1938**, 54, 528.

[47] Vonnegut, B., Neubauer, R.L. *J. Colloid Sci*. **1952**, 7, 616.

[48] Vonnegut, B., Neubauer, R.L. *J. Colloid Sci.* **1953**, 8, 551.

[49] Drozin, V.G. *J. Colloid Sci.* **1955**, 10, 158.

[50] Mack, L.L., Kralik, P., Rheude, A., Dole, M. *J. Chem. Phys*. **1970**, 52, 4977.

[51] Clegg, G.A., Dole, M. *Biopolymers* **1971**, 10, 821.

[52] Teer, D., Dole, M. *J. Polymer Sci.* **1975**, 13, 1985.

[53] Dole, M., Cox Jr., H.L., Gieniec, *J. Adv. Chem. Ser*. **1973**, 125, 73.

[54] Iribarne, J.V., Dziedzic, P.J., Thomson, B.A. *Int. J. Mass Spectrom. Ion Phys*. **1983**, 50, 331.

[55] Blakely, C.R., McAdams, M., Vestal, M.L. *J. Chromatogr*. **1978**, 158, 264.

[56] Blakely, C.R., Carmody, J.J., Vestal, M.L. *Clin. Chem*. **1980**, 16, 1467.

[57] Blakely, C.R., Carmody, J.J., Vestal, M.L. *J. Am. Chem. Soc*. **1980**, 102, 5931.

[58] Yamashita, M., Fenn, J.B. *J. Phys. Chem*. **1984**, 88, 4451.

[59] Aleksandrov, M.L., Gall, L.N., Krasnov, V.N., Nikolaev, V.I., Pavlenko, V.A., Shkurov, V.A. *Dokl. Akad. Nauk SSSR* **1984**, 277, 379.

[60] Alexsandrov, M.L., Gall, L.N., Krasnov, V.N., Nikolaev, V.I., Pavlenko, V.A., Shkurov, V.A., Baram, G.I., Gracher, M.A., Knorre, V.D., Kusner, Y. S. *Bioorg. Khim*. **1984**, 10, 710.

[61] Smith, R.D., Barinaga, C.J., Udseth, H.R. *Anal. Chem*. **1988**, 60, 1948.

[62] Mylchreest, I.C., Hail, M.E. United States Patent 5,122,670, June 16, 1992.

[63] Meng, C.K., Mann, M., Fenn, J.B. *Z. Phys. D* **1988**, 10, 361.

[64] Hiraoka, K., Fukasawa, H., Matshushita, F., Aizawa, K. *Rapid Commun. Mass Spectrom*. **1995**, 9, 1349.

[65] Imatani, K., Smith, C. *Am. Lab*. **1996**, 28, 29.

[66] Wilms, M., Mann, M. *Int. J. Mass Spectrom. Ion Processes* **1994**, 136, 167.

[67] Search for "electrospray" on www.ingenta.com.

[68] Wang, H., Agnes, G.R. *Anal. Chem*. **1999**, 71, 3785.

[69] Marky, L.A., Breslauer, K.J. *Biopolymers* **1987**, 26, 1601.

[70] Cheng, X., Gao, Q., Smith, R.D., Jung, K.-E., Switzer, C. *Chem. Commun*. **1996**, 747.

[71] Sannes-Lowery, K.A., Griffey, R.H., Hofstadler, S.A. *Anal. Biochem*. **2000**, 280, 264.

[72] Leize, E., Jaffrezic, A. ,Van Dorsselaer, A. *J. Mass Spectrom*. **1996**, 31, 537.

[73] Jørgensen, T.J.D., Roepstorff, P., Heck, A.J.R. *Anal. Chem*. **1998**, 70, 4427.

[74] Davidson, W.R., Kebarle, P. *J. Am. Chem. Soc*. **1976**, 98, 6133.

[75] Dzidic, I., Kebarle, P. *J. Phys. Chem*. **1970**, 74, 1466.

[76] Bouchard, F., Hepburn, J.W., McMahon, T.B. *J. Am. Chem. Soc*. **1989**, 111, 8934.

[77] Kemper, P.R., Bushnell, J., Van Koppen, P., Bowers, M.T. *J. Phys. Chem*. **1993**, 97, 1810.

[78] Peschke, M., Blades, A.T., Kebarle, P. *J. Phys. Chem. A* **1998**, 102, 9978.

[79] Hoyau, S., Norrman, K., McMahon, T.B. Ohanessian, G. *J. Am. Chem. Soc.* **1999**, 121, 8864.

[80] Ervin, K.M., Armentrout, P.B. *J. Chem. Phys*. **1985**, 83, 166.

[81] Schultz, R.H., Crellin, K.C., Armentrout, P.B. *J. Am. Chem. Soc*. **1991**, 113, 8590.

[82] Rodgers, M.T., Ervin, K.M., Armentrout, P.B. *J. Chem. Phys*. **1997**, 106, 4499.

[83] Woodin, R.L., Beauchamp, J.L. *J. Am. Chem. Soc*. **1978**, 100, 501.

[84] Holland, A.W.P.M., Lindsay, D.M., Peterson, K.I., Castleman, Jr., A.W. *J. Am. Chem. Soc*. **1978**, 109, 6039.

[85] Sallans,L., Lane, K.R., Freiser, B.S. *J. Am. Chem. Soc*. **1989**, 111, 865.

[86] Van der Hart, W. *J. Mass Spectrom. Rev*. **1989**, 8, 237

[87] Wiley, K.F., Cheng, P.Y., Bishop, M.B., Duncan, M.A. *J. Am. Chem. Soc*. **1991**, 113, 4721.

[88] Faulk, J.D., Dunbar, R.C. *J. Am. Chem. Soc*. **1992**, 114, 8596.

[89] Afzaal, S., Freiser, B.S. *Chem. Phys. Lett*. **1994**, 218, 254.

[90] Cooks, R.G., Patrick, J.S., Kotiaho, T., McLuckey, S.A. *Mass Spectrom. Rev*. **1994**, 13, 287.

[91] Cooks, R.G., Wong, P.S.H. *Acc. Chem. Res*. **1998**, 31, 379.

[92] Cooks, R.G., Koskinen, J.T., Thomas, P.D. *J. Mass Spectrom*. **1999**, 34, 85.

[93] Miessler, G.L., Tarr, D.A. "Chemistry of the Main Group Elements," Inorganic Chemistry, Prentice Hall, Inc., Englewood Cliffs, NJ, 1991, pp. 227-230.

[94] Kebarle, P. *J. Mass Spectrom*. **1997**, 32, 922.

[95] Ikonomou, M.G., Blades, A.T., Kebarle, P. *Anal. Chem*. **1990**, 62, 957

[96] Hiraoka, K., Kudaka, I. *Rapid Commun. Mass Spectrom*. **1990**, 4, 519.

[97] Ogorzalek Loo, R.R., Udseth, H.R., Smith, R.D. *J. Phys. Chem.* **1991**, 95, 6412.

[98] Ogorzalek Loo, R.R., Udseth, H.R., Smith, R.D. *J. Am. Soc. Mass Spectrom*. **1992**, 3, 695.

[99] Young, D.-S., Hung, H.-Y., Liu, L.K. *Rapid Commun. Mass Spectrom*. **1997**, 11, 769.

[100] Frensdorff, H.J. *J. Am. Chem. Soc.* **1971**, 93, 600.

[101] Kempen, E.C., Brodbelt, J.S., Bartsch, R.A., Jang, Y., Kim, J.S. *Anal. Chem*. **1999**, 71, 5493.

[102] Goolsby, B.J., Brodbelt, J.S., Adou, E., Blanda, M. *Int. J. Mass Spectrom*. **1999**, 193, 197.

[103] Blanda, M.T., Farmer, D.B., Brodbelt, J.S., Goolsby, B.J. *J. Am. Chem. Soc*. **2000**, 122, 1486.

[104] Yoshida, M., Tsuzuki, S, Goto, M., Nakanishi, F. *J. Chem. Soc., Dalton Trans*. **2001**, 1498.

[105] Lopes, N.P., Stark, C.B.W., Hong, H., Gates, P.J., Staunton, J. *Analyst* **2001**, 126, 1630.

[106] Fukushima, T., Matsuda, Y., Hashimoto, H., Arakawa, R. *Electrochem. and Solid-State Lett*. **2001**, 4, A127.

[107] Temesi, D., Law, B. *LC-GC* **1999**, 17, 626.

[108] Tsuzuki, S., Yoshida, M., Uchimaru, T., Mikami, M. *J. Phys. Chem. A* **2001**, 105, 769.

[109] Cubero, E., Luque, F.J., Orozco, M. *Proc. Natl. Acad. Sci. USA* **1998**, 95, 5976.

[110] Mecozzi, S., West, Jr., A.P, Dougherty, D.A. *J. Am. Chem. Soc.* **118** (1996) 2307.

[111] Stone, J.A., Vukomanovic, D. *Int. J. Mass Spectrom*. **2001**, 210/211, 341.

[112] Klassen, J.S., Anderson, S.G., Blades,A.T., Kebarle, P. *J. Phys. Chem*. **1996**, 100, 14218.

[113] Rodgers, M.T., Armentrout, P.B. *J. Phys. Chem. A* **1997**, 101, 2614.

[114] Evans, C.S., Startin, J.R., Goodall, D.M., Keely, B.J. Rapid *Commun. Mass Spectrom*. **2001**, 15, 1341.

[115] Schalley, C.A., Castellano, R.K., Brody, M.S., Rudkevich, D.M., Siuzdak, G., Rebek, Jr., J. *J. Am. Chem. Soc.* **1999**, 121, 4568.

[116] Stone, J.A., Vukomanovic, D. *Int. J. Mass Spectrom*. **2001**, 210/211, 341.

[117] Tao, W.A., Zhang, D., Nikolaev, E.N., Cooks, R.G. *J. Am. Chem. Soc.* **2000**, 122, 10598.

[118] Gaussian 98 (Revision A.*7*), M. J. Frisch, G. W. Trucks, H. B. Schlegel, G. E. Scuseria, M. A. Robb, J. R. Cheeseman, V. G. Zakrzewski, J. A. Montgomery, Jr., R. E. Stratmann, J. C. Burant, S. Dapprich, J. M. Millam, A. D. Daniels, K. N. Kudin, M. C. Strain, O. Farkas, J. Tomasi, V. Barone, M. Cossi, R. Cammi, B. Mennucci, C. Pomelli,

C. Adamo, S. Clifford, J. Ochterski, G. A. Petersson, P. Y. Ayala, Q. Cui, K. Morokuma, D. K. Malick, A. D. Rabuck, K. Raghavachari, J. B. Foresman, J. Cioslowski, J. V. Ortiz, A. G. Baboul, B. B. Stefanov, G. Liu, A. Liashenko, P. Piskorz, I. Komaromi, R. Gomperts, R. L. Martin, D. J. Fox, T. Keith, M. A. Al-Laham, C. Y. Peng, A. Nanayakkara, C. Gonzalez, M. Challacombe, P. M. W. Gill, B. G. Johnson, W. Chen, M. W. Wong, J. L. Andres, M. Head-Gordon, E. S. Replogle and J. A. Pople, Gaussian, Inc., Pittsburgh PA, 1998.

[119] Weast, R.C., ed., CRC Handbook of Chemistry and Physics, 60th ed., "Buffer Solutions," CRC Press, Inc, Boca Raton, FL, 1979, pp. D-148.

[120] Bhushan, R., Martens, J. *Biomed. Chromatogr*. **1998**, 12, 309.

[121] Kelly, M.A., Vesting, M.M., Fenselau, C.C., Smith, P.K. *Org. Mass Spectrom*. **1992**, 27, 1143.

[122] Mansoori, B.A., Volmer, D.A., Boyd, R.K. *Rapid Commun. Mass Spectrom*. **1997**, 11, 1120-1130.

[123] Kebarle, P., Tang, L. *Anal. Chem*. **1993**, 65, 972A-986A.

[124] Guo, B.C., Conklin, B.J., Castleman, A.W., Jr. *J. Am. Chem. Soc*. **1989**, 111, 6506.

[125] Lias, S.G., Liebman, J.F., Levin, R.D. *J. Phys. Chem. Ref. Data* 1984, 13, 695.

[126] Straub, R.F.; Voyksner, R.D. *J. Am. Soc. Mass Spectrom*. **1993**, 4, 578-587.

[127] Temesi, D.; Law, B *LC-GC* **1999**, 17, 626-632.

[128] Evans, C.S.; Startin, J.R.; Goodall, D.M.; Keely, B.J. *Rapid Comun. Mass Spectrom.* **2001**, 15, 1341-1345.

[129] Hopfgartner, G.; Bean, K.; Henion, J. *J. Chrom*. **1993**, 647, 51-61.

[130] Jones, L.; Atkins, P. Chemistry: Molecules, Matter, and Change, 4th ed., W.H. Freeman and Co., New York, 2000, p. 302.

VITA

Kevin Albert Schug was born in Blacksburg, Virginia on May 4, 1975. Upon graduation from Blacksburg High School in 1993, he attended Virginia Polytechnic Institute and State University part-time for one year prior to attending the College of William and Mary. He received a Bachelor of Science in Chemistry from William and Mary, along with a minor in Classical Civilizations, in 1998. During undergraduate studies, he performed research with Professor William Starnes in polymer-related research. In the summer of his sophomore year, he worked with Professor Harold McNair at Virginia Tech. In the summer of his junior year, he was employed as an intern with the quality assurance department at S. C. Johnson & Wax in Racine, Wisconsin performing analysis of pesticide degradation in holding tanks by gas chromatography. Following graduation, he enrolled as a graduate student at Virginia Tech under Professor Harold McNair. During his time there, he was involved as a lecture and laboratory instructor for ACS sponsored short courses in gas chromatography, gas chromatography-mass spectrometry, liquid chromatography, and sample preparation techniques. He also performed a summer internship in the Dipartmento Pharmacia at the University of Messina, Sicily, Italy, under Professor Giovanni Dugo. After completing his Ph.D. degree from Virginia Tech in 2002 in the field of electrospray ionization mass spectrometry, he pursued post-graduate research with Professor Wolfgang Lindner at the University of Vienna in Austria.